Spring 2011

The Effects of Weak Collisions on Nonlinear Plasma Kinetics

Carrie E. Black
University of New Hampshire, Durham

The Effects of Weak Collisions on Nonlinear Plasma Kinetics

BY

Carrie E. Black

B.S., University of Vermont (2006)

Dissertation

Submitted to the University of New Hampshire
in Partial Fulfillment of
the Requirements for the Degree of

Doctor of Philosophy

in

Physics

May 2011

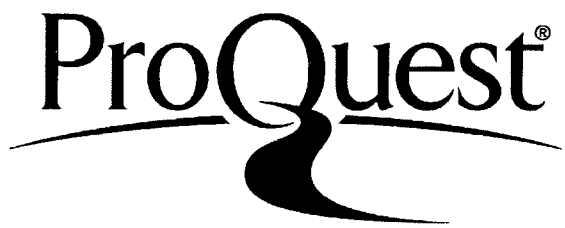

ProQuest LLC
789 East Eisenhower Parkway
P.O. Box 1346
Ann Arbor, MI 48106-1346

This has been examined and approved.

advisor, Amitava Bhattacharjee

Peter Paul Professor, Department of Physics

Kai Germaschewski

Assistant Professor of Physics

Martin Lee

Professor of Physics

James Connell

Associate Professor of Physics

Dawn Meredith

Associate Professor of Physics

3/27/11

Date

DEDICATION

With love to Stephen, whose daily encouragement and support kept me on the path.

And for my father, the original Dr. Black.

ACKNOWLEDGMENTS

I would like to thank my advisor, Dr. Amitava Bhattacharjee, for the extraordinary opportunities I have been afforded while under his tutelage. His imaginative approach to physics never fails to make one think in new and unexpected ways. For these experiences, I am truly grateful. I have learned much from him beyond how to do science and count myself very fortunate to have been a member of the Center for Integrated Computation and Analysis of Reconnection and Turbulence (CICART).

I wish to thank two people in particular, without whom this project would have been almost impossible: Dr. C. S. Ng and Dr. Kai Germaschewski. Their patient guidance in my early days and continued collaboration has been invaluable.

To Dr.'s Marty Lee, Jim Connell, Dawn Meredith, Dick Kaufmann, and Barrett Rogers, thank you for the many wonderful and probing discussions. I always came away with a renewed vigor for the work. I would also like to extend my thanks for the critical reading of this thesis.

Finally, I would be remiss if I did not thank the many members of CICART and the UNH Space Science Center who have been both colleagues and friends. A special thanks goes to Doug Larson for the answers to my many Zaphod/UNIX/random questions.

I owe a debt of gratitude to the Space Plasma Theory/ CICART Program Manager, Amber Perkins. She has been a tireless advocate for graduate students professionally and, more importantly, in a human capacity. Her shoulder to cry on and keen understanding that science is not without its emotional side helped me keep it together when I would rather have given up.

I also wish to thank my fellow graduate students, particularly my cube-mates Liwei Lin, Lei Ni, Liang Wang, and Matt Gorby. They have been supportive, open, and always good for a laugh.

TABLE OF CONTENTS

LIST OF TABLES

LIST OF FIGURES

ABSTRACT

The Effects of Weak Collisions on Nonlinear Plasma Kinetics

by

Carrie E. Black
University of New Hampshire, May, 2011

Kinetic plasma behaviors have long been of interest to those studying space and laboratory plasmas. For instance, kinetic plasma instabilities are widely believed to be responsible for the generation of anomalous resistivity in reconnection layers, providing a possible mechanism for fast reconnection. The concept of Landau damping is fundamental to such wave kinetic instabilities in space, and is treated typically within the framework of the collisionless Vlasov equation. It has become clear in recent theoretical and experimental work that weak collisions are a singular perturbation on the collisionless theory, and qualitatively alter the results of the collisionless theory. In particular, it has been demonstrated by C. S. Ng, A. Bhattacharjee, and F. Skiff that the Case-Van Kampen continuous spectrum, which are the underlying eigenmodes of the collisionless system, are completely eliminated and replaced by a discrete spectrum (hereafter referred to as the NBS spectrum). The NBS spectrum includes Landau-damped roots as exact eigenmodes, but is significantly broader, including a larger spectrum of discrete roots. We discuss the implications of these results for two nonlinear applications, the plasma wave echo and the ion acoustic instability, by means of a new Vlasov code that has been modified to include the Lenard-Bernstein collision operator. We show that the existing collisional theories for the echo, which fail to account for the discrete collisional spectrum, come close, but do not quite yield the appropriate collisional damping rates. Of greater practical importance to problems involving dissipation and anomalous transport is the generation of anomalous resistivity due to microinstabilities. As a specific example, we consider the ion acoustic wave. We compare our numerical findings with the anomalous resistivity estimates of A. Galeev and R. Z. Sagdeev for both collisionless and weakly collisional systems. In the regime of applicability of the theoretical estimates, the

agreement is good within an order of magnitude.

CHAPTER 1

Introduction

One of the unique properties of plasmas is that the particles which constitute the plasma and the waves resulting from their motion can interact. These wave-particle interactions occurring in the linear and nonlinear regimes are conservative, and are treated properly in the framework of kinetic models. There is a delicate relationship between individual particle motion and the collective behavior of the plasma. As is demonstrated by Landau damping, relatively few particles can have a dramatic impact on the collective. The field response of a plasma to stimuli is the collective response (behavior) of the plasma. In the study completed here, the fields are electrostatic. The particle behavior is given by the particle distribution functions.

Fluid models, which are often used to treat low-frequency waves (e.g., magneto-hydrodynamic waves), cannot be used to describe these kinetic interactions in detail. Kinetic waves and, in particular, the wave-particle interactions are altered in interesting ways by the introduction of particle collisions. The types of collisions that occur depend on plasma properties. There can be hard sphere scattering (neutral-neutral collisions), Coulomb (charge-charge) collisions, charge exchange, and creation and annihilation processes due to collisions. The interest for the work presented here is focused on small angle Coulomb collisions.

In a natural plasma, there are always some collisions. When collisions are extremely weak, i.e. when the system scale is much smaller than the collision scale, the system can be considered to be collisionless. When collisions are very strong, the

fluid approximations can be utilized. (See Ichimaru [Ich73]) There is also at least one intermediate regime which spans the collisionless and highly collisional limits. We focus on the weakly collisional limit which borders the collisionless regime. The bounds of the weakly collisional regime can be difficult to determine in natural data. Here, the effects of collisions are typically modeled using perturbation methods, but this must be done with care. We will show that when weak collisions are a singular perturbation, they significantly alter the mode spectrum. The weakly collisional plasmas are, in general, more difficult to work with analytically than the collisionless or highly collisional limits. In this work, weak Coulomb collisions are modeled with the Lenard-Bernstein operator and their effects are explored numerically for two different applications - the plasma wave echo (PWE) and the current driven ion acoustic instability (CDIAI). It is important to point out that the collisions, modeled by a particular operator, have a similar effect on different kinetic waves. Electron-electron collisions, for instance, have the same type of effect on the plasma wave that they do on the ion acoustic wave.

1.1 Previous Experimental Measurements and Existing Theories of Weakly Collisional Kinetic Modes

The work we discuss here is the motivation for the derivation of the weakly collisional plasma modes. The experimental work is done for the ion acoustic problem. Typical experiments require the use of a probe which generates a potential sheath around it when the potential applied to a grid varies temporally. Estabrook and Alexeff [EA72] examine pseudowaves numerically and experimentally and described the consequences of this. Ions are accelerated through the sheath in bursts. After leaving the sheath, these bunched particles travel ballistically. These free-streaming particles are called pseudowaves since they look like waves in phase space, but do not interact

self consistently with the electric fields. They demonstrate that the presence of these waves indicates there are modes which have been ignored because they are also not represented by the usual dispersion relations.

Sarfaty, Skiff and De Souza-Machado [SSMS96] present ion acoustic data from a new experimental method. They implement a laser induced fluorescence method, which eliminates the necessity for a probe, to measure particle distributions in phase space. The Krook collision operator is used to model the collisional effect on the ion acoustic wave and good agreement is found with the experiment. They present observational evidence of the wave-particle resonance in the phase space distribution for a weakly collisional, weakly magnetized plasma. This finding is compared with the assumed form of the distribution given by Stix [Sti92]. This form includes the classic assumption of Su and Oberman [SO68] for the temporally damped collisional wave effect on the distribution. Sarfaty et al. show that in the resonance regime, the Su and Oberman form is a poor fit. They show, most importantly, that the collision frequency obtained from the fit is two orders of magnitude smaller than found by other experimental methods.

Skiff, De Souza-Machado, Noonan, Case, and Good [SSMN+98] point out that modes outside of the collective modes, i.e. the full eigenmode spectrum, are almost always ignored under the assumption that they will settle down before the collective modes set in. It was thought, [SO68], that the weak collisions in a real system will cause these transients (free-streaming particles) to decay with $\exp(-at^3)$ or $\exp(-bx^3)$ while having little effect on the collective first order behavior. The free-streaming particles will decay quickly with collisions and have very little or no measurable effect on the electric field/waves. However, there should be measurable evidence of this decay under some nonlinear conditions. Skiff correctly sites that this Su and Oberman result is actually derived for the region near resonance and does not apply

to the nondispersive, free-streaming behavior on which pseudowaves and the plasma wave echo are dependent.

What is interesting about the work of Skiff in the weakly collisional regime is that despite the fact that Lenard and Bernstein actually recover a discrete spectrum in their solutions, they never discuss this. In the fluid limit the discrete spectrum is well known and the collisionless limit has a continuous spectrum, but the intermediate regime of weakly collisional systems has had little examination. Skiff et al. point out that the Vlasov picture neglects particle discreteness effects. This means that all particles move independent of each other, accept through interaction with the self-consistent electric field. The Coulomb operator introduces particle coupling "linking" the infinite degrees of freedom into a discrete spectrum. They believe this effect to be a generic property of Coulomb collisions for the linear modes.

This was followed by De Souza-Machado et al [DSMSS99] who present the Hermite expansion method for solving the eigenmodes of the collisional Vlasov-Poisson system with collisions modeled by a linearized Fokker-Planck equation. They show that the distributions are reasonably described by a sum of a few eigenfunctions derived for the spatially damped ion acoustic wave. This means that a) the Lenard-Bernstein operator models the particle collisions for a real system sufficiently well and b) there is now a good model for the resonance region. This prompted a new analytical look at the modes of the weakly collisional plasma wave. Ng, Bhattacharjee, and Skiff (NBS) [NBS99] show that the eigenmodes of the plasma, those of the particle distribution, become a discrete set when collisions are introduced. This discretization had long been ignored under the assumption that continuity of modes quickly dissipates and is of no importance. In this paper, they argue that the Su and Oberman result is dependent on the continuum. The NBS formulation shows that discretization of the spectrum is a key feature of the weakly collisional system, in part because one of these

discrete modes contain the Landau damped solution. Skiff points out that the fluid, high collisionality limit is known to have a discrete spectrum but the collisionless limit has a continuous eigen-spectrum. They note this means that the presence of collisions fundamentally alters the eigenmode spectrum. They believe this is a generic effect of Coulomb collisions whereby the collisions couple modes in the continuum, creating a discretized spectrum.

For better comparison with the existing collisional theories [SO68] and to test the NBS predictions, numerical analysis of the plasma wave and the plasma wave echo were carried out in the first part of the work presented in this thesis. Because the Skiff experiments were on the ion acoustic modes and the ion waves have greater application than the plasma waves, the second part of this work is on the current driven ion acoustic wave and instability. The effect of Coulomb collisions on the instability and the "anomalous" resistivity it generates are examined.

1.2 Plasma Wave Echo

The plasma wave echo gives great insight into the behavior of a weakly nonlinear system. It requires a very quiet system to exist and therefore is seen only in laboratory plasmas. The plasma wave echo is in a class of entropy conserving phenomena that includes the well known nuclear magnetic resonance (NMR). NMR, which led to many significant advances in medicine and materials science, is simply due to the interference of two magnetic pulses in a polarized material. The result is that the material emits a magnetic pulse at a resonant frequency. The plasma wave echo is an electrostatic analog. In the plasma echo, two different electric wave perturbations interfere causing the plasma to emit an electric pulse.

The echo is highly sensitive to collisions making it ideal for the study of weak collisions on plasma waves. In particular, it provides an opportunity to examine the

effect that collisions have on particles resonant with the wave. Collisionality in physical systems is extremely difficult to determine. If analytical models of collisionality could be resolved with numerical and laboratory experiments, the plasma wave echo could be used as a diagnostic for determining collisionality in a lab setting. To this end, some laboratory experiments have been performed by Spentzouris, Ostiguy, and Colestock [SOC96]. Their data was fit to the only existing theory, that of Su and Oberman [SO68] . The classic result of Su and Oberman demonstrates how collisions of the Lenard-Bernstein type between particles, which are resonant with the echo wave, Modify the echo amplitude. They predict that the echo should damp super exponentially ($\exp(-\beta t^3)$) in time. Spentzouris et al. find that their data fits this theory nicely. However, it is inherently difficult to independently verify the real collisionality.

Using numerical methods, we will test how well the Su and Oberman theory fits the collisional and fully nonlinear Vlasov-Poisson system. As we have seen for the linear analysis, the Su and Oberman theory must be applied carefully to the appropriate regimes. Even more care must be taken for application to the nonlinear regime. In the work presented, the echo is generated numerically for various collision frequencies. It is shown that the Su and Oberman form for the collisional echo fits the data well and recovers a collision frequency that agrees reasonably well with the expected value. However, this leaves many open questions about the nature of the nonlinear modes. This work also suggests that the collisional effects on the particle distribution function need to be revisited analytically, perhaps, beginning with a re-evaluation of the asymptotic matching used between the resonant and non-resonant regions.

1.3 Ion Acoustic Instability

Ion acoustic waves are the focus of the second part of this work. They are prevalent in many natural and laboratory systems and belong to a class of kinetic drift waves which can be unstable. They are different from the classic $E \times B$, gradient, and curvature drift waves. In this case the drift is an initial condition rather than a result. The kinetic drift waves are of interest in a wide range of fields from dusty plasmas [MD05] and laser and fusion plasmas [DRB+05],[SDR+06], [BMRT05], [IH84] to space plasmas [DG75], [LT88]. Microinstabilities arising from these drift waves are of interest for those studying magnetic reconnection as well [Tre01], [BE06]. Analytically, the ion acoustic wave is relatively simple. In the cold ion limit, the 2-species Vlasov-Poisson system decouples easily making the system predictable in the linear and weakly nonlinear regimes. Numerically, the linear behavior can be predicted for a larger range of temperature and wave numbers. However, a definitive prediction for nonlinear behavior does not exist. Here we present results in the weakly nonlinear regime and compare with other existing theories.

The drift wave instabilities scatter particles about the resonance so dramatically that significant changes to transport properties arise. Measurable anomalous resistivity results from the instabilities [Tho63], [Sti92]. The study of anomalous transport in plasmas often coincides with studies of anomalous resistivity. This kinetic resistivity can only be estimated analytically in the linear regime and for restricted parameters. Numerically, the resistivity can be examined in the linear and nonlinear regimes. We compare the analytical estimates to the numerical results and show that they agree up to the onset of the nonlinear regime. Wave properties are compared with other numerical studies. We show good agreement with other Vlasov-Poisson studies, but not with existing Vlasov-Ampere studies.

Examined here are the effects of weak Lenard-Bernstein collisions on the growth of

the instability and the resulting anomalous resistivity. Different particle collisions will have different effects on the instability. The electron plateau formation, for example, is directly impacted by electron-electron and electron-ion collisions. These work to Maxwellianizes the distribution. Ion-ion collisions have a more subtle impact on the instability. They introduce a viscosity which slows the wave and also equilibrate the ion distribution. This is discussed in further detail in chapter 5.

Various collision operators have previously been examined for their effect on the current driven ion acoustic wave, although the Lenard-Bernstein operator has not. Most notably for this study is the work of Kulsrud and Shen [KS66]. Collisions between the different species have different impacts on ion acoustic waves. Here we show how ion-ion and electron- electron collisions effect the quasilinear saturation of the current driven ion acoustic instability. In this work, it is demonstrated that the Lenard-Bernstein operator behaves qualitatively as predicted by other operators belonging to the Landau-Fokker-Planck family. We show that the quantitative agreement between results of Krook operators [Ste71] and the data is reasonable. Also examined, are the effects of various collisionalities on the wave-particle resistivity. It is shown that the ion-ion collisions decrease the resistivity, which is calculated from the electron distribution. Electron-electron collisions are shown to increase the total resistivity.

1.4 Scope of Thesis

In this thesis, two nonlinear phenomena are examined numerically in collisionless and collisional systems. The plasma wave echo and ion acoustic instability are studied with the use of a new Vlasov-Poisson solver. This parallel solver makes use of a Hermite spectral scheme for the velocity dependence of the system. We employ a very large velocity space and implement the full Lenard-Bernstein collision operator.

Beginning in chapter 2, the collisionless and collisional modes of the particle distribution and the resulting collective behavior modes (those of the electric field) are derived analytically. In chapter 3, the code used to carry out this study is introduced and important benchmarks are shown for the linear collisionless modes. In this chapter, we present for the first time, numerical evidence that the least damped NBS eigenmode well describes the weakly collisional plasma wave. We also present evidence that other NBS modes are sustainable in the system. This work is followed in chapter 4 by a study of the collisional plasma wave echo. This is significant because the classic analytical estimates for the effect of collisions on the echo are for the Lenard-Bernstein operator and this is the first numerical study of this specific topic.

In chapter 5, the linear ion acoustic modes are derived analytically and are benchmarked on the Kinetic Code. The current driven ion acoustic modes are also shown analytically and numerically. Growth of the instability occurs as predicted and saturation of the instability coincides with the formation of the quasilinear plateau in the electron distribution function. We compare our saturation values with other numerical studies. We show that the Vlasov-Ampere studies saturate at a much lower energy than the Vlasov-Poisson studies. This is believed to be due to electron phase space holes not seen in the Poisson studies and whose origin is currently debated. The current methods for predicting saturation are discussed and shown to be inadequate for absolute predictions. Anomalous resistivity data are also presented and compared with other studies.

This is followed in chapter 6 by a study of collisions in the instability growth rate and saturation. We show the impact of ion-ion and electron-electron collisions on the wave-particle scattering of electrons. Finally, chapter 7 concludes this thesis with an overview of the findings presented.

Appendix A shows the detailed echo derivation. Appendix B contains the deriva-

tion of the quasilinear equation. Finally, Appendix C describes various collision operators and their conservation properties.

CHAPTER 2

Electrostatics

The study of collisions in a plasma begins with the analysis of the modes supported by a collisionless electron plasma. The simple plasma wave is due to the oscillation of electrons about the massive and stationary, neutralizing ions. Traditionally, the modes of the collective behavior such as the self-consistent fields are examined and little attention is paid to the actual eigenmodes of the entire system, the modes of the distribution. Solving for the full distribution is a challenge.

This began with the work of Vlasov [Vla45], Langmuir and Tonks [TL29], and Landau [Lan46], who all solve for modes of the plasma wave in the electrostatic regime. The classic results given by these works for the collective behavior were ground breaking, in particular, that of Landau. He accurately predicted how the resonance interaction would occur and its effect on the wave. The result is fascinating because the wave that is made up of the particles interacts with the particles almost as though they are independent quantities.

Shortly thereafter, the work of Case [Cas59] and Van Kampen [van55] gave the distribution modes for the collisionless electrostatic plasma. These modes are a continuum and collective behaviors are achieved through interference of multiple modes. This continuum of eigenmodes means that there are infinite degrees of freedom in the system. That is, each particle is considered to move independent of any effects from surrounding particles. There is no coupling. It is no wonder, then, that distribution modes have been ignored. The van Kampen modes offer no further insight into

plasma behavior at this point.

When collisions are introduced, things change. These processes are inherently difficult to model as seen in nature and the analytical forms are just as difficult to solve. Highly simplified forms such as the Bhatnagar-Gross-Krook operator (BGK or Krook) [BGK54] are limited in their regime of validity. However, their tractable nature helps to guide the development of solutions for more complicated forms such as the Fokker-Planck operator. In this work, we focus on an operator for weak collisions presented by Lenard and Bernstein [LB58]. They show that the eigenmode spectrum is discrete and that the Langmuir waves are modified by a damping component proportional to the collision frequency. However, there is no discussion of the consequences of the spectrum discretization.

Karpman [Kar67] and Su and Oberman [SO68] followed this work by solving for the impact of collisions on the resonant regime of the distribution only. They show collisions have a super exponential damping contribution. However, this finding is dependent on the continuous spectrum as Karpman notes. Su and Oberman state that their result has impact on the free-streaming particles that are central to the plasma wave echo. This is discussed in detail in this chapter 4.

Ng, Bhattacharjee and Skiff [NBS99], [NBS04], derive the complete set of eigenmodes for the full Lenard-Bernstein Vlasov-Poisson system. These modes are those of the distribution modes and are discrete. They also recover the Landau damped solution in the limit of zero collisions. This work shows that the $\exp(-\nu t^3)$ behavior as predicted by Su and Oberman is not in the mode structure of the plasma. It could potentially exist in interactions of modes and this motivates the study of the collisional plasma wave echo. We begin here with a review of the plasma wave modes and eigenmodes for both the collisionless and weakly collisional systems.

This chapter begins, in section 2.1, with a description of the kinetic approach

to plasmas. Sections 2.2 and 2.3 contain derivations of the Langmuir and Case-Van Kampen modes. Section 2.4 describes the Lenard-Bernstein collision operator and its effect on the wave modes. In section 2.5, we examine the derivation of Su and Oberman and discuss the implications of the solution. In section 2.6, we derive the true eigenmodes of the full Lenard-Bernstein collisional plasma, the NBS modes. Here we examine the conflict with Su and Oberman and its motivation for examining the plasma wave echo and the ion acoustic instability. Section 2.7 contains a summary of the important points in this chapter and a brief discussion of what the mode analysis of the plasma wave implies for ion acoustic waves.

2.1 Kinetic Plasma Theory

The kinetic approach to plasmas centers on the particle distribution function, f. The distribution is a function of space, velocity and time and defines the number of particles per unit of space and velocity, or the number density per velocity volume element..

$$n_s(\mathbf{r},t) = \int f_s(\mathbf{r},\mathbf{v},t)d^3v \tag{2.1}$$

Bulk properties of the system are found by taking moments of the distribution. Shown in equation 2.1 is the zeroth moment, the number density. The first moment gives the average particle momentum and the second moment gives the average energy. From these, the bulk flow velocity (fluid velocity) and the average temperature can be found.

$$n_s(\mathbf{r},t)u_{s,0}(\mathbf{r},t) = \int v f_s(\mathbf{r},\mathbf{v},t)d^3v \tag{2.2}$$

$$\frac{m_s}{2}n_s(\mathbf{r},t)u_{s,th}^2(\mathbf{r},t) = \frac{m_s}{2}\int v^2 f_s(\mathbf{r},\mathbf{v},t)d^3v - n_s(\mathbf{r},t)\frac{m_s}{2}u_{s,0}^2(\mathbf{r},t) \tag{2.3}$$

Boltzmann's equation was first applied to a plasma by Vlasov in 1945 and from then on, the equation bore his name when in the context of a plasma.

$$\frac{\partial f_s}{\partial t} + \mathbf{v} \cdot \nabla f_s + \mathbf{a} \cdot \nabla_v f_s = 0 \tag{2.4}$$

The acceleration, a, is found from the force applied to the particles, in this case, from an applied electric field. This nonlinear partial differential equation requires one other equation to meet the closure requirement. We choose to use Poisson's equation to solve for the electric field.

$$\frac{\partial f_s}{\partial t} + \mathbf{v} \cdot \nabla f_s + \frac{q_s \mathbf{E}}{m_s} \cdot \nabla_v f_s = 0 \tag{2.5}$$

$$\nabla \cdot \mathbf{E} = \frac{\mathbf{q_s}}{\epsilon_\mathbf{o}} \int_{-\infty}^{\infty} \mathbf{f_s}(\mathbf{v}) \mathbf{d^3 v} \tag{2.6}$$

The nonlinearity in the third term of equation 2.5 is the source of many challenges in solving this system. When taking the perturbative approach, this challenge can be eliminated by solving recursively for high orders. In this study, we work with the first and second order approximations, confining ourselves to the weakly nonlinear regime at most.

2.2 Collisionless Wave Modes

2.2.1 Plasma Waves

There are two approaches to this problem, the initial value and boundary value methods. In the initial value problem, we assume a real wavenumber and solve for a complex frequency. These waves will damp in time. In the boundary value problem, we assume a real frequency and solve for a complex wavenumber. These waves will damp spatially. Plasma waves were found independently by Vlasov [Vla45] and by

Langmuir and Tonks [TL29].

$$\frac{\partial f}{\partial t} + v\frac{\partial f}{\partial x} + \frac{qE}{m}\frac{\partial f}{\partial v} = 0 \tag{2.7}$$

$$\nabla^2\Phi = \frac{q}{\epsilon_o}\int_{-\infty}^{\infty} f(v)dv \tag{2.8}$$

In this work, we focus on the temporal problem beginning with the solutions to the linearized, single species, 1d, Vlasov-Poisson system, 2.9.

$$\begin{aligned} &\frac{\partial f_1}{\partial t} + v\frac{\partial f_1}{\partial x} + \frac{qE_1}{m}\frac{\partial f_0}{\partial v} = 0 \\ &\frac{\partial E_1(x,t)}{\partial x} = \frac{q}{\epsilon_o}\int_{-\infty}^{\infty} f_1(x,v,t)dv \end{aligned} \tag{2.9}$$

Note here that E_1 contains the externally applied field and the self consistent first order response. The equilibrium (Maxwell) distribution is given by f_0. By Fourier transforming (2.10) the system in space and Laplace transforming (2.11) it in time, the plasma response to the externally applied field is found to be given by eq 2.12.

$$\begin{aligned} f(x) &= \frac{1}{\sqrt{2\pi}}\int_{-\infty}^{\infty} f(k)e^{ikx}dk \\ \widetilde{f}(k) &= \frac{1}{\sqrt{2\pi}}\int_{-\infty}^{\infty} f(x)e^{-ikx}dx \end{aligned} \tag{2.10}$$

$$\begin{aligned} f(t) &= \frac{1}{2\pi i}\int_{b-i\infty}^{b+i\infty} \widetilde{f}(p)e^{pt}dp \\ \widetilde{f}(p) &= \int_0^{\infty} f(t)e^{-pt}dt \\ p &= \gamma - i\omega \end{aligned} \tag{2.11}$$

See Appendix A.2 for the complete details. The roots of the electrostatic wave can be found by solving for the dielectric function equal to zero. We call this the dispersion

relation as shown in equation 2.13.

$$\widetilde{\phi}_1 = \frac{\widetilde{\phi}_{ext}}{\epsilon(p,k)} \tag{2.12}$$

$$\epsilon(p,k) = 1 - \frac{ie^2}{m\epsilon_0 k}\int_{-\infty}^{\infty}\frac{df_0/dv}{p+ikv}dv = 0 \tag{2.13}$$

$$\epsilon(p,k) = 1 - \frac{ie^2}{m\epsilon_0 k}\left(P\int_{-\infty}^{\infty}\frac{df_0/dv}{p+ikv}dv + 2\pi i Res\left[\frac{df_0/dv}{p+ikv}, p=ikv\right]\right) = 0 \tag{2.14}$$

$$Res[\frac{df_0/dv}{p+ikv}, p=ikv] = \frac{1}{(n-1)!}\frac{d^{n-1}}{dz^{n-1}}df_0/dv|_{p=ikv} \tag{2.15}$$

$$Res[\frac{df_0/dv}{p+ikv}, p=ikv] = df_0/dv|_{p=ikv} \tag{2.16}$$

$$\epsilon(p,k) = 1 - \frac{ie^2}{m\epsilon_0 k}P\int_{-\infty}^{\infty}\frac{df_0/dv}{p+ikv}dv - 2\pi i\frac{ie^2}{m\epsilon_0 k}df_0/dv|_{p=ikv} = 0 \tag{2.17}$$

Here ϕ is the electric potential. Specifically ϕ_1 (eq 2.12) is the response to the externally applied potential. The dispersion relation contains a singularity at $p = -ikv$, making the roots difficult to find. However, roots are easily found for a small resonance contribution. In this regime, the roots display a one to one relationship between frequency and wavenumber. From the long wavelength approximation, we find the Langmuir modes.

$$\omega^2 = \omega_{pe}^2 + \gamma k^2 v_{th,e}^2 \tag{2.18}$$

The well-known Bohm-Gross dispersion relation comes about by setting $\gamma = 3$.

2.2.2 Landau Damping

Landau [Lan46] furthered the theory by finding a solution that includes the resonances. The basic idea is that at resonance the wave and distribution will exchange energy. The classic analogy is to that of a surfer on a wave. When the surfer travels at the wave speed, he or she gains energy and the wave looses it. If there are a few more particles moving a little slower than phase velocity than the number of particles moving a little faster than phase velocity, the wave will lose energy to the particles.

This is accomplished by casting the frequencies into the complex plane. It means that the electric waves have a complex and, therefore, an inherent damping component. This is the phenomena of Landau damping. We can show that the damping rate has a dependence on the derivative of the distribution function. The dielectric function can be separated into real and imaginary components by using the Plemelj relation to solve the integral. This gives a principal value integral which is all real and the residue component which is imaginary. See Appendix A for complete details. We set real and complex terms of the dielectric function equal to zero, separately. With simple algebraic manipulation, we recover:

$$\gamma = \frac{k\pi\omega_{pe}^3}{|k|2k^2}\frac{df_0}{dv}|_{v_z=\omega/k} \tag{2.19}$$

This demonstrates that the wave will gain or loose energy to the particles in accordance with the values of the derivative of the distribution at the waves phase velocity. There are many solutions to the dielectric function. It is rewritten in the following form for a Maxwellian distribution and called the plasma dispersion relation.

$$D(k,p) = 1 + \frac{1}{(k\lambda_D)^2}[1 + \zeta Z(\zeta)] = 0 \tag{2.20}$$

where

$$\zeta = \sqrt{\frac{m}{2k_BT}}\left(\frac{ip}{k}\right) \tag{2.21}$$

$$z = \sqrt{\frac{m}{2k_BT}}v_z \tag{2.22}$$

$$Z = \int_C \frac{1}{\sqrt{\pi}}\frac{ze^{-z^2}}{z-\zeta}dz \tag{2.23}$$

A consequence of accounting for the resonance is that we find there is no longer a one to one relationship between the wavenumber and frequency. The solution for a single wavenumber is found to be a set of infinite discrete complex frequency pairs with negative imaginary components. The solutions have been tabulated in the well-known

book by Fried and Conte [FC62]. The solutions can also be generated numerically. We will see in chapter 3 that many of these modes Landau damp away very quickly leaving a least damped mode whose damping rate is described as in equation 2.19. This is sometimes referred to as the Landau root or the Landau damped solution. It should be noted here that these solutions are not eigenmodes of the system, but rather modes of the collective behavior and a consequence of eigenmode interference. This is explored further in the next section.

2.3 Collisionless Eigenmodes

Initial value and eigenvalue problems are fundamentally different problems. The initial value problem yields roots dependent on an excitation given at $t = 0$. From this we can determine all modes that will be excited in the system. The normal mode, in this case the eigenvalue problem, gives us the set of all possible frequencies that are excitable based on the fundamental characteristics of the system. From this we get the set of all possible modes. The field modes were derived using initial condition information via a Laplace transform in time. The normal modes of the system are found from a Fourier transform in time which carries no initial condition information.

It is also important to note that from Poisson's equation it is possible to have many different forms of the distribution function that integrate to the same density. Thus, an electric field does not map to a single distribution function, but the reverse is true. The distribution function is the fundamental entity in the equation and its modes are the full normal modes of the system.

The modes of the distribution function, the Case-Van Kampen modes are found using the normal mode analysis. The Vlasov-Poisson system is Fourier transformed in space and time. By solving Poisson's equation for the potential and substituting

it into Vlasov's equation we recover equation 2.24.

$$\left(v - \frac{\omega}{k}\right) \tilde{f}_1(\omega, k, v) = \left(\frac{\omega}{k}\right)^2 \frac{\partial \tilde{f}_0(\omega, k)}{\partial v} \int_{-\infty}^{\infty} dv \tilde{f}_1(\omega, k, v) \tag{2.24}$$

$$\begin{aligned} \tilde{f}_1(\omega, k, v) =& P\left[\frac{(\omega/k)^2 \partial \tilde{f}_0(\omega, k)/\partial v}{v - \frac{\omega}{k}}\right] \\ &+ \delta(v - \frac{\omega}{k}) \left(1 - P \int_{-\infty}^{\infty} dv \frac{(\omega/k)^2 \partial \tilde{f}_0(\omega, k, v)/\partial v}{v - \frac{\omega}{k}}\right) \end{aligned} \tag{2.25}$$

The genius of Van Kampen [van55] was to recognize that the solutions are functions which are a continuous spectrum. They are highly singular (delta-function like) and an infinite number of modes exist in a continuum along the real axis of the complex frequency (or wavenumber) plane. This is in contrast to a discrete spectrum which may contain an infinite number of modes, but are at distinct and discrete locations on the complex plane. Landau damping occurs due to the destructive interference of the continuum of modes. Case [Cas59] later demonstrated that these modes are a complete set. In summary, the true eigenmodes of the collisionless Vlasov-Poisson system are the highly singular Case-Van Kampen modes. Landau damping is the long-time remnant of an initial perturbation which can be written as a linear superposition of Case-Van Kampen modes, but is not itself an eigenmode of the system. In the next section, we show how these modes are impacted when collisions are introduced.

2.4 Collisional Wave Modes

There are many types of collision operators for different types of collisions. The most simplistic forms of collisions are elastic and inelastic collisions. In the elastic collisions we assume single large angle, hard sphere collisions occur. When we consider charged particles of thermal speeds, the collisions occur through the electric fields of the colliding particles. These long range interactions result in glancing blows. These small angle collisions have a greater effect on the velocity of a particle than on the

position. This makes the system significantly more difficult to handle analytically. The Fokker-Planck family of equations accounts for drag and/or diffusive effects on the particle velocity.

The introduction of collisions into the Vlasov system is an interesting problem. The distribution function is a fluid description of the plasma in so far as it is treated as a continuum. It is a fluid of sorts in phase space. The idea is that the collision operator introduces the first particle discreteness effects into the system. That is, that macroscopic variables fluctuate because of the random motion of the individual particles.

We begin by assuming a Markovian process, i.e., one whose probability density functions exhibit time dependence based on only their value at the previous time step. That is, they have a short memory. They only remember the most recent encounter. A non-Markovian process has a dependence on all previous experiences [Ris89]. We treat particle collisions as introducing Brownian motion in velocity space. The collisional description, then, shows the Brownian motion of an fluid element in the electron phase space distribution. The random Coulombic collisions which occur on the discrete particle scale cause friction and diffusion of the continuum in phase space.

Equation 2.26 shows the Fokker-Planck operator.

$$\left(\frac{\partial f}{\partial t}\right)_C = \nabla_v \cdot \left[\left\langle \frac{\Delta \mathbf{v}}{\Delta t} \right\rangle_s f_s\right] + \frac{1}{2}\nabla_v \nabla_v : \left[\left\langle \frac{\Delta \mathbf{v} \Delta \mathbf{v}}{\Delta t} \right\rangle_s f_s\right] \tag{2.26}$$

The first term, the dynamical friction vector, accounts for drag imposed by the collision in velocity space. The second term is the diffusion tensor. The Krook operator mentioned earlier accounts only for drag as in equation 2.27.

$$\left(\frac{\partial f}{\partial t}\right)_C = \nu f \tag{2.27}$$

Appendix C contains descriptions of these and other common forms for Coulomb collisions in a plasma including conservation properties.

Lenard and Bernstein [LB58] derived the modes of the plasma wave with a reduced Fokker-Planck type equation. By assuming a single dimension in space and velocity and a constant collision frequency, the Lenard-Bernstein operator is obtained (RHS of 2.28). This operator conserves particle number and momentum. The Maxwellian is the equilibrium distribution.

$$\frac{\partial f}{\partial t} + v\frac{\partial f}{\partial x} + \frac{qE}{m}\frac{\partial f}{\partial v} = \nu\frac{\partial}{\partial v}\left[vf + v_{th}^2\frac{\partial f}{\partial v}\right] \tag{2.28}$$

Here ν is the constant collision frequency. Lenard and Bernstein proceeded to solve the system by Fourier transforming in space and velocity and Laplace transforming in time. Ultimately they find that collisions introduce a damping term equal to the collision frequency. In the long wavelength limit, a modified Bohm-Gross dispersion relation is recovered. In the limit of $\nu \to 0$, collisional damping is a small perturbation to Landau damping.

$$\omega = \omega_p + \frac{3k^2v_{th}^2}{\omega_p} - i\nu \tag{2.29}$$

Turning our attention now to the behavior of the collisions at resonance, we see that the collision operator is a highly singular perturbation in the limit of weak collisions $\nu \to 0$. The result does not asymptote to the collisionless limit. This appears non-intuitive. The diffusive term in the operator is a dominant contributor in the resonance region. Asymptotic analysis identifies this type of problem as an interior-layer problem and prescribes a method for matching regions to obtain a complete and smooth solution.

2.5 Su and Oberman

V. I. Karpman [Kar67] and Su and Oberman [SO68] take the first steps to this solution by solving for the behavior near the resonance. Karpman treats it with a Green's function. Su and Oberman solve it using a boundary layer method. The

distribution is split into resonant and non-resonant parts. In the non-resonant regime, the collision operator reduces to a small perturbation which to zeroth order is ignored. This means that the collisions have no effect in the non-resonant regime when they are infrequent. In the resonant regime, this assumption cannot be made. There is a significant contribution from the collision operator. The second (or higher) order derivative multiplied by a small constant is the signature of a singular perturbation. The second order derivative oscillates dramatically as the distribution evolves.

Equation 2.30 is then solved for the distribution using a Laplace integral method frequently used in asymptotic methods [Hin91], [BO99]. The result is that the collisions damp the distribution at a rate of $exp(-\nu\omega_{pe}t^3)$. Typically, this solution is patched together with the solution for the non-resonant distribution [Sti92]. This result shows that in the limit of weak collisions, the damping in the resonance regime is more significant than the damping of the wave mode. It is interesting to note that Karpman states explicitly that Coulomb collisions very rapidly damp the singular solutions through diffusion. He goes on to comment on the work of BGK and notes that the inclusion of collisions, no matter how weak, eliminates the delta function from the continuous solution. Thus collisions have fundamentally altered the system. Until the work of Skiff, the consequences of this go unexplored.

$$\frac{\partial f_1}{\partial t} + v\frac{\partial f_1}{\partial x} + \frac{qE_1}{m}\frac{\partial f_0}{\partial v} = \nu v_{th}^2 \frac{\partial^2 f_1}{\partial v^2} \tag{2.30}$$

$$f_{1,res}(x,v,t) = f_{1,collisionless} exp(-\nu\omega_{pe}t^3) \tag{2.31}$$

Su and Oberman's result is used as the classic result for weak collisional effects on the particle distributions. However, there is a discrepancy between this result and the known result from Lenard and Bernstein for collisional effects on the collective behavior which has a νt behavior. Perhaps extending the asymptotic matching analysis to higher orders would reveal a more complete solution.

2.6 Collisional Eigenmodes: The NBS Set

As previously mentioned the measurements of Skiff et al. [SSMN+98] did not recover the Su and Oberman contribution which prompted Ng, Bhattacharjee, and Skiff (NBS [NBS99]) to search for the eigenmodes of the Vlasov-Poisson system with the full Lenard-Bernstein operator. A normalized Vlasov-Poisson system was Fourier transformed in space and time and then Hermite transformed in velocity space. Equation 2.32 shows the Hermite transform. The Hermite basis is implemented for velocity purpose for a few reasons. First, the Hermite polynomials have a wave-like structure. We will see in the next chapter that this is important for recovering velocity filamentation of the distributions due to ballistic particle motion. Second, their recursion relations reduce the collision operator to a single term. This makes the system much easier to solve than, for instance, Fourier transforming in velocity.

$$f_1(v) = \sum_{n=0}^{\infty} a_n(\Omega) H_n(v) e^{-v^2} \tag{2.32}$$

$$\begin{aligned} a_1 &= \sqrt{2}\Omega a_0 \\ a_2 &= (\Omega + i\mu)a_1 - \frac{1+\alpha}{\sqrt{2}} a_0 \\ a_{n+1} &= \sqrt{\frac{2}{n+1}} \left((i\mu n + \Omega) a_n - \sqrt{\frac{n}{2}} a_{n-1} \right) \quad n \geq 2 \end{aligned} \tag{2.33}$$

A recursion relation was found for the distributions, equation 2.33. See appendix C.7 for a full derivation. Numerical analysis of the recursion relation recovered a discrete spectrum of modes, hereafter called the NBS modes, in the complex plane. Figure 2-1 was taken from [NBS99] and shows the eigenmodes in the complex wavenumber plane. The behavior is analogous for solutions to the temporal problem. There are two branches of modes. One diverges along the imaginary axis. These modes decay very quickly. The other branch approaches the Landau roots in the limit of zero collisions.

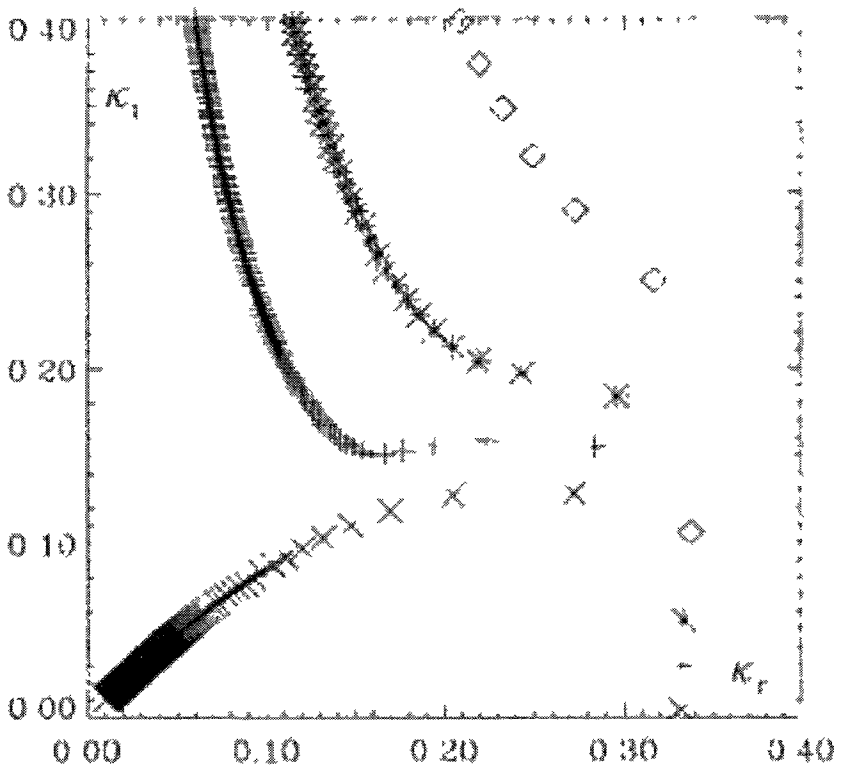

Eigenvalues on the complex κ plane for the spatial evolution problem with $\alpha = 1.6$. ($\diamond$) $\mu = 0.1$, ($*$) $\mu = 0.05$; (·) $\mu = 0.025$, (∘) Landau roots ($\mu = 0$).

Figure 2-1: NBS Eigenmodes in the Complex k-Plane
The eigenmodes published by NBS in [NBS99]. Here $\alpha = (1/k\lambda_{De})^2$ and $\mu = \nu/(\sqrt{2}k\lambda_{De}v_{th})$.

$$\omega_i = \gamma + i\nu \tag{2.34}$$

The least damped of these modes obeys equation 2.34, where γ is the Landau damping rate. This is consistent with the findings of Lenard and Bernstein in the limit of long wavelengths.

Figure 2-2 shows a least-damped NBS eigenfunction for a temporally damped collisional plasma wave. The function itself is complex and both parts contain interior

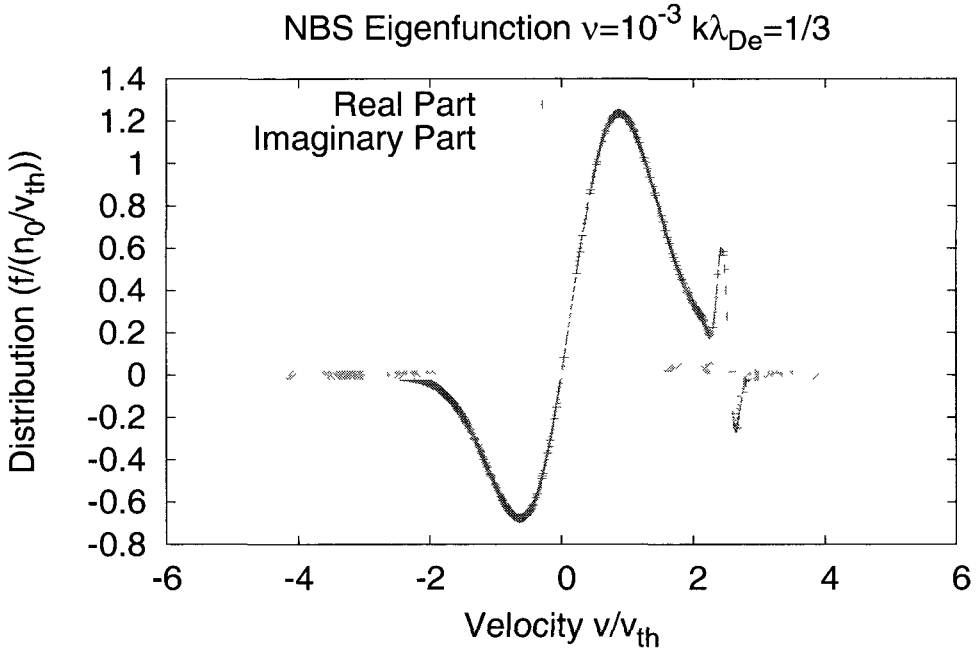

Figure 2-2: NBS Eigenfunction for $\nu = .001\sqrt{2}kv_{th}$
This is the eigenfunction for the least damped NBS eigenmode for $k = 1/3$. Note the layer at $v/v_{th} \approx 2.5$.

layer structures as described in the previous section. To construct a physical function out of this complex one, the real part must be taken.

In the collisional case, the Landau damping behavior is inherent in the modes of the

distribution. This is in contrast to the collisionless case where Landau damping is a long-time behavior due to phase mixing. It should be noted that while the spectrum change is significant, the long time behavior of the system is only modified by a perturbation to the damping rate, $-\nu$. A system will settle to a single eigenmode in the long time limit and the The NBS analysis shows that the least damped collisional eigenmode contains the information on the collisionaly modified Landau damped solution.

This work calls into question the result of Su and Oberman. Their treatment of the distribution indicates that their model is implicitly dependent on the continuous spectrum. Since they do not recover the discrete nature of the modes, something is missing from their model to explain the complete behavior, unless the $\exp(-\nu t^3)$ behavior could arise from a sum of exponentially decaying terms which are now recovered by multiple approaches.

Shortly after the NBS paper, Short and Simon [SS02] argued that the NBS modes are sufficient to describe the collective behavior only. They show that there are two branches of the spectrum, one which describes the collective motion of the particles and one which describes the motion of the free-streaming particles. They also recover the Su and Oberman damping rate and comment that it is not necessary to assume the continuous spectrum to recover it. Since then, the NBS modes were shown to form a complete set [NBS04]. They argue that since the distribution is the more fundamental than the collective behavior, i.e., electric field, the distribution modes are the true complete eigenmodes of the system. For the Lenard-Bernstein system, these modes are the NBS modes.

These modes should also be able to describe nonlinear phenomena based on linear interactions such as the plasma wave echo. The work of Su and Oberman was done in the context of the plasma wave echo, although the analysis is for a first order response

Theory	System	Transforms	Solve	Result
Case-Van Kampen	no collisions	Fourier x,t	f	continuous spectrum modes of f
Landau	no collisions	Fourier x Laplace t	ϵ	discrete spectrum modes of ϵ
Lenard and Bernstein	LB collisions	Fourier x,v Laplace t	$f(\epsilon)$	discrete spectrum modes of ϵ
NBS	LB collisions	Fourier x,t Hermite v	f	discrete spectrum modes of f
Su and Oberman	LB collisions at resonance	Fourier x,t dom. bal. v	f	long time limit

Table 2.1: Electrostatic Modes
Here are the Vlasov-Poisson electrostatic mode theories for the collisionless and collisional systems in a map. Also included is the work of Su and Oberman who do not find modes, but rather predict the long time behavior using the dominant balance method.

to a single perturbation. If it is indeed a natural behavior of the plasma, it should be recoverable through numerical experiments on the collisional Vlasov-Poisson system. This has motivated the following work on the plasma wave echo and will be examined further in future chapters.

2.7 Conclusion

Here we have derived the wave modes and the eigenmodes, those of the distribution, for the collisionless and collisional Vlasov-Poisson systems. We have shown that in the collisionless plasma the eigenmodes are continuous and collective behavior, such as the electric field and Landau damping of the field, comes about through interference of these modes. In the collisional system, the complete set of eigenmodes was found by NBS to be discrete and to recover the damping rate of Lenard and Bernstein. This calls into question the regime of validity for the Su and Oberman solution. Their work was written to be applied to the plasma wave echo and was subsequently carried out by O'Neil [O'N68]. Numerical studies of the plasma wave echo are carried out in the

following chapters to examine the real behavior of these equations with and without collisions.

The mode structures examined here are also of importance to the ion acoustic part of this thesis. Collisional impacts on the ion acoustic wave are analogous to those of the plasma wave. The collisional two-species Vlasov-Poisson system is even harder to solve analytically than the single species system for the plasma wave. We are fortunate, then to be guided by the work presented thus far. In the ion acoustic chapters we will discuss how the wave-particle resonances are effected by collisions and what it implies for the nonlinear regime.

CHAPTER 3

Kinetic code

The numerical approach used in this work permits an examination of the analytical estimates made on the Vlasov-Poisson system. We are able to test nonlinear predictions that are difficult to verify with real life experiments. To carry out the kinetic studies of collisional effects in an electrostatic plasma, we make use of a Vlasov-Poisson simulation code called the Kinetic Code. Vlasov solvers are a unique class of codes that solve for particle distribution evolution using numerical fluid methods rather than solving for individual particles as particle tracing or particle-in-cell (PIC) codes do. Representing a continuum in the discrete format of the computer introduces its own challenges. But, PIC and cloud in cell (CIC) codes are inherently noisy and this can disrupt the fine structures that develop in time and phase space. Vlasov solvers can resolve these structures [SH98], but require significant computational resources to run in multiple dimensions. A single spatial dimension is sufficient to examine the physics of the electrostatic waves and is implemented here. Velocity resolution has typically been the stumbling block for such methods. In the code described here, we take advantage of parallelization to implement very high velocity resolution.

The Kinetic Code was written by Kai Germaschewski in C language and loosely based on a Hermite spectral method presented in Schumer and Holloway [SH98] for velocity dependance of the distributions. This collisionless, electron code (single species with a stationary ionic background) was modified to include Lenard-Bernstein collisions and a second species (ions) for the study of the ion acoustic instability.

In section 3.1 we give an overview of what the Kinetic Code solves. Section 3.2 gives a detailed description of how the code solves the Vlasov-Poisson system. Section 3.3 shows benchmarks of the code for the collisionless Langmuir waves. Section 3.4 contains benchmarks of the code for the collisional plasma wave modes. A study of the NBS eigenfunction behavior in the code was made is section 3.4.1. Finally, in the conclusion 3.5 we discuss future plans for development of the Kinetic Code.

3.1 Code Description

The main purpose of the Kinetic Code is to evolve the particle distribution according to the Vlasov-Poisson system of equations. This nonlinear, parallel code was written for a single particle species in one spatial dimension, one velocity dimension and in time. The basic operation is as follows. The simulation is initialized with a perturbation to the distribution function. The electric field is then calculated from Poisson's equation. This is inserted into Vlasov's equation which is used to find the change to the distribution function over some time interval. This process is repeated until some chosen time to end the simulation.

The first version of the code for the plasma wave studies used a non-dimensional version of the Vlasov-Poisson system. Space is scaled by electron Debye length, λ_{De} and time by inverse electron plasma frequency, ω_{pe}^{-1}. The Vlasov and Poisson equations are also scaled by electron mass, m_e, charge, q_e, and particle number density, n_0.

$$\frac{\partial f}{\partial t} + v\frac{\partial f}{\partial x} + \frac{qE}{m}\frac{\partial f}{\partial v} = 0 \tag{3.1}$$

$$\nabla \cdot E = \frac{q}{\epsilon_o}\int_{-\infty}^{\infty} f(v)\partial v \tag{3.2}$$

The normalizations are given in equations 3.3 - 3.5.

$$t = \frac{t'}{\omega_p} \qquad x = \lambda_D x' \tag{3.3}$$

$$v = v_{th} v' \qquad f = \frac{n_0}{v_{th}} f' \tag{3.4}$$

$$E = \frac{e n_0 \lambda_D}{\epsilon_o} E' \tag{3.5}$$

The system in its non-dimensional form is seen in equations 3.6 and 3.7.

$$\frac{\partial f'}{\partial t'} + v' \frac{\partial f'}{\partial x'} + E' \frac{\partial f'}{\partial v'} = 0 \tag{3.6}$$

$$\nabla' \cdot E' = \int_{-\infty}^{\infty} f'(v') dv' \tag{3.7}$$

The distribution in its non-dimensional form is very easy to transform to the Hermite basis as is explained later. Note here that $v_{th,e} = \sqrt{(k_B T_e / m_e)}$.

$$f_0(x, v) = \frac{n_0}{\sqrt{2\pi} v_{th}} e^{-\left(\frac{v}{2 v_{th}}\right)^2} \tag{3.8}$$

$$f_0(x, v) = \frac{n_0 f'}{v_{th}} \tag{3.9}$$

$$f' = \frac{e^{-\left(\frac{v}{\sqrt{2} v_{th}}\right)^2}}{\sqrt{2\pi}} \tag{3.10}$$

Boundary conditions are set for the distribution in space and velocity in accordance with the physical system. Periodic boundary conditions are applied to the single spatial dimension to approximate an infinite system. This is sufficient for studies of generic electrostatic waves. Box and grid sizing must be chosen carefully so as to appropriately resolve the details of the distribution while maximizing efficiency of resources. The box needs to be at least as large as the longest wavelength studied. The grid spacing should be at least $1/16^{th}$ of the smallest wavelength desired, if not smaller. Grid cells are indexed from 0 to $N_x - 1$, where $N_x = L_x / \Delta x$.

The distribution approaches zero exponentially as $v \to \infty$. To capture this, velocity space it must be several times the thermal velocity. A Hermite spectral scheme

was implemented with a velocity scale, U, as in Schumer and Holloway [SH98]. The Hermite spectral values are not usually on the same scale as the physical system being modeled. To ensure that there is appropriate resolution, the spectral velocities, $v_{hermite}$, are scaled to the system velocities, u_{system} so that $u_{system} = v_{hermite}U$. In the non-dimensional form of Vlasov-Poisson for the plasma wave, $U < 1$.

In general, a very high order Hermite polynomial (i.e., $N_v = 20000$ or higher) was chosen for the velocity spectrum. The spectral values (i.e., where the Hermite polynomial equals zero) are not equi-spaced, which imposes a nonuniform grid on velocity space. The spectral grid is symmetric about zero and there is higher resolution near the origin than at the bounds. The number spectral velocities is given by the number (order) of the Hermite polynomial. The odd numbered Hermite polynomials have odd numbers of a spectral velocities including one of zero. The even numbered polynomials have spectral values symmetric about zero only. We have chosen to implement the even numbered Hermite spectrum in the code for simplicity of counts in the code.

The code uses MPI to run on multiple nodes. As we require very high velocity resolution to run experiments such as the plasma wave echo, we have chosen to parallelize with respect to velocity. The velocity grid is divided up among the processors. Each one calculates the Vlasov-Poisson system for its local space. Some calculations require information from grid cells not stored on that processor. In this case, it reads from ghost cells which contain the necessary information. A typical run operates optimally on 16-64 processors for 2-3 days, depending on system parameters.

3.2 Simulation Model

What follows here is a description of the implemented schemes for space, time, and velocity evolution. We begin with the equilibrium distribution being the Maxwellian.

To initialize the system, the equilibrium must be perturbed.

$$f_0(x, v, t = 0) = \frac{n_0}{\sqrt{2\pi} v_{th}} e^{-\left(\frac{v}{\sqrt{2} v_{th}}\right)^2} \tag{3.11}$$

Perturbations to the distribution, f_1, for both collisional and collisionless trials are given a generic functional form seen in equation (3.12) and in figure 3-1

$$f_1(x, v) = \frac{sin(kx)}{\sqrt{2\pi} v_{th}} e^{-\frac{v^2}{2 v_{th}^2}}. \tag{3.12}$$

The total initial condition is $f = f_0 + \alpha f_1$. The perturbation size which determines the linearity of the system is set by α. For α on the order of 10^{-3} or less, the system is very linear. For larger values, $\alpha \sim 10^{-2}$, trapping effects become increasingly prevalent.

The electron equilibrium distribution was chosen to be the Maxwell-Boltzmann distribution while the cold, stationary ions are given by a delta function.

$$f_{ion}(v, t = 0) = \frac{n_0}{\sqrt{2\pi}} \delta(v) \tag{3.13}$$

This gives a background field of zero. The perturbed distribution leads to the perturbed electric field, $E^{(1)}$, through Poisson's equation. The electric field properties are evaluated for comparison with theory.

$$\frac{dE^{(1)}}{dx} = \frac{1}{\epsilon_o} \int_{-\infty}^{\infty} (q_i f_i^{(1)}(v) + q_e f_e^{(1)}(v)) dv \tag{3.14}$$

$$E^{(1)}(x) = \frac{e}{\epsilon_o} \int \int_{-\infty}^{\infty} (f_i^{(1)}(v, x') - f_e^{(1)}(v, x')) dv dx' \tag{3.15}$$

The plasma wave is excited when ions are cold, stationary and unperturbed, ions and the electrons are Maxwellian and nondrifting, and the electric field is given by:

$$E^{(1)}(x) = \frac{e n_0}{\epsilon_o} \int \int_{-\infty}^{\infty} \left(\frac{\delta(v)}{\sqrt{2\pi}} - \frac{\alpha_e e^{-\left(\frac{v}{\sqrt{2} v_{th,e}}\right)^2}}{\sqrt{2\pi} v_{th,e}} sin(kx) \right) dv dx' \tag{3.16}$$

$$= \frac{e n_0}{\epsilon_0 k} (1 - \alpha_e cos(kx)) \tag{3.17}$$

For thermal, nondrifting ions and electrons, which gives ion acoustic waves, the electric field is:

$$E(x) = \frac{-q}{\epsilon_0 k}\frac{n_0}{\sqrt{2\pi}}cos(kx)\int_{-\infty}^{\infty}\left(\alpha_i\frac{e^{-\left(\frac{v}{\sqrt{2}v_{th,i}}\right)^2}}{v_{th,i}} - \frac{\alpha_e e^{-\left(\frac{v}{\sqrt{2}v_{th,e}}\right)^2}}{v_{th,e}}\right)dv \tag{3.18}$$

$$= \frac{en_0}{\epsilon_0 k}cos(kx)(\alpha_i - \alpha_e) \tag{3.19}$$

The current driven ion acoustic wave is stimulated by thermal, nondrifting ions and drifting electrons. The initial electric field is the same. Note that the initial field does not carry temperature dependance and that it is the same as the ion acoustic wave.

$$E(x) = \frac{e}{\epsilon_0 k}\frac{n_0}{\sqrt{2\pi}}cos(kx)\int_{-\infty}^{\infty}\left(\alpha_i\frac{e^{-\left(\frac{v}{\sqrt{2}v_{th,i}}\right)^2}}{v_{th,i}} - \frac{\alpha_e e^{-\left(\frac{v-v_{drift,e}}{\sqrt{2}v_{th,e}}\right)^2}}{v_{th,e}}\right)dv \tag{3.20}$$

$$= \frac{en_0}{\epsilon_0 k}cos(kx)(\alpha_i - \alpha_e) \tag{3.21}$$

When applying a spectrum of waves as the initial condition, the electric field for the current driven ion acoustic wave is given as follows.

$$E(x) = \sum_n \frac{en_0}{\epsilon_0\sqrt{2\pi}}\int_{-\infty}^{\infty}\int_{-\infty}^{\infty}\left(\frac{\alpha_i}{v_{th,i}}e^{-\frac{v^2}{2v_{th,i}^2}} - \frac{\alpha_e}{v_{th,e}}e^{-\frac{(v-v_{d,e})^2}{2v_{th,e}^2}}\right)sin(k_n x)dvdx \tag{3.22}$$

$$= \sum_n \frac{en_0(\alpha_e - \alpha_i)}{\epsilon_0}\frac{cos(k_n x)}{k_n} \tag{3.23}$$

$$= \sum_n E_n cos(k_n x) \tag{3.24}$$

Each of these cases are used in the data presented in this work.

3.2.1 Hermite Spectrum

The Hermite polynomials contain a natural oscillation making them easier to fit to certain systems than sums of sines and cosines. Here the orthonormal properties are exploited as well, but the distribution function needs to be renormalized and the

Hermite polynomials need to be implemented in their orthonormal form.

$$\int_{-\infty}^{\infty} H^m(v)H_n(v)e^{-v^2}dv = 2^n\pi n!\delta_n^m \tag{3.25}$$

$$f(v) = \sum_n c_n\psi_n(v) \tag{3.26}$$

The symmetric Hermite basis is given in equation 3.27 .

$$\psi_n(v) = \psi^n(v) = a_nH_n(v)e^{-v^2/2} \tag{3.27}$$

One of barriers to high resolution in the Hermite spectral scheme lies in the Hermite transform. For large values of velocity, the Hermite polynomials explode and the exponential term drops rapidly to zero. It is difficult, then, to obtain real numbers at large velocity values. This is mitigated somewhat by carrying the exponential through the transform as is done for the symmetrically weighted basis. For comparison, the antisymmetric basis is given by equation 3.28.

$$\psi_n(v) = a_nH_n(v),\ \psi^n(v) = a_nH_n(v)e^{-v^2}, \tag{3.28}$$

Regardless of the the symmetry of the basis the coefficients, a_n, are the same.

$$a_n = \frac{1}{\sqrt{2^n\pi n!}} \tag{3.29}$$

Note that the orthonormality condition holds.

$$\int_{-\infty}^{\infty} \psi^m(v)\psi_n(v)dv = \delta_n^m \tag{3.30}$$

The symmetric form of the Hermite recursion relations are given as follows:

$$v\psi^n(v) = \sqrt{\frac{n+1}{2}}\psi^{n+1} + \sqrt{\frac{n}{2}}\psi^{n-1}(v) \tag{3.31}$$

$$\frac{d}{dv}\psi^n(v) = -\sqrt{\frac{n+1}{2}}\psi^{n+1} + \sqrt{\frac{n}{2}}\psi^{n-1}(v) \tag{3.32}$$

The Hermite polynomial values are calculated from a recursion relation which we extend to the distribution function here.

$$\psi_0 = e^{-\frac{v^2}{2}} \tag{3.33}$$

$$\psi_1 = \sqrt{2}ve^{-\frac{v^2}{2}} \tag{3.34}$$

$$\psi_n = \sqrt{\frac{2}{n}}\psi_{n-1} - \sqrt{\frac{n-1}{n}}\psi_{n-2} \tag{3.35}$$

We have explored the basic tools that are implemented in the code. Now we discuss in detail the processes that use them. When the code is initialized, the phase space grid is calculated. The spatial grid is simple because it is uniform and calculated from a predetermined interval. The velocity grid is found by locating the spectral velocities. This routine and the others for calculating the initial hermite coefficients are found in Fortran Routines for Spectral Methods [Fun93]. These methods rely on the relation between the Hermite polynomials and the Laguerre polynomials. The Laguerre spectral velocities are located using a Newton's Methosd. As it turns out, this process can be quite time consuming for large order polynomials. We limit the order of the polynomial to $N_v = 1024$. This provides sufficient resolution to initialize the distribution.

Once these values have been located, the distribution is calculated. The velocity boundary condition is applied at this point as well. The spectral velocities are symmetric about $v = 0$. The $f(\pm v_{max}) = 0$ condition is applied at the $n_v = 0$ and $n_v = 1024$ locations. After this, the distribution is Hermite transformed and allowed to evolve through a much larger velocity space, typically, $N_v \geq 20000$.

The Hermite transform itself consists of calculating the coefficients, c_n, for the expansion. Note that here the velocity is the scaled velocity. Begin by calculating the weights of the Hermite polynomials. The discrete analog of the velocity integral

is given by equation 3.36.

$$\int_{-\infty}^{\infty} f(v)dv \approx \sum_{i=0}^{N} w_i^n f(\xi_i^N) \tag{3.36}$$

The weights are given by:

$$w_i = \frac{\sqrt{\pi}}{N}[\tilde{H}_{N-1}(xi_i^N)] \tag{3.37}$$

Now the coefficients can be calculated.

$$c_n = \frac{1}{2^n n!\sqrt{\pi}} \int_{-\infty}^{\infty} f(v)H_n(v)e^{-v^2}dv \tag{3.38}$$

$$\approx \frac{1}{\pi^{1/4}} \sum_{i=0}^{N-1} f(\xi^N)\tilde{H}_n(\xi_i^N)w_i^N \tag{3.39}$$

These coefficients, c_n, are calculated for each point in space and are then advanced in the Vlasov equation using the recursion relations for velocity evolution and the finite difference methods for spatial evolution. This is examined in the next section.

$$f(v,x) = \sum_{n=0}^{\infty} c_n\psi_n(v_{us})e^{-v_{us}^2/2} \tag{3.40}$$

$$= \sum_{n=0}^{\infty} c_n(x)a_n H_n(v_{us})e^{-v_{us}^2/2} \tag{3.41}$$

The inverse Hermite transform is only used for generating the phase space distribution data. This is fortunate because it runs into numerical limitations. The inverse transform is simply a summation of all polynomials at each velocity as seen in equation 3.41. However, the exponential term seen here carries the unscaled velocity. All of the scaling information is stored in the coefficients, c_n. This limits the value of the maximum velocity for which the computer will return a real number. Any input larger than this number yields an output of infinity or not-a-number. The maximum usable velocity is obtained from the $N_v = 1024$ polynomial. This limits the output region to approximately $(-7v_{th,e}, 7v_{th,e})$.

3.2.2 Spatial Scheme

A finite (central) difference scheme is used to spatially evolve the distribution. It is just a difference of a function over the point of interest. This is seen in the following equation. The only term in the Vlasov equation that uses this is the second one, $v\frac{\partial f}{\partial x}$.

$$\frac{\partial f(n_x)}{\partial x} = \frac{f(n_x+1) - f(n_x-1)}{2\Delta x} \tag{3.42}$$

$$\tag{3.43}$$

The spatial bounds are calculated in a simple manner.

$$f(n_x = 0) = f(n_x = N_x) \tag{3.44}$$

Where it is necessary to calculate gradients across the boundary, use the following. Note that the count starts at $n_x = 0$.

$$\frac{df(n_x = N_x)}{dx} = \frac{f(n_x = N_x - 1) - f(n_x = 0)}{2\Delta x} \tag{3.45}$$

3.2.3 Explicit Time Stepping

For each time step the following steps are taken.

$$f(t + \Delta t) = f(t) + \Delta f \tag{3.46}$$

$$\Delta f = \left[-v\frac{\partial f(t)}{\partial x} - \frac{qE(t)}{m}\frac{\partial f(t)}{\partial v}\right]\Delta st \tag{3.47}$$

First, the $v\frac{\partial f}{\partial x}$ term is calculated at $f(t)$. This term is written in the code as the finite difference scheme shown above combined with the Hermite recursion relation for vf given in equation 3.31. Next Poisson's equation is solved for the electric field, $E(t)$, and multiplied by $\frac{\partial f(t)}{\partial v}$. Each term in Vlasov's equation is summed and multiplied by the time interval. It is then added to the existing distribution.

Each time step is split into two pieces. For example, the spatial term is advanced in two successive steps each of size $\Delta t/2$. First the ΔX term is calculated at time,

t, as described above. This is multiplied by half the time interval and then added to the distribution as seen below. The new distribution is then used to calculate a new ΔX which is then added to the initial distribution.

$$\Delta X(t) = v\frac{\Delta f(t)}{\Delta x} \tag{3.48}$$

$$f(t + \frac{\Delta t}{2}) = f(t) + \Delta X(t)\frac{\Delta t}{2} \tag{3.49}$$

$$\Delta(t + \frac{\Delta t}{2})X = v\frac{\Delta f(t + \frac{\Delta t}{2})}{\Delta x} \tag{3.50}$$

$$f(t + \Delta t) = f(t) + \Delta X(t + \frac{\Delta t}{2}))\Delta t \tag{3.51}$$

Poisson's equation is solved next for the electric field. First, the density is calculated by performing a velocity integral over the distributions. This is accomplished by summing the over the Hermite coefficients with corresponding weightings as in equation 3.36. Only the $n = 0$ term survives the integration (summation). A tridiagonal matrix is solved for the potential, Φ. The spatial gradient yields the electric field. The velocity gradient term exploits the hermite recursion relation. As does the collision operator.

$$\frac{qE(x,t_a)}{m}\frac{\partial f(x,v,t_a)}{\partial v} = \sum_{j_v=0}^{N_v-1}\frac{eE}{U\sqrt{2}m}\left(\sqrt{j_v+1}f(x,j_v+1) - \sqrt{j_v}f(x,j_v-1)\right) \tag{3.52}$$

3.2.4 CFL Condition

The Courant-Freidrichs-Levy (CFL) [CFL67] condition is a necessary condition for stability of partial differential equations solved by explicit time stepping. It basically says that the simulation time step must be less that the time it takes for a wave to travel from one grid point to the next. The value of C depends on the scheme being used, the equation being solved, and is on the order of 1.

$$\frac{u\Delta t}{\Delta x} \leq C \tag{3.53}$$

Here, u is the speed of the fastest moving particle, Δx is the spatial grid size and Δt is the time step. If the CFL condition has not been met, it is quite obvious in the simulation data. The collective properties (electric field and particle densities) grow explosively. This condition is easily met.

3.2.5 Filamentation:Velocity Convergence

All Vlasov solvers are limited numerically by velocity space filamentation of the distribution functions. Velocity shearing of the phase space distributions is a natural consequence of the free-streaming particles. This behavior is modeled by the first two terms of the Vlasov equation, the ballistic terms. This is discussed further with the collisional plasma wave echo in section 4.4. Klimas [Kli87] also gives a detailed discussion. The concept may be illustrated as follows. We begin at $t = 0$ with a

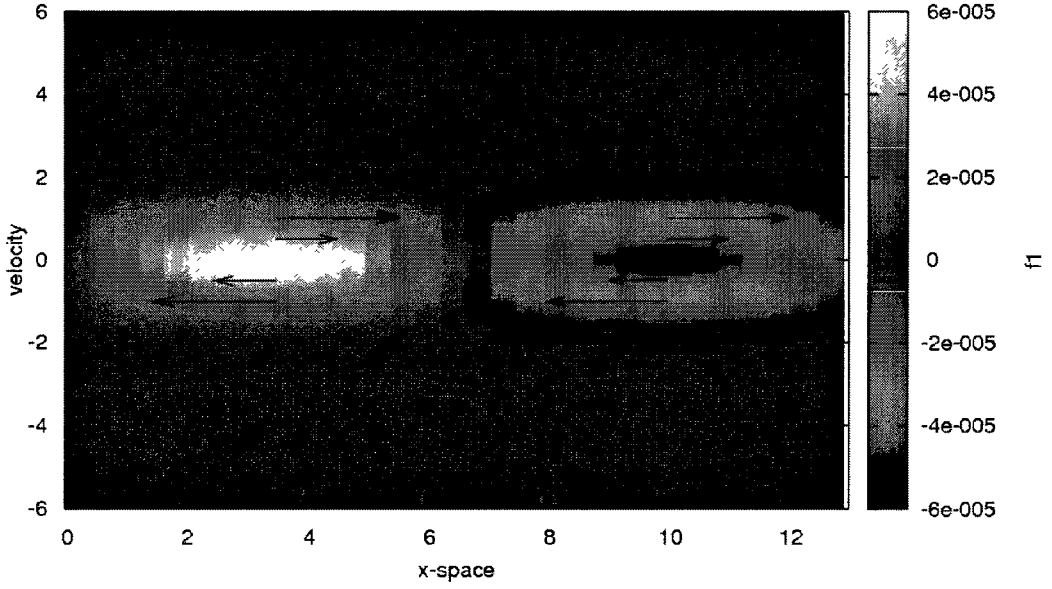

Figure 3-1: Filamentation in phase space at $t\omega_{pe} = 0$
A typical sine wave perturbation to the code, f_1, at $t = 0$ in phase space. The initial perturbation will shear in velocity space as indicated by the arrows.

distribution of a generic type as in eq. (3.12) and seen in Fig.(3-1). At some later

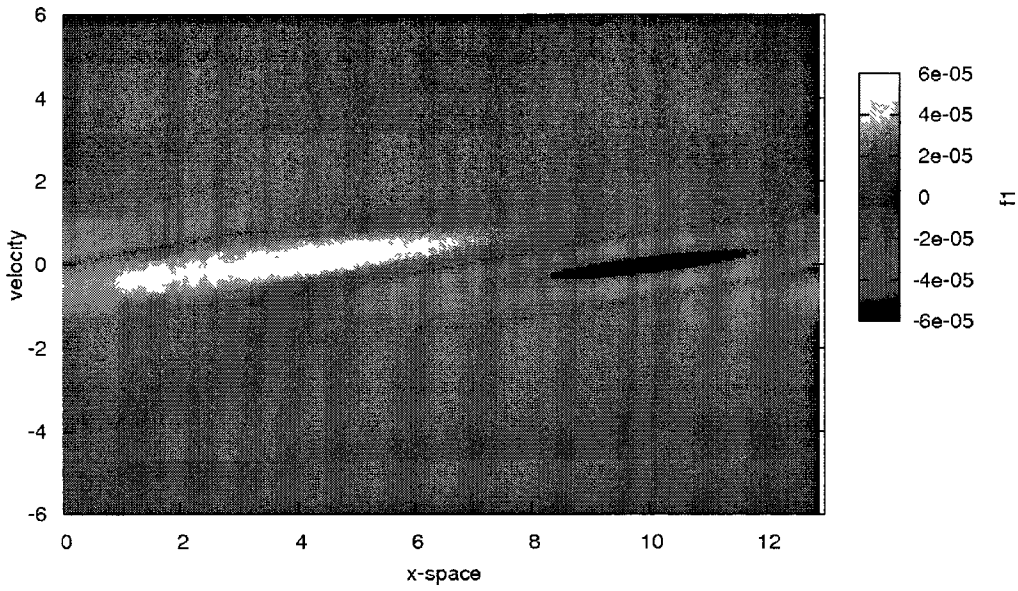

Figure 3-2: Filamentation in phase space at $t\omega_{pe} = 4$
At some later time, $t\omega_{pe} = 4$, the filaments are beginning to form. Note the dark blue creeping in from left of the graph for v > 0. The periodic boundary condition aids in 'looping' the distribution around in space.

time, particles with large velocities will have moved further in space than those with smaller velocities, Fig. (3-2). As time increases, these filaments become increasingly finer (Fig.(3-3)). It is here that we can see how useful the Hermite spectral method is. The natural oscillations in the Hermite polynomials are easily fit to the filamentation of the distribution.

At some point, the filament widths become smaller than the velocity grid size. It is here that we encounter a phenomenon called recurrence. A more convenient way to view this is in the transformed velocity space. At $t = 0$, the perturbation is launched at the beginning of Hermite space. As time advances, the perturbation moves through the space eventually reaching the end. At recursion time, the perturbation reverses its direction. Remnants of the perturbation traveling in both directions will interfere causing an artificial growth in the electric field. See figure 3-4. Once recursion time has been identified, we are sure to end the simulations well before it.

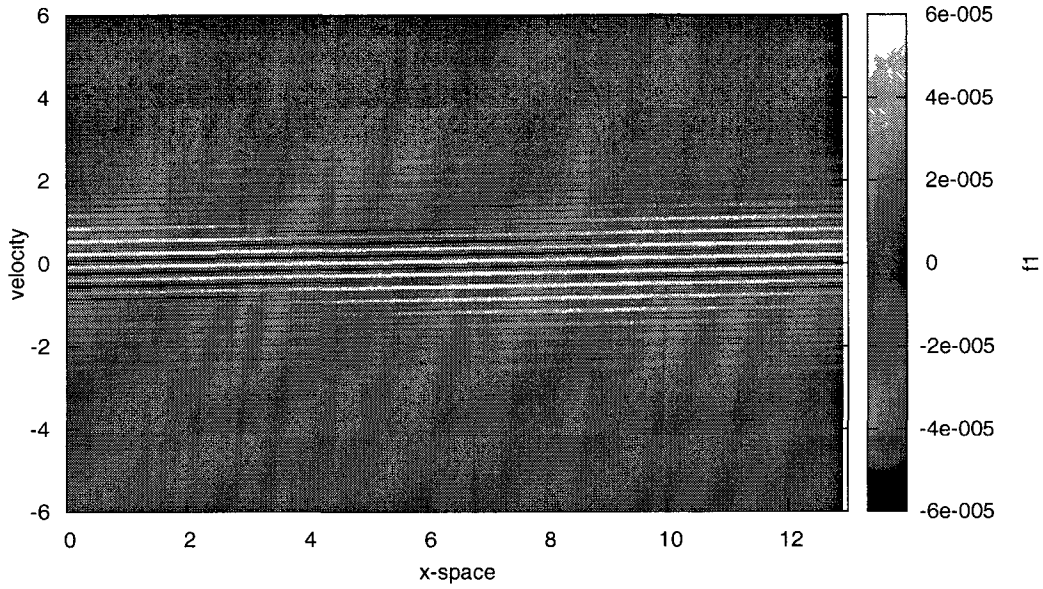

Figure 3-3: Filamentation in phase space at $t\omega_{pe} = 40$
At $t\omega_{pe} = 40$ many filaments have developed.

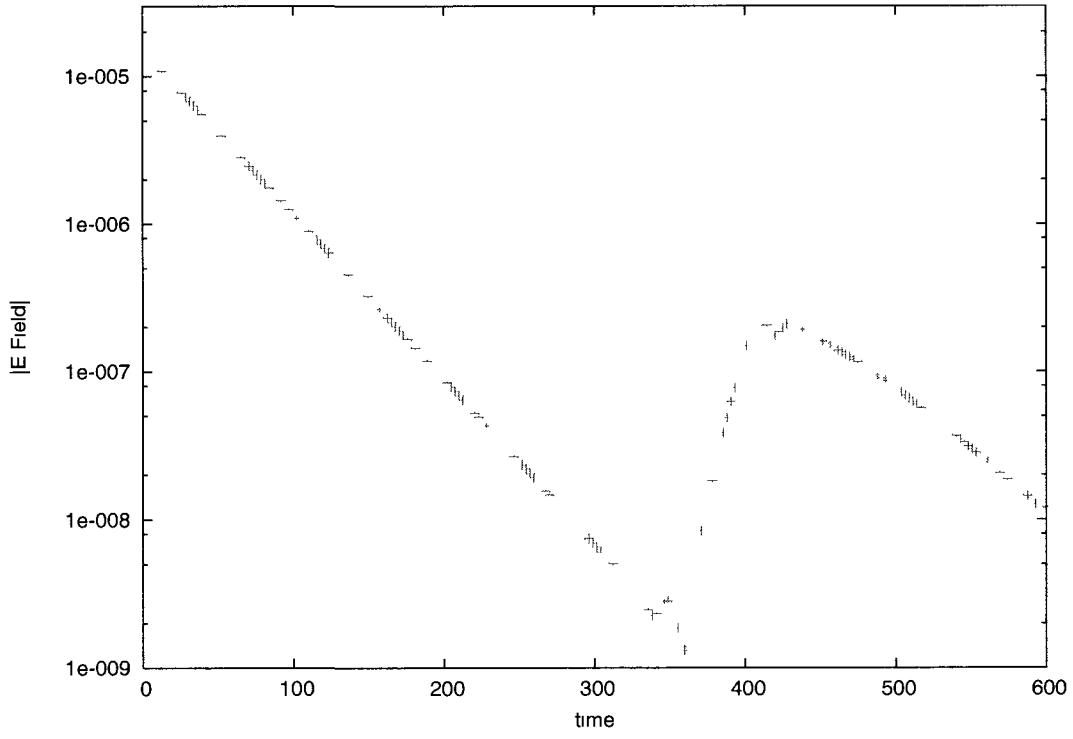

Figure 3-4: Recursion effect in the electric field
The growth in the electric field at $t\omega_{pe} = 400$ is due to recursion. This particular case was for 512 Hermite modes.

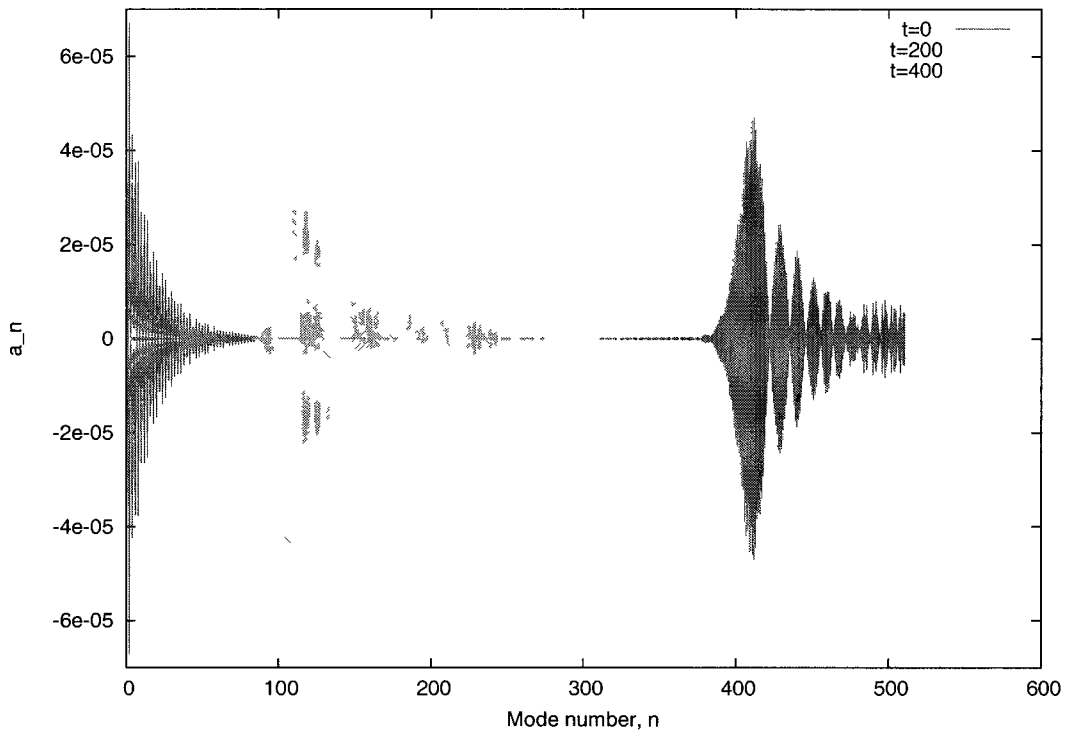

Figure 3-5: Recursion effect in Hermite space
A symmetrically weighted Hermite space representation of recursion. At $t = 0$, the perturbation (in red) is located at the beginning of the Hermite space. At $t\omega_{pe} = 200$ (in green), the perturbation has moved in the space. Note the small bump in front of the large peak. At $t\omega_{pe} = 400$ (in blue), this small bump has been reflected. The interference of these reflected parts with the forward moving components is responsible for the growth of the electric field as seen in fig. 3-4.

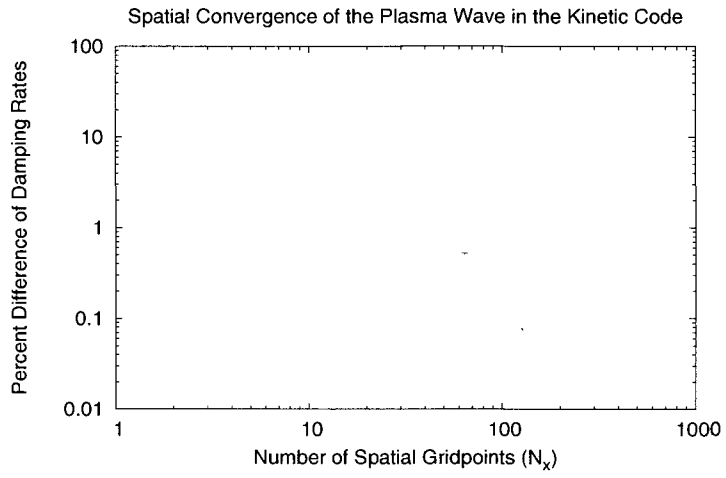

Figure 3-6: Spatial convergence of the Langmuir wave
Spatial Convergence of the simulation. For $k\lambda_D = 1/3$, the electric field damping rate at the maximum is compared with the damping rate from the converged result ($N_x = 256$). As the number of points in the spatial domain increases, the error drops quadratically.

The recursion time is estimated by Schumer and Holloway [SH98] as seen in eq 3.54. Here k is the wavenumber of the excited wave and U is the velocity scale factor.

$$\tau_{recur} \sim \frac{\pi\sqrt{N_v}}{kU} \tag{3.54}$$

We find that once velocity space convergence has been reached, i.e., that the amplitudes of the electric field no longer vary with decreased velocity interval, increased velocity resolution can extend the validity of the simulation in time.

3.2.6 Spatial Convergence

Because the code is parallel in velocity space only, increased spatial resolution requires much more processing time than increased velocity resolution. Spatial convergence at a converged velocity setting is shown here. Fig. 3-6 shows that the damping rate of the maximum electric field converges to the theory as the spatial resolution increases.

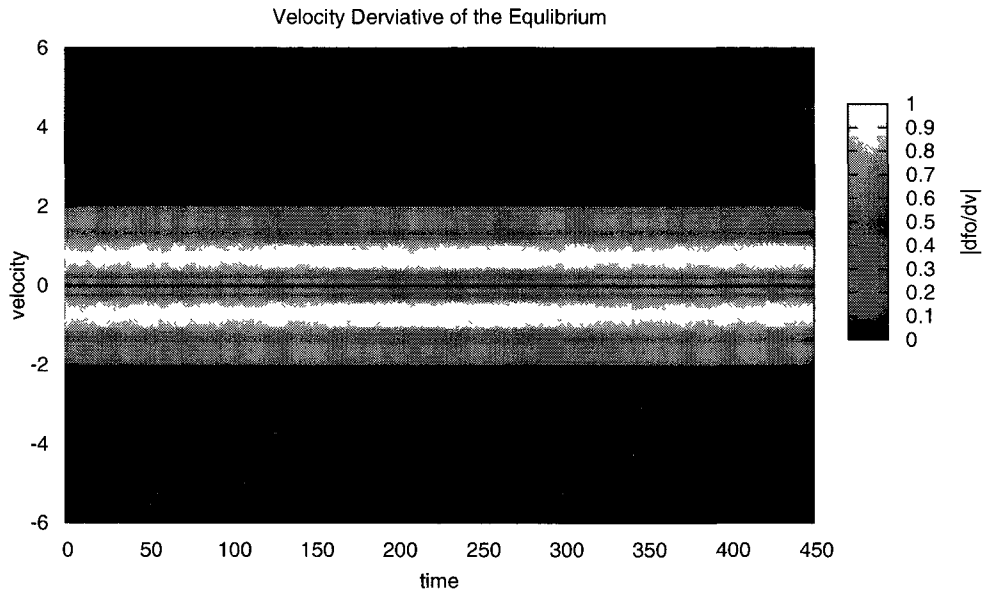

Figure 3-7: The velocity derivative of f_0 in time
The velocity derivative of the equilibrium distribution as function of time. This is always much larger than the velocity derivative of the perturbation (Fig.(3-8))

3.2.7 Linearity

The linearity condition is tested here on trials of a generic perturbation. This is a check that the modes recovered from the code will agree with those from theory.

$$\left|\frac{\partial f_0}{\partial v}\right| \gg \left|\frac{\partial f_1}{\partial v}\right| \tag{3.55}$$

Derivatives in velocity of the perturbation become large as time advances due to filamentation. However, the amplitudes remain small when compared to the equilibrium derivative. This is seen in figures 3-7 and 3-8

3.3 Collisionless Benchmark: Langmuir wave

The collisionless regime was benchmarked with roots of the plasma dispersion relation (fig. 3-9) found from a numerical plasma dispersion function solver written by C. S. Ng in Fortran 77. It is referred to in this document as the Plasma Dispersion Function

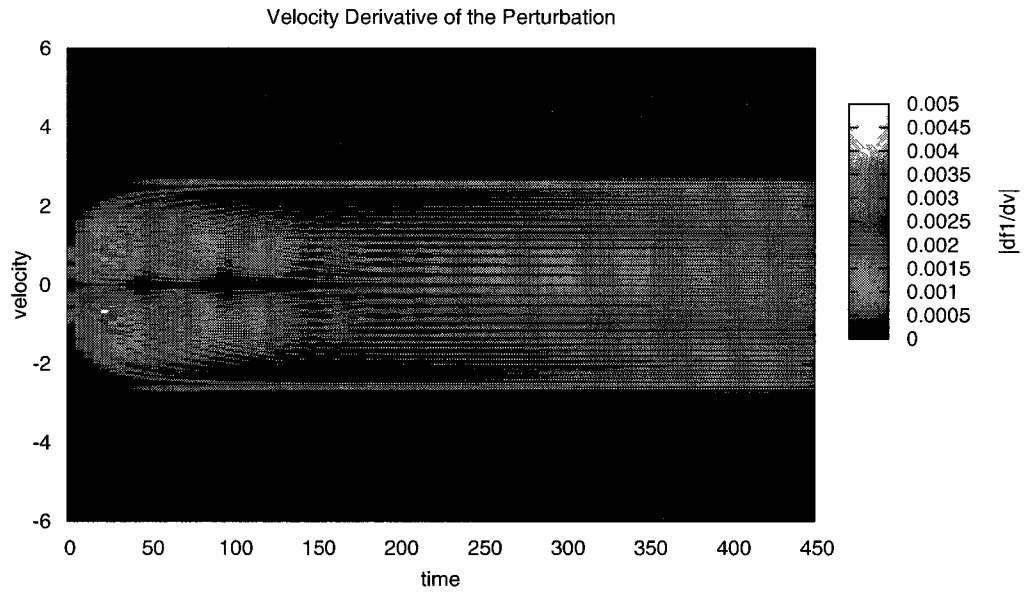

Figure 3-8: Velocity derivative of f_1 in time
The velocity derivative of the perturbation as function of time. This is the magnitude of the derivative. Note that after some transient behavior, the derivative settles into a steady growth. This particular perturbation has an initial magnitude of 1e-3. It is larger than that of the data we will analyze later. For all times that will be analyzed, the perturbation's derivative is order of magnitude smaller than the derivative of the equilibrium shown in Fig. (3-7)

Parameter	Value
nx	64
nv	20000
α	10^{-4}
lx	$2\pi/k$
U	0.15
dt	0.01

Table 3.1: Parameters for benchmarking the Langmuir wave
The wavelength is varied and system size along with it.

(PDF) solver. The dispersion relation is given by eq 3.56.

$$1 + \left(\frac{\omega_{pe}}{k v_{th}}\right)^2 (1 + \zeta_e Z(\zeta_e)) = 0 \tag{3.56}$$

Where $\zeta_e = \omega/(\sqrt{2}kv_{th})$ and $Z(\zeta)$ is the plasma dispersion function. Using the recursive forms of the small and large argument expansions of the plasma dispersion function, exact roots of ζ are found for regimes that are not well described by the simple forms found in the previous chapter. The relation above is used to recover the real and complex components of ω for a given wavenumber, k. Very good agreement is found between the Kinetic Code and the PDF Solver.

3.4 Collisional Langmuir Benchmarks

Collisions have been added to the code via the Lenard-Bernstein operator (RHS of equation 3.57).

$$\frac{\partial f}{\partial t} + v\frac{\partial f}{\partial x} + \frac{qE}{m}\frac{\partial f}{\partial v} = \nu \frac{\partial}{\partial v}\left[vf + v_{th}^2 \frac{\partial f}{\partial v}\right] \tag{3.57}$$

The entire collision operator reduces to a single term when Hermite transformed. This term is implemented along with the $E\frac{\partial f}{\partial v}$ term.

$$HT\left[\left(\frac{\delta f}{\delta t}\right)_C\right] = \nu n \psi_n \tag{3.58}$$

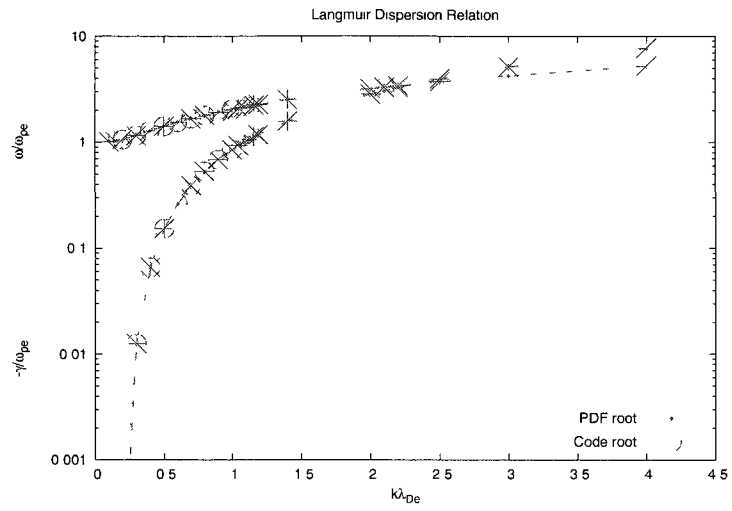

Figure 3-9: The Langmuir Dispersion Relation
The upper plots show the frequency of oscillation normalized by plasma frequency. The lower plot shows the damping rate normalized by plasma frequency. "PDF root" is the roots from the Plasma Dispersion Function Solver. "Code root" is the result from the Kinetic Code.

A simple relation given by NBS, equation 3.59, predicts the damping rate for the least damped mode of the plasma wave. Exact roots were also compared from a collisional NBS solver written by C. S. Ng in Fortran 77. The modes are found numerically by matching the large and small n limits of the Hermite expansion coefficients on a grid in the complex frequency plane. This allowed us to perform benchmarks with both the generic function and an eigenfunction as perturbations. Table 3.2 shows that the generic (sine wave) perturbation (eq. 3.12) nicely recovers the NBS predictions.

$$\gamma_{coll} = \gamma_{Landau} - \nu_{coll} \tag{3.59}$$

3.4.1 NBS Eigenmode study

The NBS modes were shown to be a complete set of eigenmodes by [NBS04], so here we search for numerical evidence of this as well. First, we examine the behavior of a single

μ	Ω_i NBS	Ω_i Kinetic Code	Percent Difference
0	-0.0548864	-0.0541404	1.36
0.00001	-0.0548937	-0.0541542	1.35
0.0001	-0.0549601	-0.0542592	1.28
0.001	-0.0556237	-0.0540314	2.86
0.01	-0.0622458	-0.0617001	.88
0.1	-0.1270101	-0.1263660	.51

Table 3.2: NBS Benchmark of Kinetic Code
Damping rates for various collision frequencies, μ, recovered from simulations compared to those predicted by the NBS modes. Here $\mu = \nu/(\sqrt{2}v_{th}k)$, $\Omega = \omega/(\sqrt{2}v_{th}k)$, and $k\lambda_{De} = 1/3$.

NBS eigenmode with the Kinetic Code. We show that the least damped collisional eigenmode is evolved in the Kinetic Code as predicted by NBS. This illustrates that the NBS modes are indeed eigenmodes of the distribution.

Next, the NBS modes are examined as a basis. Ideally, one would be able to recover hundreds of eigenfunctions so that any function could be decomposed into an NBS basis. We will show shortly that this is not presently possible. In any event, the response of the plasma to the recoverable eigenfunctions is examined by studying field damping rates and the weighting of eigenfunctions in the evolving distribution.

We begin by examining how the exact NBS eigenfunctions are generated. The eigenfunctions are calculated by Fourier transforming the collisional VP system in space and time and assuming the velocity dependence of the distribution to go as the sum of Hermite polynomials.

$$f(v) = \sum_{n=0}^{\infty} a_n H_n(v) e^{-v^2}. \tag{3.60}$$

NBS describe the recursion relation by which Ω_n and the corresponding Hermite coefficients, a_n, may be found. Note that f(v) is then found via equation 3.60 and that the coefficients and thus the function f(v) are complex. The full NBS eigenfunction perturbation for the Kinetic Code uses the real part only and has the form of equation

μ	Ω_i NBS	Ω_i code	Percent Difference
0.01	-0.0622458	-0.062049	.32
0.1	-0.1270101	-0.126813	.16

Table 3.3: Eigenfunction Benchmark of Kinetic Code
Damping rates for differing collision frequencies, μ, the eigenfunction perturbation tests are compared to the prediction of the NBS modes. Here $\mu = \nu/(\sqrt{2}v_{th}k)$, $\Omega = \omega/(\sqrt{2}v_{th}k)$, and $k\lambda_{De} = 1/3$.

3.61, where $t = 0$.

$$f(x,v,t) = (f_r(v)cos(kx - \omega_r t) - f_i(v)sin(kx - \omega_r t))e^{\omega_i t} \tag{3.61}$$

Least damped modes were applied for two different collisional frequencies as seen in Table 3.3. There is very nice agreement in the electric field damping rates between the NBS prediction and Kinetic Code results.

The distribution is analyzed next. The least damped NBS eigenmode should advance in time according to equation 3.61. Distributions are generated from this equation and then compared with the distribution output from the Kinetic Code. Figure 3-10 shows the root mean square error between theses two set of distributions. The agreement is quite nice until the system has damped out significantly. This indicates that the collisional Vlasov-Poisson system supports the NBS modes as eigenmodes of the distribution.

Attention is now turned to the NBS basis. To determine the weightings of eigenfunctions in the evolving distribution, the functions Ng's Eigenfunction Solver need to be renormalized to exploit the orthonormal property of the NBS eigenmodes. Specifically, the distributions that will be used as initial conditions in the Kinetic Code need to be put in the adjoint form to exploit orthogonality. The adjointedness is shown

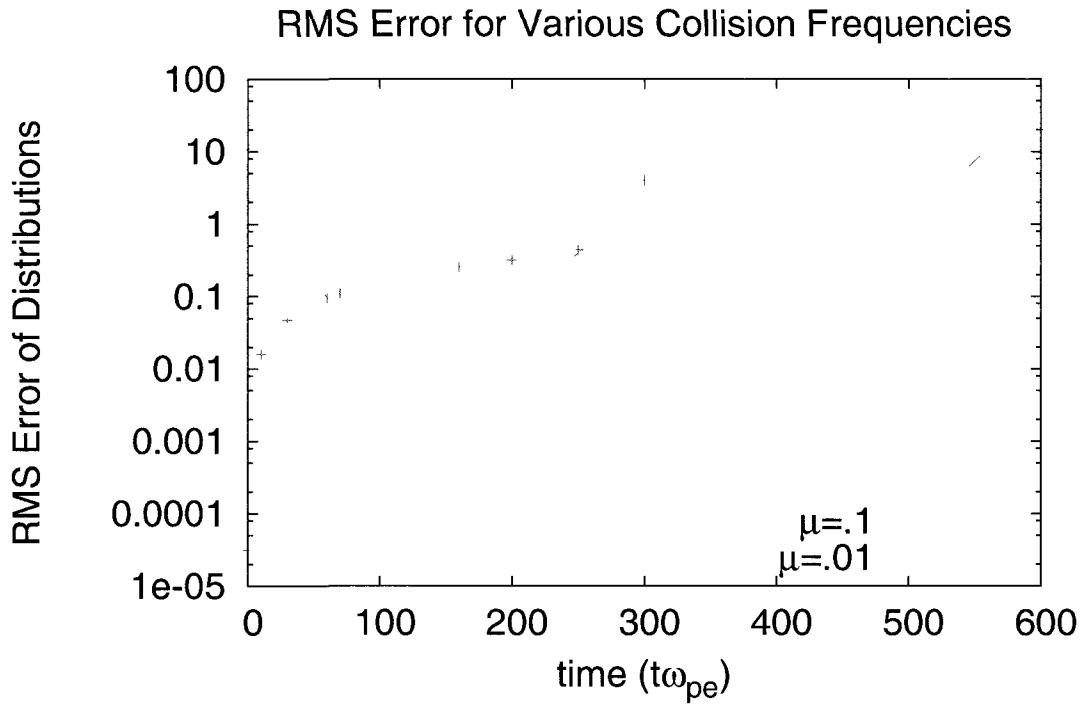

Figure 3-10: RMS Error in time for Least Damped Eigenfunctions
Here $\mu = \nu/(\sqrt{2}v_{th}k)$ and $k\lambda_{De} = 1/3$.

below. The distribution function is known to have the following form.

$$g(x,v,t) = \sum_n b_n g_n(v) e^{-i\Omega_n t + ikx} \tag{3.62}$$

$$b_n = \int_{-\infty}^{\infty} g(v) G_n(v) dv \tag{3.63}$$

The orthogonality definition is given in equation 3.63. Now, take some function, g, which is a sum of NBS eigenfunctions, g_n, and weighted by b_n. The functions G_n and g_n are adjoint. We need to generate G_n to calculate the weights, b_n. From Ng's eigenfunction solver we have an eigenfunction $f_n(v)$, which is a sum of (the orthonormal) Hermite polynomials, H_l. It needs to be normalized into the adjoint form, $g_n(v)$ by finding coefficients, a_n ,which differs in definition from the a_n used earlier in the chapter.

$$f_n(v) = \sum_l c_{n,l} H_l(v) e^{-v^2/2} \tag{3.64}$$

$$g_n(v) = a_n f_n(v) \tag{3.65}$$

$$G_n(v) = A_n \sum_l C_{nl} H_l(v) \tag{3.66}$$

Begin by imposing orthonormality on g_n and G_n.

$$1 = \int_{-\infty}^{\infty} g_n(v) G_n(v) dv \tag{3.67}$$

We know from [NBS04] that the $G_n(v)$ is related to g_n.

$$G_n(v) = g_n(v) e^{v^2} + \frac{\alpha}{\sqrt{\pi}} \int_{-\infty}^{\infty} g_n(v') dv' \tag{3.68}$$

$$\alpha = \frac{1}{k^2} \tag{3.69}$$

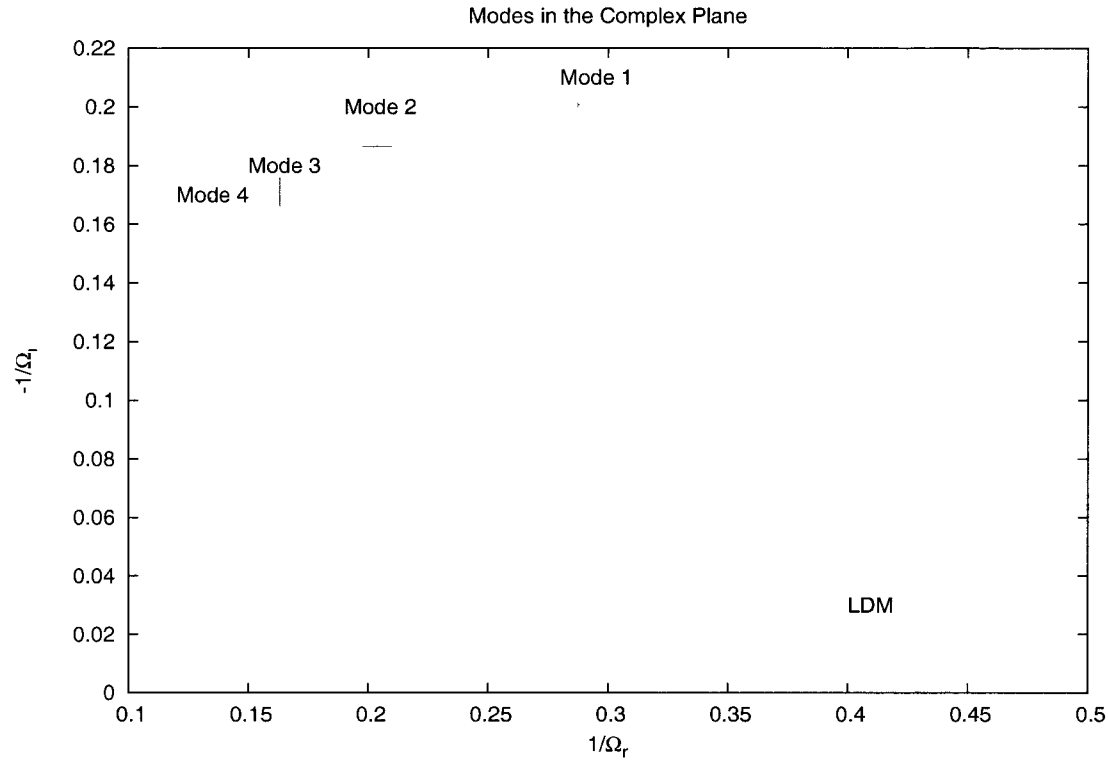

Figure 3-11: Eigenmodes in the Complex Frequency Plane.
Higher order modes become increasingly compact in the complex plane.

The coefficients for adjoint normalization are easily found to be:

$$1 = \int_{-\infty}^{\infty} g_n(v) \left[g_n(v) e^{v^2} + \frac{\alpha}{\sqrt{\pi}} \int_{-\infty}^{\infty} g_n(v') dv' \right] dv \tag{3.70}$$

$$= \int_{-\infty}^{\infty} \left[g_n^2(v) e^{v^2} + \frac{\alpha g_n(v)}{\sqrt{\pi}} \int_{-\infty}^{\infty} g_n(v') dv' \right] dv \tag{3.71}$$

$$= \int_{-\infty}^{\infty} \left[(a_n f_n(v))^2 e^{v^2} + \frac{\alpha a_n f_n(v)}{\sqrt{\pi}} \int_{-\infty}^{\infty} a_n f_n(v') dv' \right] dv \tag{3.72}$$

$$1 = a_n^2 \int_{-\infty}^{\infty} \left[(f_n(v))^2 e^{v^2} + \frac{\alpha f_n(v)}{\sqrt{\pi}} \int_{-\infty}^{\infty} f_n(v') dv' \right] dv \tag{3.73}$$

$$a_n = \left[\int_{-\infty}^{\infty} \left[(f_n(v))^2 e^{v^2} + \frac{\alpha f_n(v)}{\sqrt{\pi}} \int_{-\infty}^{\infty} f_n(v') dv' \right] dv \right]^{-1/2} \tag{3.74}$$

Strictly speaking, the coefficients, a_n, are calculated numerically from equation 3.74. In general, we choose to generate g_n from the Kinetic Code and G_n from the eigenfunction solver. Now we have all the tools to do the work and, in theory, we could

generate any eigenfunction from the NBS set using this method. However, as seen in figure 3-11, the modes become compact toward the origin making it difficult to recover them accurately. They also become increasingly oscillatory requiring great accuracy to recover their functional forms appropriately. Difficulties have been encountered in accurately recovering these modes to very high precision in the simulation code. This difficulty is due to the inherent challenges of doing high order hermite transforms. One of the symptoms of this is in the orthonormality testing.

We are able to apply only two modes with good precision. A third mode is presented that is not in good agreement and shows the nature of the problem. In this study a perturbation from a sum of three eigenmodes is applied in the Kinetic Code. Figure 3-11 shows the location of the these eigenmodes in the complex plane. Orthonormality tests of the eigenfunctions from the eigenfunction solver showed that the least damped mode (LDM) and mode 1 behaved very well for all tested functions. Mode 2, however, displayed normality when tested with itself, but poor orthogonality when tested with other functions. Nevertheless, a perturbation of the form $.5Mode2 + .25Mode1 + .25LDM$ was applied to the Kinetic Code. Figure 3-12 shows the weightings of the various modes in this perturbation as a function of time. As expected, modes 1 and 2 damp very quickly and the least damped mode dominates from that time on. The damping rates exhibited by the LDM and Mode 1 agree with their root. Mode 2 contains oscillations which prevent a linear damping rate from being well determined. In general, these tests show that the well resolved eigenfunctions are supported by the collisional Vlasov-Poisson system. The single least damped mode models the long time behavior, thus showing that interference of modes is not responsible for Landau damping in collisional systems.

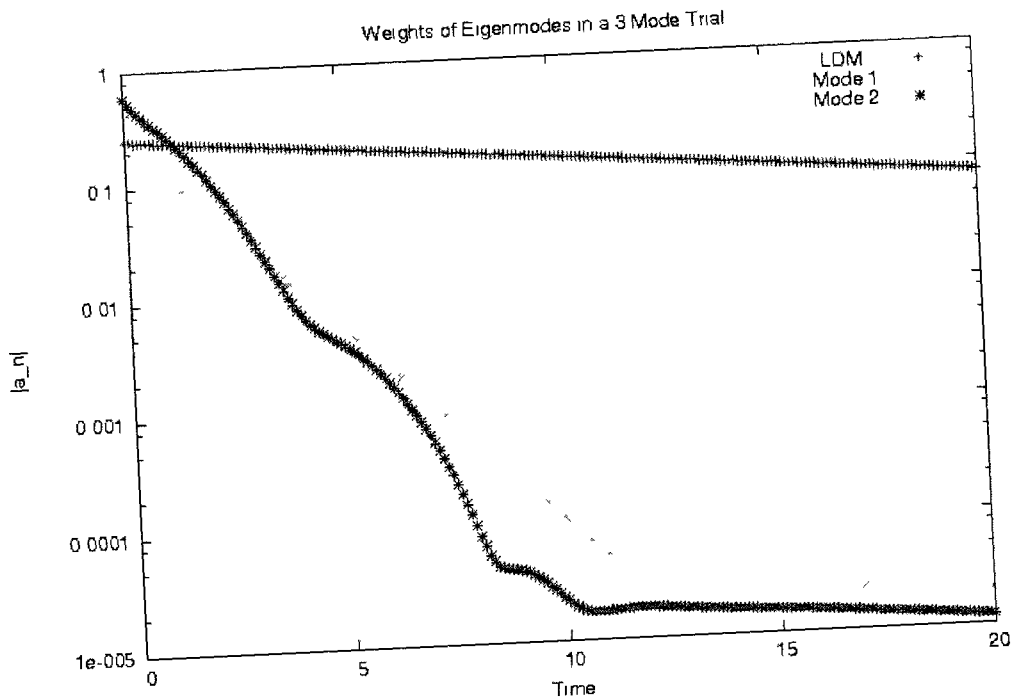

Figure 3-12: Weights of a three eigenmode perturbation as a function of time.

3.5 Discussion and Conclusion

In this chapter we have introduced the Kinetic Code used for numerical experiments in this thesis. The simulation model was described including important limitations imposed by the Hermite method. We have shown that the code recovers the collisionless plasma wave modes as well as the collisional NBS modes. The eigenfunctions of the collisional modes have been tested in the Kinetic Code as well and show expected behavior.

Future plans for this code include the implementation of a parallel scheme for the spatial dimension. This would significantly speed up the processing time required for very high velocity resolution.

Now that the Kinetic Code has been benchmarked in the collisional and collisionless regime, we will examine the plasma wave echo in the following chapter.

CHAPTER 4

Plasma Wave Echo

4.1 Introduction

The plasma wave echo was first shown analytically by Tom O'Neil in 1966 [O'N65]. The spatial and temporal echoes were derived by O'Neil and Gould [OG68]. The echo was later found in laboratory plasmas by Malmberg and Wharton in 1968 [MWGO68]. It gives great insight into the behavior of a weakly nonlinear system and is ideal for examining the effects of weak collisions on the eigenmodes of the system, those of the distribution. Collisional studies of the echo were done by Su and Oberman, and O'Neil [O'N68].

The plasma echo demonstrates the time reversibility (entropy conservation) of the collisionless system by recalling stored wave information to the macroscopic state, the electric field [Bel06]. The microscopic state is that of the phase space distribution. First, we begin by analyzing Landau damping in a collisionless plasma. This is entropy conserving. There is no loss of information to heat. Usually, a macro state maps to many micro states as collisions evolve the system. A Landau damped macroscopic state corresponds to a single microscopic state. Wave information is stored in the phase space filamentation of the distribution which occurs while Landau damping transfers energy out of the wave to the distribution. When two waves have Landau damped out, their combined information can be recalled from the microscopic state to the macroscopic state. This is the echo.

Since the echo is dependent on the characteristics of phase space filamentation, it is dependent mostly on the "free-streaming" particles. That is, those particles which are not scattered by wave resonance. This must be examined carefully because once the second wave has been applied, there are many high order interference waves to account for. The echo environment is excellent for studying the effects of collisions on resonant particles because of this. Collisions destroy filamentation information by scattering particles in phase space, thus altering if not completely preventing the echo. The classic work of Su and Oberman offers the only analytical guidance for the effects of collisions on the echo, but must be applied with care.

As we have discussed previously, the behavior of the collisional plasma wave echo was predicted in Su and Oberman's 1968 paper [SO68]. They show that the damping of first order resonant particles goes as $exp\,(-\nu t^3)$. This damping rate does not appear in the linear electric field, but could be seen in the nonlinear electric field as suggested by Su and Oberman. Though not explicitly shown, it is assumed that the collisional damping remains unchanged when the constructive interference of two such sets of particles creates the echo and that the echo will damp in this manner. O'Neil [O'N68] takes this approach when solving the collisional echo. This approach should not be taken for a full second order analysis of the collisional problem. It has neglected the damping that occurs for the non resonant particles.

Skiff et al. [SSMN$^+$98] proposed that the spectrum for a weakly collisional plasma contains degrees of freedom (modes) that had previously been ignored under the assumption that they were transients that decayed very quickly. The resulting work of NBS was then questioned by Short and Simon [SS02] who claimed that there are two branches of the spectrum, one which describes the collective motion of the particles and one which describes the motion of the free-streaming particles. They found via asymptotic analysis that the NBS modes describe only the collective motion. They

argue that free-streaming perturbations to the distribution respond to collisions as predicted by Su and Oberman. This has led to a reevaluation of the plasma wave echo and free-streaming particles in the weakly collisional system.

It is important to examine the definition of free-streaming particles as the echo phenomenon is dependent on the motion of these particles. In the purest sense, free-streaming or ballistic motion is defined by $x = x_0 + v_0 t$. There are no forces or perturbative effects on these particles. If we begin with a plasma made up of particles moving randomly with no applied forces or fields and assume no Coulomb effects between particles, we can state that all particles are free streaming. This is our standard initial condition. In our simulation, the particles are Maxwellian and non interacting. If a known electric field with some spatial and time dependence is applied to the plasma, as an antenna might, all particles will respond to it as we see from $F = qE$. The particle trajectories are then altered so that they are now defined by $x = x_0 + vt + qE(x,t)t^2/(2m)$. It is easy to show that in the case of an impulse perturbation, the trajectories are written as $x = x_0 + (v_0 + qE(x_0, t_0)/m)t$.

If no further forces are applied to these particles they will free-stream at their new velocities given by $v_0 + qE/m$. The perturbation to the particle trajectories is very important. It is through these trajectories that the filamentation of the distribution function occurs. This is how the wave information is stored in the distribution. This structure is necessary for the plasma wave echo.

One of the unique characteristics of phase space filamentation is that it does not alter the characteristics of the self consistent electric field. As was discussed in the eigenmode analysis, there is nothing to prohibit a single electric field from developing from many different velocity distributions. We see this in that the electric field characteristics are unaltered by the evolution of the filaments, i.e., plasma frequency remains unchanged as does the Landau damping rate.

Next, we consider the difference between resonant and non resonant particles. As Landau damping occurs, the resonant particles will have their trajectories further modified due to scattering from the wave-particle interaction. One must be careful, then, about referring to resonant particles as free-streaming.

In the case of the echo, two perturbations are made to the system. Each different wavenumber forms filaments at different angles in the phase space distributions. There are now at least two waves propagating in the plasma each with its own resonance. As we have seen from echo theory, there are also multiple interaction waves. These echo waves also have their own resonances with the particles. The echo occurs when an interaction wave becomes the dominant wave in the system. In phase space, very fine filaments give way to a single large structure whose characteristics are defined by the interaction wave. This is most easily shown in movie form.

When discussing collisional echo it is extremely important to appropriately define "free-streaming" particles. As seen in the electrostatics chapter, the Lenard-Bernstein collision operator contains an interior layer in the solution for the limit of weak collisions. This layer is centered on the resonance. Su and Oberman solve asymptotically for the behavior of the particles in the layer and term them "free-streaming particles". The exterior, non resonant part of the distribution is assumed to be completely unaffected by the collisions.

Here the assumption is that the particles that free-stream (are non-resonant with the wave) in response to a perturbation are unaffected by collisions to first order until they become resonant with the wave and form the echo at which point they are damped super exponentially by collisions. In reality, non-resonant particles are damped by collisions as well, but in a different manner. It is perhaps poor terminology to say that any particles in a collisional system free-stream as (in the case of the Lenard-Bernstein operator) all particles have their trajectories modified. The

introduction of collisions kills free-streaming in principle. We know from the work of Lenard and Bernstein that those non-resonant particles are suffering an exponential decay due to collisions. Su and Oberman's result belongs in some time regime, but the total decay of the echo needs to include the exponential decay component.

In this chapter, we set out to determine what effects Lenard-Bernstein collisions actually have on the Vlasov-Poisson echo since it is difficult to do experimentally. The studies presented here show the Lenard-Bernstein collisions do modify the echo significantly. We show that the echo can occur with weak collisions. Most significantly, we show that the collisional echo fits well to the Su and Oberman theory and recover collision frequencies that are close to the applied value. The very weakly collisional data recovers better fits than those with increasing collisionality.

This chapter begins with an examination of echo theory in section 4.2 and benchmarks from the Kinetic Code in section 4.3. Section 4.4, examines the theory of Su and Oberman and the implications of the NBS modes for the echo. We also demonstrate here that the Su and Oberman result is fairly well recovered in section 4.5. Section 4.6 contains concluding remarks regarding the advancement of the theory as well as a brief discussion of future and ongoing studies.

4.2 Collisionless Echo Theory

As previously mentioned, the plasma wave echo is the interaction of two first-order perturbations. To see this, we begin by expanding the Vlasov-Poisson system to second order. The second order potential, $\phi^{(2)}$ is solved by Fourier transforming in space and Laplace transforming in time. The solutions for $\phi^{(1)}$ and $f^{(1)}$ are used from the first order analysis. For some externally applied potential, the second order field response is given in equation 4.1. This equation contains the two external perturbations, ϕ_a and ϕ_b to the plasma and three dispersion functions, ϵ. Equation 4.4 shows

that these dispersion functions belong to each of the three waves in the system; the perturbations (k_1 and k_2) and the interaction wave (k_3). See appendix A.1 for full details.

$$\widetilde{\phi}^{(2)} = \frac{-\omega_p e}{4\pi^2 k^2 m \epsilon(p,k)} \int_{-\infty}^{\infty} dv \frac{k}{(p+\imath k v)^2} \times \left[\int_{-\infty}^{\infty} dk' \int_{b-\imath\infty}^{b+\imath\infty} dp' \frac{\bar{k}' k' \widetilde{\phi}_{ext}(\bar{p}', \bar{k}')}{\epsilon(\bar{p}', \bar{k}')(\bar{p}' + \imath \bar{k}' v)} \frac{df_0}{dv} \frac{\widetilde{\phi}_{ext}(k', p')}{\epsilon(p', k')} \right] \tag{4.1}$$

Here $\bar{k}' = k - k'$ and $\bar{p}' = p - p'$. Substitute a double impulse external field, then solving for cross terms and poles, the most dominant contributor is found to be equation 4.4, where τ is the time the second wave is applied.

$$\phi_{ext} = \phi_a cos(k_1 x)\delta(\omega_p t) + \phi_b cos(k_2 x)\delta(\omega_p (t-\tau)) \tag{4.2}$$

In equation 4.4, τ' is the time at which the echo reaches its peak.

$$k_3 = k_2 - k_1 \tag{4.3}$$

$$\phi_2(k_3) = \frac{e\phi_a \phi_b k_1 k_2 i \tau'}{4 m k_3} \times \int_{-\infty}^{\infty} dv \frac{\frac{df_0}{dv} e^{\imath k_3 v(\tau' - t)}}{\epsilon(-k_1, ik_1 v)\epsilon(k_2, -ik_2 v)\epsilon(k_3, -ik_3 v)} \tag{4.4}$$

$$\tau' = \frac{k_2 \tau}{k_2 - k_1} \tag{4.5}$$

While it is difficult to determine the exact value of the echo peak, we can see that the value is approximately $\Phi^2_{echo} \sim \Phi^1_a \Phi^1_b$. Noting that this interaction can occur for any high order (second, third, etc.), any echo peak may be approximated as $\Phi^{m+n}_{echo} \sim \Phi^m_a \Phi^n_b$. This is given by Malmberg et al. [MWGO68] from wave-wave interaction theory. They show that the relation agrees well with theory for the third order echo. The echo time can be found for higher orders as well by noting that the echo comes about approximately from the following equation.

$$\Phi_{echo} \sim (e^{-\imath k_b (t-\tau)})(e^{\imath v k_a t}) \tag{4.6}$$

The higher order terms are found by multiplying orders of this together.

$$\Phi_{echo}^{m+n} \sim (e^{-\imath k_b(t-\tau)})^m (e^{\imath v k_a t})^n \tag{4.7}$$

The corresponding echo time is given by:

$$t_{echo}^{m+n} = \frac{mk_2\tau}{mk_2 - nk_1} \tag{4.8}$$

Later, in figure 4-2, we show that the high order echoes are recovered by the Kinetic Code. The echo shape is quite challenging to determine analytically, but the rising and falling rates of the echo can be estimated and are given in O'Neil and Gould [OG68]

$$\gamma_{rising} = \gamma_1 \frac{k_3}{k_1} \tag{4.9}$$

$$\gamma_{falling,1} = \gamma_2 \frac{k_3}{k_2} \tag{4.10}$$

$$\gamma_{falling,2} = \gamma_3 \tag{4.11}$$

Note that for $k_1 = k_3$, the rising rate is the same as the damping rate of the first impulse. The falling rate can also have the same value as the rising rate.

4.3 Echo Benchmarks

The collisionless echo characteristic found in the previous section (echo time, amplitude, and rising and falling rates) are used to benchmark the numerical results presented here. We have benchmarked the Kinetic code with the work of Galeotti et al. [GCP06] who were the first to publish numerical results of the plasma wave echo. The applied conditions are given in table 4.1 and the echo peak value is show in fig 4-1. The echo wavenumber $k_3 = k_1$ and the peak value is predicted to occur at $t\omega_p = 1600$. The actual echo peak value occurs at $t\omega_p = 1602$. There is also a noticeable structure on either side of the peak. These oscillations are also seen by Galeotti, and are not easily described by the analysis of the echo.

Parameter	Value
N_x	32
N_v	20000
α (both perturbations)	10^{-6}
τ	800
wavenumber 1, $k_1\lambda_D$	.4
wavenumber 2, $k_2\lambda_D$	.8
lx	$4\pi/.4$
U	.15

Table 4.1: Echo parameters
The parameters used for benchmarking the plasma wave echo

We find that the peak value differs from that found by Galeotti; it is larger by about a factor of 1.7. Note that the actual peak value does not agree well with the approximate prediction of theory. Wave-wave theory estimates a peak value of 10^{-12}. Simulations recover a peak value of 10^{-10}.

$$\phi_{echo} \sim \phi_1^m \phi_2^n \tag{4.12}$$

$$\sim 10^{-6}10^{-6} = 10^{-12} \tag{4.13}$$

However, the rising and falling rates of the echo follow theory nicely. The rising and the falling rates both have a value of $\gamma_1 = \gamma_3$. The decay rate from the root of $k_1\lambda_D = .4$ is $0.00778\omega_{pe}$. The decay rate from the root of $k_1\lambda_D = .8$ is $0.022389\omega_{pe}$. From the trial data presented here, we found the rising rate of the echo to be $.00785\omega_{pe}$ and the falling stage to be $.0074\omega_{pe}$. The rising and falling stages show reasonable agreement with the theoretical predictions and the findings of Galeotti et al.

We have also recovered higher order echoes as demonstrated in figure 4-2. For any echo such as this one where $k_2 = 2k_1$, the echo appears at $t_{echo} = 2\tau$. This places the echo at $t = 1200$ and the third order echo at $t = 800$. Note that the third order echo seen here applies to $m = 2$, $n = 1$ as calculated from 4.8. This third order echo is actually slightly shifted from the expected values, but is well within reasonable error. Now that we have demonstrated that the plasma wave echo is recovered appropriately

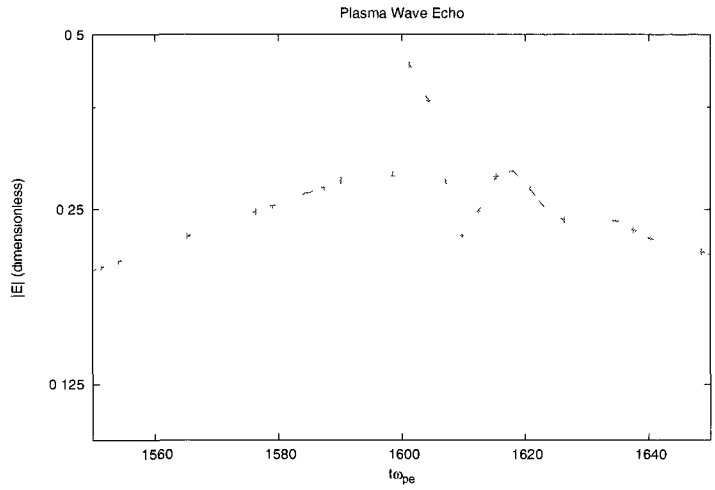

Figure 4-1: Echo benchmark of Kinetic Code with existing numerical studies
The peak value of the plasma wave echo multiplied by 10^9 from Galeotti et al. [GCP06] conditions. This result differs in magnitude from the published value by about a factor of 2.

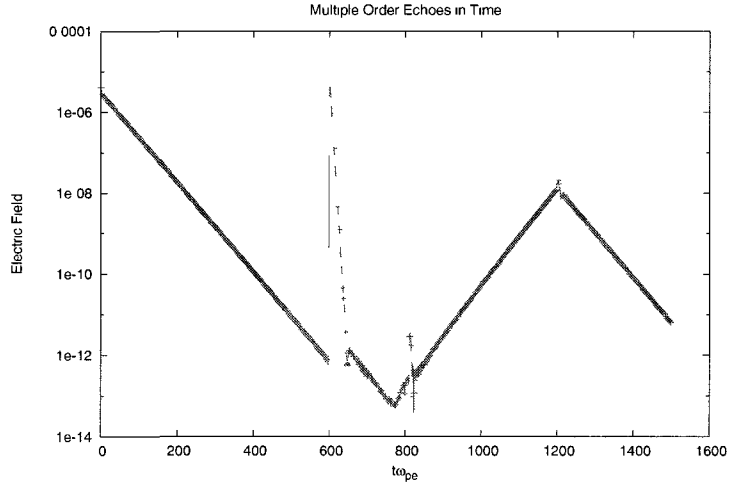

Figure 4-2: High Order Echoes
The maximum electric field in time for the maximum in space. The first wave is applied at $t\omega_{pe} = 0$. The second wave is applied at $t\omega_{pe} = 600$ and quickly Landau damps aways. The (second order) echo occurs at $t\omega_{pe} = 1200$. A third order echo is also seen at $t\omega_{pe} = 815$.

in the code, we move on to the collisional study.

4.4 Collisional Echo Theory

In this section, we discuss the form presented by O'Neil [O'N68] for the collisional echo that will be fit to the data from the Kinetic Code. The collisional term given by Su and Oberman is for a single perturbation. When O'Neil applies it to the echo, it is written as a single term where the collisional contributions for each of the two applied waves are unchanged by the interaction. For our specific case, the whole collisional echo reduces as seen below.

$$\Phi_{k_3} = \frac{e\Phi_1\Phi_2 k_1 k_2 i\tau'}{4mk_3} \times \int_{-\infty}^{\infty} dv \frac{\frac{df_0}{dv} e^{ik_3 v(\tau'-t) - D(v)\frac{k_1^2 k_3^2 \tau'^3}{3k_2^2}}}{\epsilon(-k_1, ik_1 v)\epsilon(k_2, -ik_2 v)\epsilon(k_3, -ik_3 v)} \tag{4.14}$$

The form of D needs to be determined from the collision operator. The general form for the Fokker Planck operator is written as:

$$FP(f) = -\frac{\partial}{\partial v}[D_1 f] + \frac{\partial^2}{\partial v^2}[D_2 f] \tag{4.15}$$

The collision frequency is given by the dominant term in the operator, the diffusion term.

$$\nu_{eff} = -D_2(v)\frac{k_1^2 k_3^2 \tau'^3}{3k_2^2} \tag{4.16}$$

For the Lenard Bernstein case where D_2 is independent of velocity, the effective collision frequency is

$$\nu_{eff} = \nu v_{th}^2 \frac{k_1^2 k_3^2 \tau'^3}{3k_2^2} \tag{4.17}$$

Parameter	Value
N_x	32
N_v	20000
α (both perturbations)	10^{-4}
wavenumber 1, kx	1/3
wavenumber 2, kx2	2/3
lx	6π
U	.15

Table 4.2: Parameters for the collisional echo study.
The parameters used for collisional vs. collisionless trials

4.5 Collisional Echo Findings

Here we present the effect of the collisions on the echo structure and on the echo peak value as a function of time. The data presented in figure 4-3 shows echo peak values for collisionless and collisional systems. Table 4.2 shows the parameters used for these runs. Figure 4-3 shows the echo peak structure for a single point in space. This spatial point gives the maximum value of the electric field. We can see that the echo structure is not significantly altered. Amplitudes are just reduced.

Figure 4-4 shows echo peak values as a function of time. In these trials, the parameters given in table 4.2 are used, except for N_x which was set to 64. The time that the second perturbation is applied was varied to generate this plot. Peak values were taken from the maximum location in space. We see from figure 4-4 that the echo is highly sensitive to collisions. Collisions on the order of $10^{-4}\omega_{pe}$ are sufficient to prevent the echo from forming at all. There are two structures to be pointed out. In both the collisionless and collisional results, there is a small growth and then decay of the echo peak value in the short time limit. Collisional data sets in this figure are limited in time because collisions prevent the echo from occurring at late times. The collisionless data set is limited in time as well. The initial wave will Landau damp to the numerical precision scale if left for long enough. The resulting echo peak value

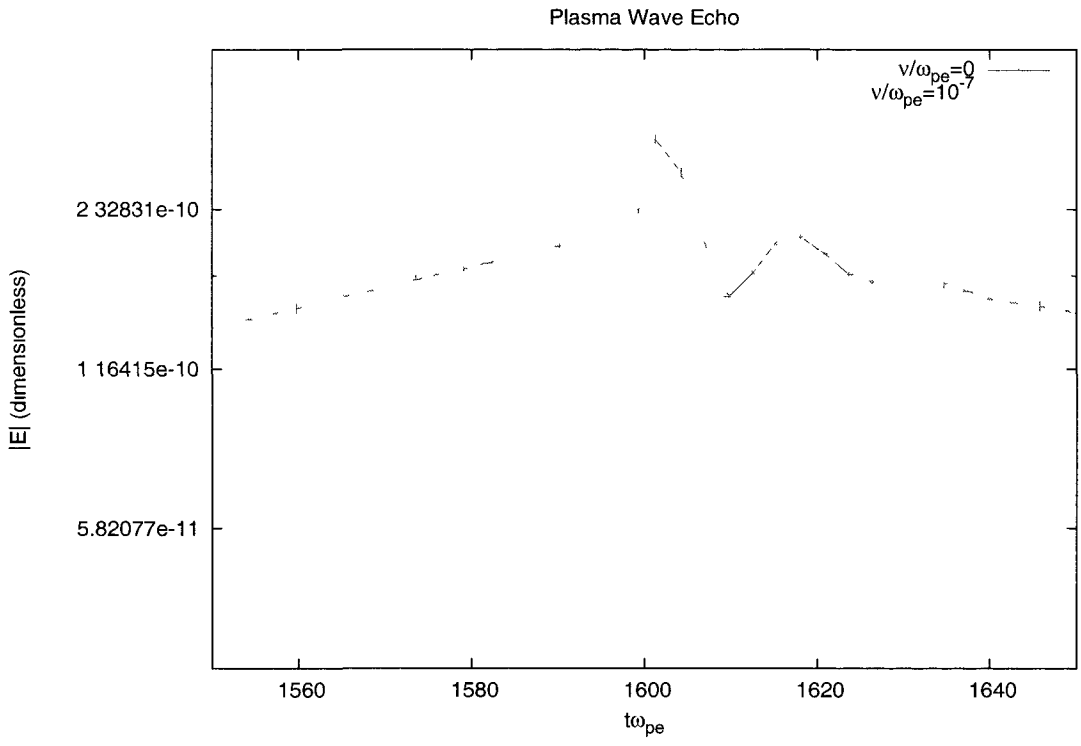

Figure 4-3: Echo Structure with Collisions

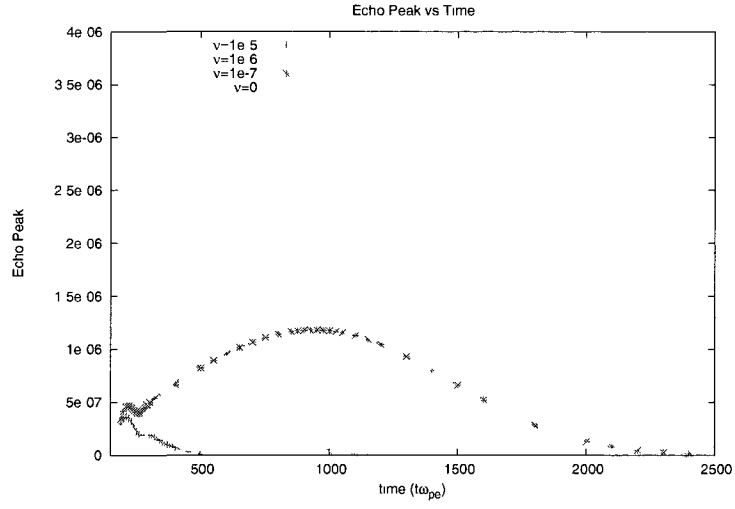

Figure 4-4: Echoes for various collision frequencies

would be questionable if the second perturbation is applied after this time.

The data presented above was fit with various forms to test the prediction of Su and Oberman and O'Neil. Following O'Neil's form, the collision frequency was non-dimensionalized for comparison with the simulation results. This yields the form:

$$\nu_{eff} = \nu v_{th}^2 \frac{k_1^2 k_3^2 \tau'^3}{k_2^2} \tag{4.18}$$

$$= \nu' \omega_{pe} v_{th}^2 \frac{1}{\lambda_D^2 \omega_{pe}^3} \frac{(k_1' k_3')^2 \tau_{non-D}'^3}{3(k_2')^2} \tag{4.19}$$

$$= \nu' \frac{(k_1' k_3')^2 \tau_{non-D}'^3}{3(k_2')^2} \tag{4.20}$$

For the wavenumbers applied in the simulations, this yields

$$\nu_{eff} = \nu \frac{\tau_{non-D}^3}{2^2 3^3} \tag{4.21}$$

This indicates that the echo should damp on the order of the applied dimensionless collision frequency. Using the eq.4.14 as a guide, the form Ate^{-Bt^3} was determined to be an appropriate structure for the data in fig. 4-4. See fig.(4-5) for an image of this fit. This fit appears to be reasonable. However, as shown in table 4.3, the resulting collision frequency does not very well recover the applied values. There is about a 14% difference for the lowest collisionality system. This increases dramatically as collisionality increases.

μ_{given}	$\nu = \mu_{given}\sqrt{2}k$	B	r^2	ν_{fit}	$\%diff$
1e-7	4.714045079e-8	3.8324e-10	0.9963	4.14e-8	14
1e-6	4.714045079e-7	3.7312e-9	0.9989	4.03e-7	17
1e-5	4.714045079e-6	3.3619e-8	0.9994	3.63e-6	30

Table 4.3: Fits of echo peak vs time to the full O'Neil form: $Ate^{-\nu t^3}$. Percent difference is between ν_{given} and ν_{fit}.

Fits to the tail regions in fig. 4-4 were also fit with just the damping component using the form $Ae^{-\nu t^3}$. These also recovered incorrect collision frequencies.

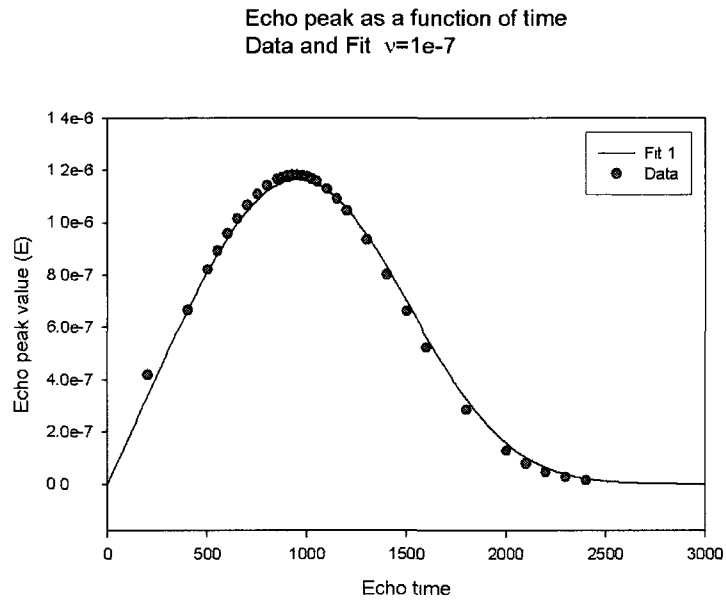

Figure 4-5: Echo data for $\nu = 1e-7$ fit to $Atexp(-Bt^3)$.

μ_{given}	$\nu = \mu_{given} * \sqrt{2k}$	B	r^2	ν_{fit}
1e-7	4.714045079e-8	1.1269e-9	0.7087	1.22e-7
1e-6	4.714045079e-7	2.9472e-9	0.9982	3.18e-7
1e-5	4.714045079e-6	2.8042e-8	0.9997	3.03e-6

Table 4.4: Fits of echo peak vs time (tail region) the SO form: $Ae^{-\nu t^3}$.

Finally study was made with a modified collision operator of just the diffusive term in the Lenard-Bernstein operator. As expected from the asymptotics, the Su and Oberman term seems to match well at late times with the Lenard-Bernstein operator. The findings presented here show that the Su and Oberman theory seems to capture most of the physics for the collisional echo. For very weak, but increasing collision frequencies, the Su and Oberman theory does consistently worse.

4.6 Conclusions and Ongoing Work

After benchmarking the collisionless echo with theory and other numerical studies, we have shown that the diffusive term in the Lenard-Bernstein operator dominates

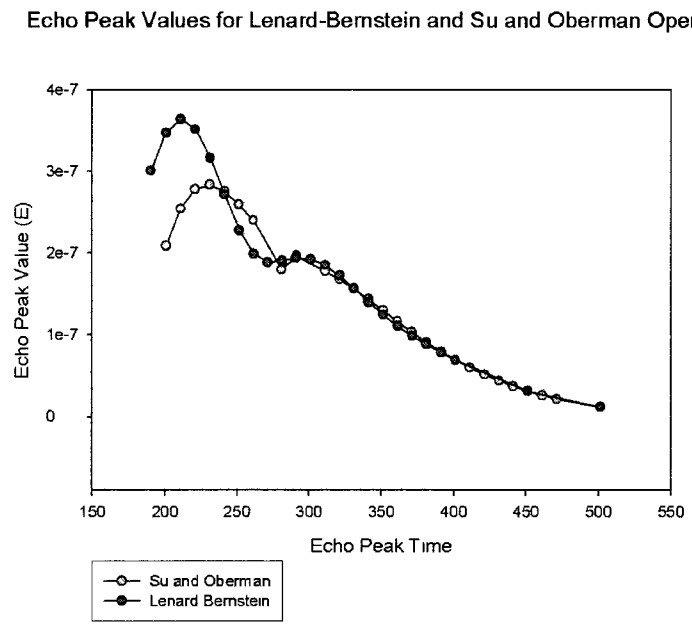

Figure 4-6: Collisional study of Su and Oberman operator and the Lenard and Bernstein operator

Echo data for $\nu = 1e-5$ for SO operator $(\partial f/\partial t)_C = \nu v_{th} \frac{\partial^2 f}{\partial v^2}$ and the full LB operator.

the echo damping as indicated by Su and Oberman. It has been shown here that the super-exponential damping, which has been attributed to free-streaming particles, captures the essence of the physics. As with asymptotic solution, it does not well describe the total collisional effects.

Short and Simon state that with very weak collisions, the collective modes can Landau damp away, leaving an appreciable free-streaming perturbation. That is, when the collective modes have Landau damped away, the information is retained in the free-streaming particles. This suggests that the free-streaming behavior exists in the long-time limit. Insofar as the Su and Oberman result describes free-streaming particles, the data presented here agrees.

This raises the issue of what the nature of the modes supported by the collisional plasma are. The discrete NBS modes eliminated the continuous spectrum, but evi-

dence of the continuous spectrum exists in the Su and Oberman echo regime. The dominant behavior in the linear regime is clearly given by the complete NBS set. There should be evidence of them in the nonlinear regime, particularly for phenomena dependent on the interference of linear waves. On the short time scales, collisions have no effect. The Su and Oberman behavior could exist on an intermediate time scale, where the continuous spectrum still exists. The long time regime has to be dominated by the eigenmodes. The data presented is restricted in time by numerical restraints. If this could be lifted, the NBS interference may be found.

Another possibility is that while the super exponential damping may be occurring for some very limited number of particles, those particles are always outnumbered by those suffering exponential decay. This decay should not be ignored as it frequently is in the weak collisionality treatments.

There are many open questions remaining and many studies to follow. The asymptotic first order analysis should be advanced to include smooth asymptotic matching of resonant and non resonant regions in the distribution. An updated collisional theory of the echo is called for that includes the exponential time damping contribution of the non resonant particles and shows the regime of validity for the Su and Oberman theory.

These investigations are not currently ongoing. However, examination of the effects of particle trapping on the collisionless and collisional echoes are currently being studied. Preliminary results show that very weak collisions can allow both the trapping and the echo to exist, but there is a larger effect by collisions on the echo than on the particle trapping.

CHAPTER 5

Ion Acoustic Instability

The ion acoustic wave (IAW) in a plasma is analogous to a sound wave in a neutral gas. The sound wave is due to pressure changes with the density of neutral atoms. It is a compressional wave. In the case of an ion acoustic waves in a plasma, an electric wave arises due to the motion of the slow, heavy ions and the response of the fast moving and light electrons. The ion acoustic waves are electrostatic waves due to the variations in particle densities. Thus, they are also a type of compressional wave [EA72].

Simple ion acoustic modes can be excited just by having two non drifting species (ions and electrons) in a system. They experience Landau damping as the plasma waves do. In the current driven case, electrons drift relative to the ions. As the drift approaches a critical value, the waves stop Landau damping. When the critical velocity is exceeded the wave experiences Landau growth. This growth continues, widening the resonance regime in the electron distribution, until it is saturated by the development of the quasilinear plateau. This prevents energy exchange between particles and the wave.

The scattering of particles that develops the plateau also generates an effective resistivity that is not derivable from the bulk properties of the system. This has been known as "anomalous" resistivity in the older literature. This resistivity was predicted by Buneman [Bun59] for the two-stream instability and then measured by Thomassen [Tho63]. This anomalous, wave-particle resistivity is examined here and

in two different temperature regimes.

In this chapter we derive the dispersion relations for the ion acoustic wave and the current driven ion acoustic wave (stable and unstable) in section 5.1. The implementation of ions in the Kinetic Code and benchmarks of the waves and instability are given in section 5.2. We examine quasilinear theory in section 5.3. Specifically, we discuss the instability saturation, quasilinear plateau formation and the high energy ion tail.

We also review the work of Sagdeev [SG69] for the form of wave-particle resistivity and compare this with the calculation from the Kinetic Code, section 5.4. These numerical results are compared with the Vlasov-Ampere study of Petkaki et al. [PFK+06] and the Vlasov-Poisson study of Hellinger and Travnicek [HTM04]. The results from the Kinetic code, show very nice agreement with the analytical estimates. This result, in part, supports the findings of Hellinger et al. who also find agreement with Sagdeev but not with Petkaki. We discuss the potential reasons for this including an examination of Hellinger's claims that the use of an unrealistic mass ratio is responsible for Petkaki's discrepancy. We show a mass convergence study which suggests that this is not the cause. The last study presented shows the anomalous resistivity for a high temperature ratio ion acoustic instability. Finally, in section 5.6, the chapter is closed with a brief discussion of future potential studies for this line of work.

5.1 Ion Acoustic Wave and Instability Theories

Here we derive the dispersion relations for the ion acoustic wave to various approximations. The plasma dispersion relation for a two species plasma with Maxwellian,

drifting electrons and Maxwellian, non-drifting ions is given in equation 5.1.

$$\epsilon(p,k) = 1 - \frac{\omega_{pe}^2}{k^2}\int_C \frac{df_{0e}/dv}{p+ikv}dv - \frac{\omega_{pi}^2}{k^2}\int_C \frac{df_{0i}/dv}{p+ikv}dv = 0 \tag{5.1}$$

This is rewritten in Z-function form (eq. 5.2), as previously seen in equations 2.20 - 2.23. It is then expanded for small ζ_i/ζ_e, where $\zeta_e = \frac{v_{th,i}}{v_{th,e}}\zeta_i$. This amounts to an expansion about $T_e/T_i \gg 1$.

$$1 + \left(\frac{\omega_{pe}}{kv_{th,e}}\right)^2 (1 + \zeta_e Z(\zeta_e)) + \left(\frac{\omega_{pi}}{kv_{th,i}}\right)^2 (1 + \zeta_i Z(\zeta_i)) = 0 \tag{5.2}$$

This is then solved using residue theory giving real and imaginary parts of the modes. Terms up to second order are kept and the real part yields the ion acoustic speed.

$$\frac{\omega}{k} = C_s = \sqrt{\frac{k_B T_e}{m_i(1+k^2\lambda^2)}} \tag{5.3}$$

Solving, then, for the complex part gives the Landau damping rate for the ion acoustic wave.

$$\frac{\gamma}{\omega} = \sqrt{\frac{\pi}{8}}\left(\sqrt{\frac{m_e}{m_i}} + \left(\frac{T_e}{T_i}\right)^{3/2} e^{-\frac{T_e}{2T_i}}\right) \tag{5.4}$$

The fourth order expansion of the plasma dispersion relation for small ζ leads to the following relation.

$$\frac{\omega}{k} = \sqrt{\frac{k_B T_e + 3T_i}{m_i}} \tag{5.5}$$

$$\frac{\gamma}{\omega} = \sqrt{\frac{\pi}{8}}\frac{\left(3+\frac{T_e}{T_i}\right)^{5/2}}{\left(9+\frac{T_e}{T_i}\right)^{3/2}}\left(\sqrt{\frac{m_e}{m_i}}\left(\frac{T_i}{T_e}\right) + e^{-\frac{T_e}{2T_i}-3/2}\right) \tag{5.6}$$

5.1.1 CDIAI Wave and instability theory

The current driven ion acoustic wave arises from a system of non-drifting ions and drifting electrons. It is important to note that in the two species problem, the wave resonates with both species. Their respective Landau behaviors both contribute to the damping or growth of the wave. For the instability to occur, the growth due to

electrons must be greater than the Landau damping due to ions. There are two ways to force the instability. Either set a very high electron drift velocity, or set a high ion to electron temperature ratio. In the limit that T_e/T_i approaches infinity, the critical velocity approaches the ion acoustic speed.

Instability theory provides guidance for determining the stability of a system based on the properties of the dispersion relation. The Nyquist criterion deals with mappings of complex ω plane onto the complex ϵ plane. It states that if the mappings include $\epsilon = 0$, the plasma is unstable. Gardner's theorem is a limiting case which states that a single humped distribution is always stable. A minimum of two peaks are necessary, but does not guarantee instability. The Penrose criteria states that the minimum between the two peaks must be deep enough. This means that the difference in drift speeds of the two species must differ by at least a factor of the thermal velocity. This is reflected in the dependence of modes on drift velocity (equation 5.9). For full details, see a textbook such as [Nic83] and [GB05] Here the dispersion relations are derived for the current driven wave. The distributions are now written as in eq 5.7.

$$f_i(v) = \frac{1}{\sqrt{2\pi}v_{th,i}} e^{-(v/v_{th,i})^2}$$
$$f_e(v) = \frac{1}{\sqrt{2\pi}v_{th,e}} e^{-(v-v_{drift})^2/v_{th,e}^2} \tag{5.7}$$

The inclusion of electron drift does not significantly alter the plasma dispersion relation. The functional form remains as in equation 5.2, where $\zeta_e = \omega/\sqrt{2}kv_{th,e} - v_{drift}$. The roots for the second order approximation for Maxwellian particles are solved as

shown previously.

$$\omega_r^2 = \frac{k^2 C_s^2}{1 + k^2 \lambda_{De}^2} \tag{5.8}$$

$$\omega_i = -|\omega_r| \sqrt{\frac{\pi}{8}} \frac{1}{(1 + k^2 \lambda_{De}^2)^{3/2}} \times \left(\left(\frac{T_e}{T_i} \right)^{3/2} exp \left[-\frac{T_e}{2T_i(1 + k^2 \lambda_{De}^2)} \right] + \sqrt{\frac{m_e}{m_i}} \left(1 - \frac{v_{drift}}{C_s} \sqrt{(1 + k^2 \lambda_{De}^2)} \right) \right) \tag{5.9}$$

Note that the sound speed is an upper limit on the possible phase velocities and that at some critical velocity the imaginary part is zero. For any drift velocity above critical velocity, the complex part is positive meaning there is growth in the wave.

$$v_{critical} = v_{th,e} \left[\sqrt{\frac{m_e}{m_i}} + \left(\frac{T_e}{T_i} \right)^{3/2} e^{-T_e/2T_i} \right] \tag{5.10}$$

5.2 Ions in the Kinetic Code

Ion acoustic waves were implemented in the Kinetic Code by inserting calculations of the Vlasov equation for ions and adding their contribution to Poisson's equation.

$$\frac{\partial f_e}{\partial t} + v \frac{\partial f_e}{\partial x} + \frac{q_e E}{m_e} \frac{\partial f_e}{\partial v} = 0 \tag{5.11}$$

$$\frac{\partial f_i}{\partial t} + v \frac{\partial f_i}{\partial x} + \frac{q_i E}{m_i} \frac{\partial f_i}{\partial v} = 0 \tag{5.12}$$

$$\nabla \cdot E = \frac{q_e}{\epsilon_o} \int_{-\infty}^{\infty} f_e(v) dv + \frac{q_i}{\epsilon_o} \int_{-\infty}^{\infty} f_i(v) dv \tag{5.13}$$

The equilibrium distributions for this case are the Maxwellian for each species.

$$f_i(v) = \frac{1}{\sqrt{2\pi} v_{th,i}} e^{-(v/\sqrt{2} v_{th,i})^2} \tag{5.14}$$

$$f_e(v) = \frac{1}{\sqrt{2\pi} v_{th,e}} e^{-(v/\sqrt{2} v_{th,2})^2} \tag{5.15}$$

Both species are perturbed at the initial condition by a sine wave whose magnitude is determined by the parameter α_i and α_e.

$$f_i^1(x, v) = \alpha_i \sin kx \frac{1}{\sqrt{2\pi} v_{th,i}} e^{-(v/\sqrt{2} v_{th,i})^2} \tag{5.16}$$

$$f_e^1(x, v) = \alpha_e \sin kx \frac{1}{\sqrt{2\pi} v_{th,e}} e^{-(v/\sqrt{2} v_{th,2})^2} \tag{5.17}$$

Parameter	Value
nx	64
nv	20000
$\alpha_i = \alpha_e$	10^{-4}
wavenumber, $kx\lambda_{De}$	.1
L_x	$2\pi/kx$
U_e	.32
U_i	.15
m_i/m_e 25	
$v_{th,e}$	1
$v_{th,i}$	varies

Table 5.1: Parameters for IAW benchmark with theory
These are the Kinetic Code parameters used for benchmarking the ion acoustic wave frequencies with the exact roots from a Plasma Dispersion Function Solver and from analytical estimates. The temperature ratio is varied by varying ion thermal velocity. The velocity scales are also varied to appropriately resolve the distributions. The values given here are for the low temperature,$T_e/T_i \leq 5$, ratio tests.

The Hermite transformations are performed for ions as they are for electrons. The ions carry their own scale, U_{ion}. Electrons and ions are calculated on the same unscaled velocity grid.

The damping rates and phase frequencies where compared primarily with the results from the Plasma Dispersion Function Solver of C. S. Ng which was modified to include the second species. It solves equation 5.2 for ζ_e. This time the roots are normalized by $\zeta_e = \omega/\sqrt{2}kv_{th,i}$ for comparison of roots with the Kinetic code.

5.2.1 IAW Benchmark

Table 5.1 gives the parameters for the temperature variation benchmark. Figure 5-1 shows that the Kinetic Code recovers the exact numerical root and is in agreement with analytical estimates as it should. For comparison, the damping rates and wave frequencies for a few temperatures are provided in Table 5.2.

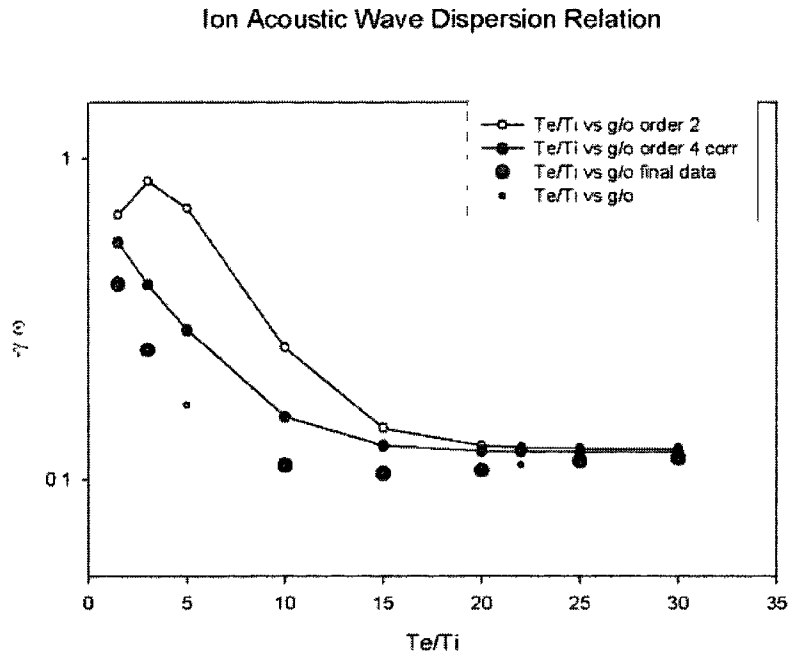

Figure 5-1: Ion acoustic wave roots with varying temperature ratio.
Shown here are the ion acoustic wave damping rates over oscillation frequencies for varying temperature ratio. Yellow circles are from the second order analytical solution. The blue circles are the fourth order analytical solution. The red circles are from roots of the numerical plasma dispersion function solver. The tiny green dots are the values recovered from the Kinetic Code. The analytical estimates converge with the exact roots as Te/Ti rises.

T_e/T_i	ω	γ
1.5	0.02699	0.011012
10	0.016634	0.001848
25	0.014697	0.001611

Table 5.2: IAW Frequencies for Varying Temperature Ratios
These rates are from the Kinetic Code. for $m_i = 25m_e$, $k\lambda_{De} = .1$, and the other parameters given in Table 5-1. They agree with the exact roots from the PDF Solver.

5.2.2 CDIAW Benchmarks

The current driven ion acoustic modes are benchmarked in two ways. In the first, the drift velocity is varied. In the second test, the temperature ratio is varied. In the first benchmark, the system is driven linearly from stability to instability as in equation 5.9. The parameters for figure 5-2 are $k\lambda_{De} = .3$, $Te = 20Ti$, and $m_i = 25m_e$. In the second benchmark, figure 5-3, the temperature ratio is varied for constant

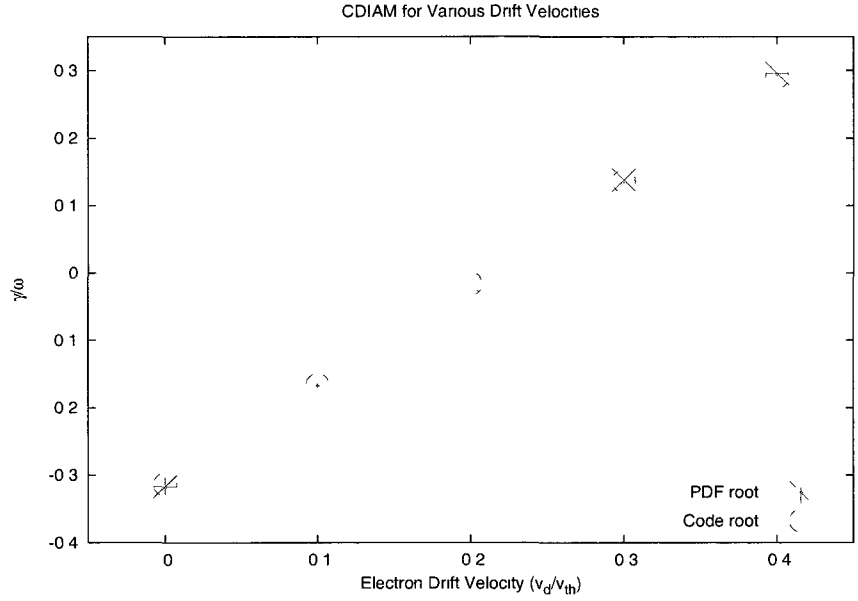

Figure 5-2: Current Driven Ion Acoustic Wave Benchmark with Varying Drift Velocity.
The red stars are the roots from the numerical plasma dispersion relation solver and the green crosses are from the Kinetic code data. As drift velocity increases, the system goes from stable to unstable.

parameters $k\lambda_{De} = .3$, $v_{drift} = .4v_{th,e}$ and $m_i = 25m_e$. The negative damping rate grows exponentially to a constant value as predicted by eq 5.9.

Figure 5-4 gives an example of the ion acoustic instability as it appears in the electric field. It has the parameters from Table 5.3, unless otherwise stated in the caption. The spatial Fourier transform of the electric field has three distinct regions.

Parameter	Value
nx	256
nv	20000
α_i	$7.76 * 10^{-5}$
α_e	$2 * 10^{-5}$
$k\lambda_{De}$	0.51
k	0.1282899 (1/m)
L_x	$4\pi/k$
U_i	6000
U_e	100000
m_e	$9.11 * 10^{-}31$ kg
m_i	$25 * m_e$
v_{drift}	$\sqrt{21.2}v_{th,e}$
T_e	2 eV
T_i	1eV
n_0	$7 * 10^6(1/m^3)$
$v_{th,e}$	592674 m/s
$v_{th,i}$	83816.7 m/s
λ_{De}	3.97 m
ω_{pe}	$1.49086 * 10^5$ Hz
ω_{pi}	$2.98 * 10^4$ Hz

Table 5.3: Parameters for Petkaki Study
This table is a complete list of the parameters implemented for the comparison study with Petkaki et al. For these parameters, $\gamma = 4583.0319Hz$, $\omega_r = 20836.067Hz$, and $v_{phase} = 162413.95m/s = .27v_{th,e}$. The ion sound speed is calculated using the fourth order expansion and is found to be $C_s = 166803m/s = .28v_{th,e}$.

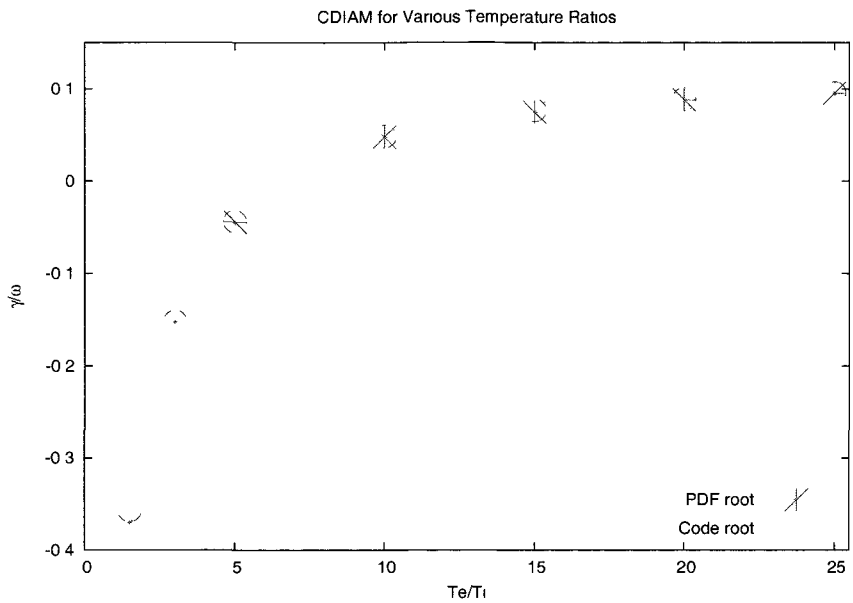

Figure 5-3: Current Driven Ion Acoustic Wave Benchmark with Varying Temperature Ratio.
The red stars are the roots from the numerical plasma dispersion relation solver and the green crosses are from the Kinetic code data. As T_e/T_i grows, the system goes from stable to unstable.

Near the initial condition, the field decays as the system settles into the most dominant mode. In the second regime, roughly $t\omega_{pe} = 50$ to $t\omega_{pe} = 220$, the linear instability is dominant. The third region is the nonlinear regime where the instability has saturated and new modes are achieved. It is also notable that the spatial electric field exhibits a change of phase velocity just before it settles into the nonlinear behavior.

Next, the spatial convergence of the saturation is tested to see that the time and peak value are stable. Figure 5-5 shows this. Note that the data points lie mostly on top of one another. From this, it is determined that 64 spatial points are sufficient to resolve quasilinear saturation.

As a final study of instability saturation convergence, a comparison of a single wave perturbation was made with a multiple wave perturbation. The multiple wave initial condition was implemented in the Kinetic Code by summing over many waves.

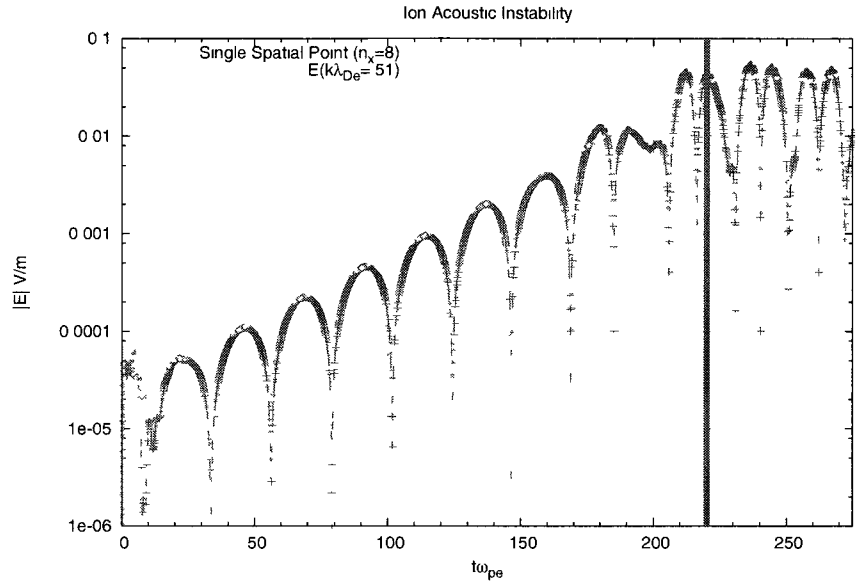

Figure 5-4: Electric Field for the Ion Acoustic instability.
The field is given for a single point in space as well as the spatial Fourier transform at the fastest growing mode. For this study $\alpha_i = \alpha_e = 10^{-4}$, $nx = 64$, $U_e = 300000$, $U_i = 40000$. The vertical line at $t\omega_{pe} = 220$ represents an estimated saturation time.

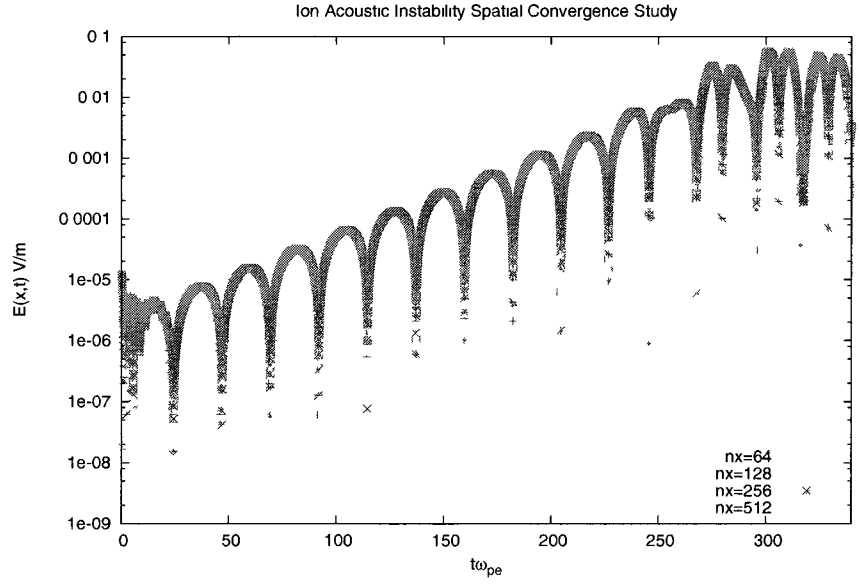

Figure 5-5: Spatial Convergence of Quasilinear Saturation
The electric field at a single point in space ($x = 10.71m$) for various spatial resolutions. The parameters for this study are given in Table 5.3.

This spectrum is actually a sum of 6 waves. The minimum wavenumber, k, is 0 and $k_n = n0.064145(1/m)$. A minimum of 16 grid points are used to resolve the smallest wavelength. To have enough spatial resolution to recover the nonlinear (interaction) waves, 128 spatial grid points are used.

$$f_i^1(v) = \alpha_i \sum_n \sin k_n x \frac{1}{\sqrt{2\pi} v_{th,i}} e^{-(v/\sqrt{2}v_{th,2})^2} \tag{5.18}$$

$$f_e^1(v) = \alpha_e \sum_n \sin k_n x \frac{1}{\sqrt{2\pi} v_{th,e}} e^{-(v/\sqrt{2}v_{th,2})^2} \tag{5.19}$$

Figure 5-6 shows that there is no significant change to the saturation value when multiple waves are added to the system. A difference in saturated value was calculated to be 0.001 V/m which is roughly a 2% difference between the two peaks. The saturation time varies between the two studies because of differing initial perturbation sizes. Figure 5-7 shows that the quasilinear saturation value of the electric field has a

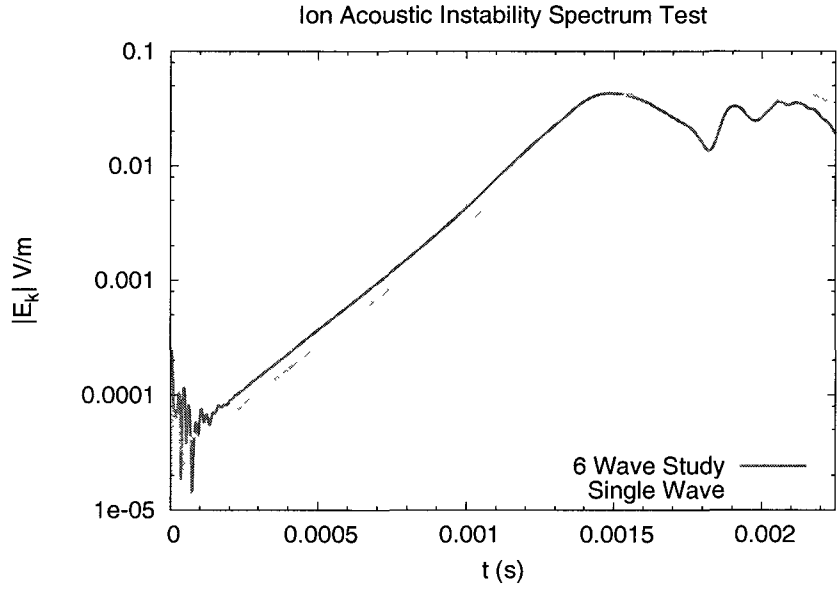

Figure 5-6: Multiple Wave Study of Quasilinear Saturation
The electric field for the fastest growing mode. The six wave study has $\alpha_e = 3.65 * 10^{-4}$ and $\alpha_i = 10^{-4}$. The rest of the parameters for the six wave run and those for the single wave run are given in Table 5.3.

dependence on drift velocity. The drift velocity sets the stability of the system. For a drift velocity less than the critical velocity, the system damps in the linear regime. Saturation is triggered by plateau development which differs with growth rates and, thus indirectly, with drift velocity.

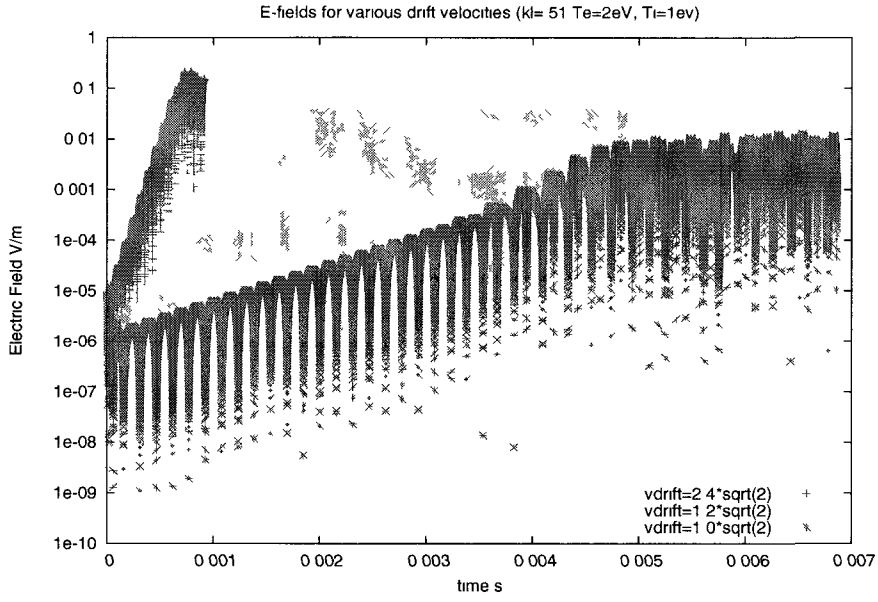

Figure 5-7: Quasilinear saturation as a function of drift velocity. As the drift velocity increases, the saturation value also increases.

From the trials presented here, we have shown that the saturation energy depends on particle drifts and temperature. The saturation time has a dependence on those quantities and also perturbation size. In the next section, we examine the theories for predicting these quantities.

5.3 Quasilinear Theory and Results

5.3.1 Saturation and Plateau

The current driven ion acoustic instability (CDIAI) is a wave-particle (Landau) resonance phenomena arising from the drift of electrons relative to ions above some critical velocity. The linear behavior of both the stable and unstable cases gives way to quasilinear behavior at some time. The electric field grows (or damps) until quasilinear saturation occurs at which point the wave levels off. This quasilinear saturation point is characterized by the formation of a plateau in the electron distribution about the wave speed. As energy is exchanged with the wave, the particles are redistributed (scattered) so that the velocity gradient smooths out. Landau damping (and growth) is dependent on this gradient. It can be easily seen that when it goes to zero, the wave will stop its growth or decay. Figure 5-8 shows the instability in the electric field at one point in space which corresponds to the distribution in Figure 5-9. Figure 5-9 shows the development of the quasilinear plateau in the electron distribution.

The prediction of the saturation time and the electric field energy at that time is still very much an open problem. Electric field energy could be determined from the initial condition and the exponential growth given from the dispersion relation. This hinges on accurate prediction of the saturation time. From Galeev and Sagdeev [GS84], the quasilinear diffusion time is predictable from the diffusion coefficient. However, this approach seems better suited to the cases where a large potential is applied at the initial condition and not for cases where the potential grows significantly. Nevertheless, we present that calculation here for comparison. The relaxation (diffusion) time is estimated below. Here, $\Delta(\omega/k)$ is twice the bounce velocity.

$$\tau_R = \frac{[\Delta(\omega/k)]^3}{e^2 \sum_k |E_k|^2/m_e^2 k^2} \tag{5.20}$$

$$= \frac{[\Delta(\omega/k)]^2}{D} \tag{5.21}$$

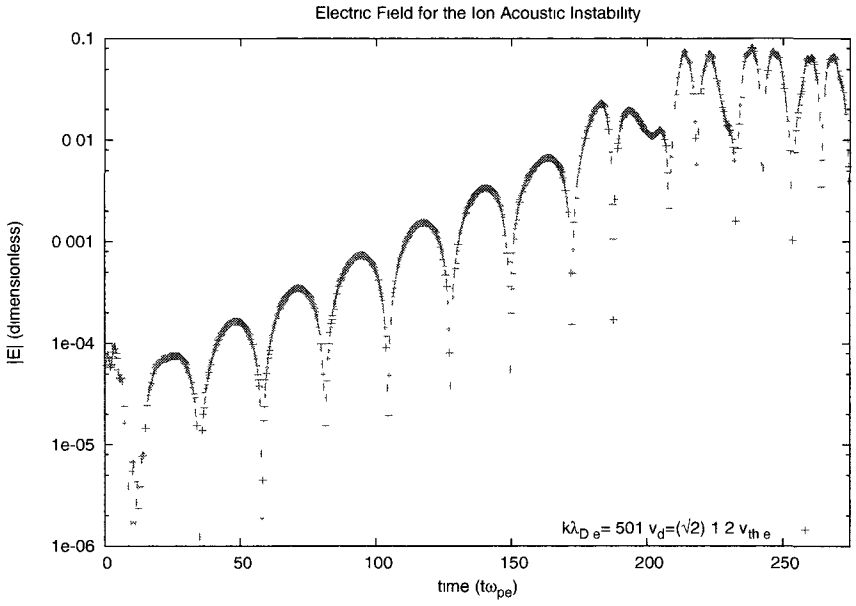

Figure 5-8: Current Driven Ion Acoustic Instability in the electric field
This is the maximum field for $T_e/T_i = 2$. At about t=200, the behavior of the electric field begins to change. This is the quasilinear saturation point.

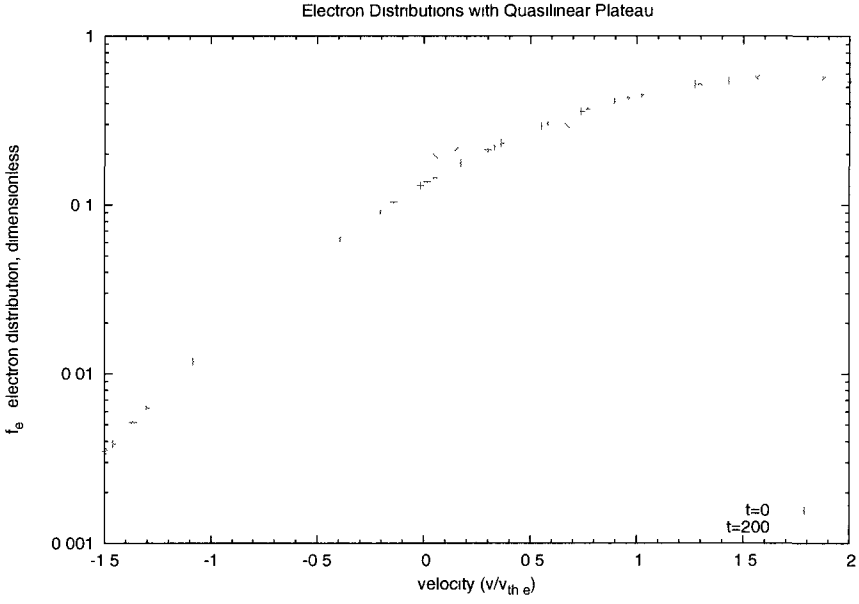

Figure 5-9: The quasilinear plateau
Electron distribution at $t\omega_{pe} = 0$ and $t\omega_{pe} = 200$ when the plateau has developed. Also plotted are the phase velocity in pink at $v = 0.27v_{th,e}$, the resonance region which is defined by the two light blue lines (given by Vedenov [Ved63]), and the ion acoustic speed (from eq. 5.3) in dark blue at $v = 0.28144v_{th,e}$.

Buchner and Elkina [BE06] estimate that the trapping frequency is approximately equal to the growth rate and estimate the saturation time eq 5.24

$$E_{sat} = \delta E_0 e^{\gamma \tau_{sat}} \tag{5.22}$$

$$\omega_t = \sqrt{\frac{eE_{sat}}{mk}} k \tag{5.23}$$

$$t_{sat} = \frac{1}{\gamma} ln \left(\frac{\gamma^2 m_e}{\delta E_0 e k} \right) \tag{5.24}$$

These estimates of saturation time are missing a vital component. They both depend on the energy at saturation time. This is problematic since it cannot be known a priori. Galeev and Sagdeev, as in other textbooks [KT73] show that the energy is dependent on the particle distributions.

$$|E_k|^2 = 2\pi^2 m_e \left(\frac{\omega_{pe}^2}{k^3} \right) n_0 \int_{v_1}^{\omega_p/k} [f_0(v, t \to \infty) - f_0(v, 0)] dv \tag{5.25}$$

The obvious problem with this is that this is written for the linear regime and assumes that the nonlinear regime is in the long time limit. Nevertheless, if the resonance regime and the quasilinear distribution is known, this form could be used. The region of the plateau, the resonance region, is given in Nicholson [Nic83] as the phase velocity plus or minus the trapping velocity. The trapping velocity changes as the instability grows.

$$\Delta v = v_{phase} - v_{trap} \tag{5.26}$$

$$v_{trap} = 2 \left(\frac{eE_1}{mk} \right)^{1/2} \tag{5.27}$$

This is first given by Vedenov [Ved63] . The idea behind this limit is straightforward. As the field grows, a potential well forms that traps particles. The trapped particle trajectories are altered. The particles distribute themselves along the well at varying rates. The space average of this redistribution is the plateau in velocity space. Figure

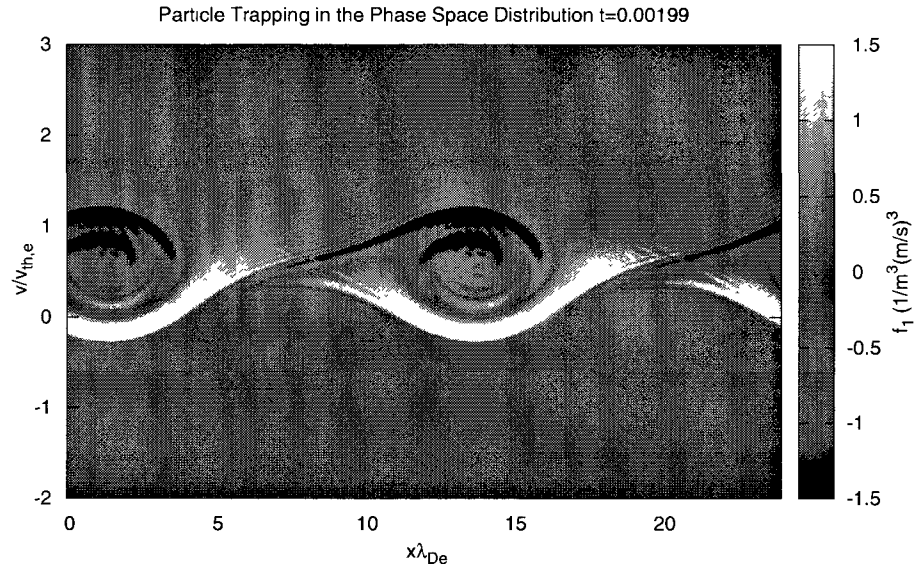

Figure 5-10: Particle Trapping in Phase Space Distributions
Electron distribution($f_1(x,v)$) in phase space shows the potential well. This is generated by the Kinetic Code.

5-10 shows the phase space distribution at a late time and that the potential well has formed. Some assumption on the analytical form of the plateau function needs to be assumed to use equation 5.25.

5.3.2 High Energy Ion Tail

Thus far, the discussion of quasilinear saturation has centered on the electron evolution. The ions are also evolved quasilinearly and have a measurable effect on the instability [IH81], [IH83], [IH84]. Like electrons, the resonant ions are scattered by the wave, attempting to form a plateau. Non-resonant ions are also diffused by a quasilinear mechanism, generating a high energy ion tail. The space averaged ion distribution grows a tail at approximately the electron thermal energy. When the tail becomes significant, the instability growth rate begins to slow. This contribution

to quasilinear evolution of the field complicates accurate prediction of the saturation energy and time.

Figure 5-11 shows the growth of the ion tail into the nonlinear regime. Near saturation, $t = 0.00199s$, the ion tail is apparent. It is apparent by comparing figures 5-11 and 5-12 that the slowing of the instability near saturation coincides with a dramatic growth in the tail. Movies of distribution evolution show this very nicely.

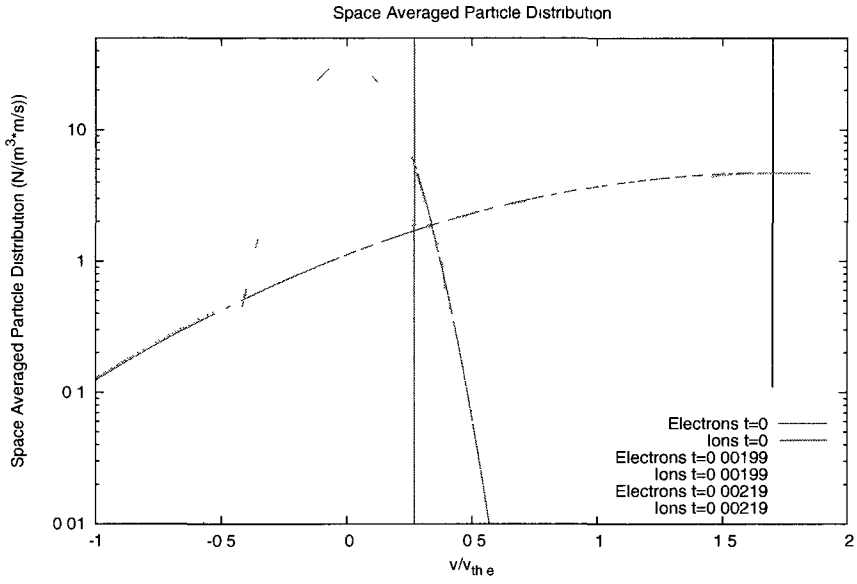

Figure 5-11: High Energy Ion Tail
Electron and Ion distributions through saturation. The vertical blue line is at the phase velocity. The vertical black line is at the electron drift speed.

We should note here that when ion-ion collisions are included, as in the next chapter, this tail is modified. The collisions will tend to "undo" the tail by their equilibrating nature.

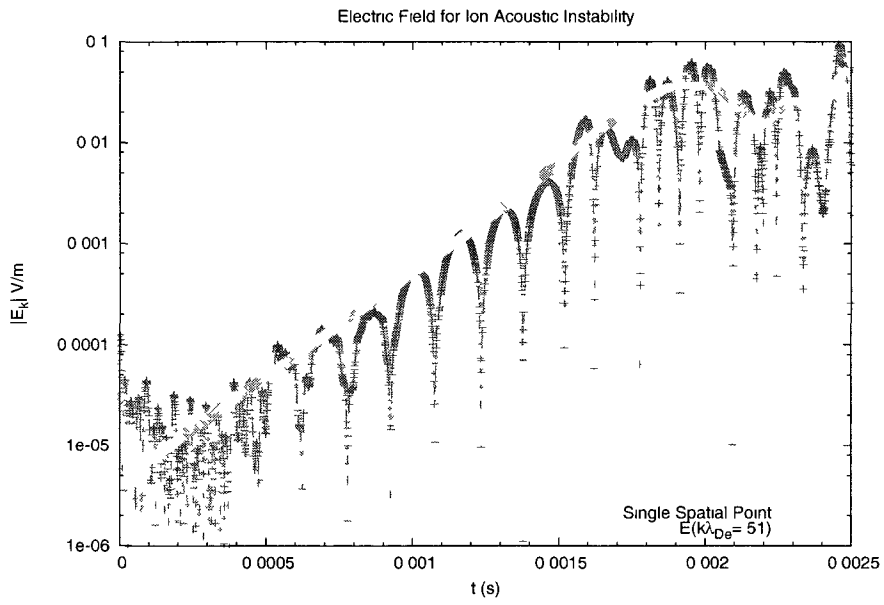

Figure 5-12: Instability from Spectrum Initial Condition
The electric field at a single point in space ($n_x = 32$) and for the fastest growing mode.

5.4 Anomalous Resistivity

The scattering of particles in phase space generates an effective collision frequency. The calculation of a total effective collision frequency needs to include both electron and ion contributions, but the focus of most studies is on the electron effective collisionality. The quasilinear plateau formed in the electron distribution induces a type of collisionless resistivity termed "anomalous" resistivity (ar). A simple force law gives the effective collision frequency as derived by Davidson and Gladd [DG75].

$$\nu = -\frac{1}{p_e}\frac{\partial p_e}{\partial t} \tag{5.28}$$

The anomalous resistivity equation is found by exploiting $qE = \eta J$ and using the definition of the current.

$$\eta = \frac{m_e}{n_e q_e^2}\left(-\frac{1}{p_e}\frac{\partial p_e}{\partial t}\right) \tag{5.29}$$

Predicting resistivity from theory is quite challenging. Various estimates exist from Galeev and Sagdeev [SG69] for different approximations, but they all use the weak quasilinear and high temperature ratio, $T_e >> T_i$, approximation.

$$\nu = \omega_{pe}\frac{\epsilon_o \delta E^2}{2nk_b T_e} \tag{5.30}$$

$$\eta = \frac{\nu}{\epsilon_o \omega_{pe}^2} \tag{5.31}$$

$$= \frac{\delta E^2}{\omega_{pe} 2nk_b T_e} \tag{5.32}$$

$$= \frac{W}{\epsilon_o \omega_{pe} nk_b T_e} \tag{5.33}$$

Energy density is calculated as $W = \epsilon_0 \delta E^2/2$. We will note later on that wave energy definition is given differently for different studies.

Since there are limited predictions from theory on the behavior of the wave-particle resistivity, results from the Kinetic Code will be compared with other numerical results. First, the resistivity calculation in the code is discussed. At each simulation time step, Δt_{sim}, the space averaged momentum is calculated. Then at each output time step, Δt_{out}, the effective collision frequency is calculated from the Davidson and Gladd form of effective collision frequency, eq. 5.28. The term $\left\langle \frac{dp_e}{dt} \right\rangle$ is calculated as seen below.

$$\left\langle \frac{dp_e}{dt} \right\rangle = \left\langle \frac{p_e(t + \Delta t_{sim}) - p_e(t)}{\Delta t_{sim}} \right\rangle \tag{5.34}$$

Figure 5-13 shows the resistivity calculated for the parameters in Table 5.3 with corresponding electric field in figure 5-4. It shows that the resistivity grows until saturation time, at which point it begins to oscillate.

5.4.1 Watt and Hellinger

Among the first researchers to perform simulations of the ion acoustic instability and anomalous resistivity were Watt, Petkaki, Horne and Freeman [WHF02], [PWHF03],

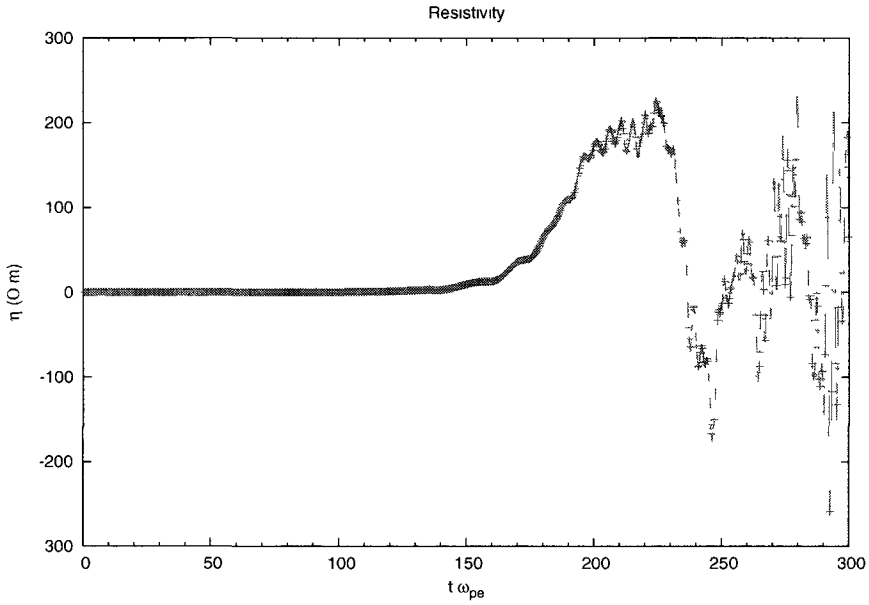

Figure 5-13: Anomalous Resistivity for the Ion Acoustic instability. For this study $\alpha_i = \alpha_e = 10^{-4}$.

[PFK+06], [PF08]. They used a Maxwell-Ampere solver with a white noise electric field for the initial condition. They use 642 spatial grid points in a periodic box and 891 velocity grid points for electrons and 289 velocity grid points for ions. The system size is set spatially to the longest unstable wavelength. They analyze the fastest growing mode. The data parameters in Table 5.3 correspond to these studies.

The test shown in figure 5-4 and 5-13 are compared with the results given in [PFK+06] to benchmark the Kinetic Code. First, it is noted that the saturation value they recover in the electric field is smaller by an order of magnitude than the data presented here. They also show a large structure in the nonlinear regime, where our result is fairly stable with only small oscillations. The resistivity, however, shows agreement in magnitude at saturation with the results of Petkaki and Freeman.

There is also a notable difference in the evolution of the phase space distributions between our results and those of Petkaki. Near quasilinear saturation and in the nonlinear regime, they show the formation of small potential wells. Our results do

not show these. Figure 5-14 shows the distribution at $t = 0.00224s$. This corresponds to the $m_i = 25m_e$ data in figure 5-16. These potential wells are believed to have a

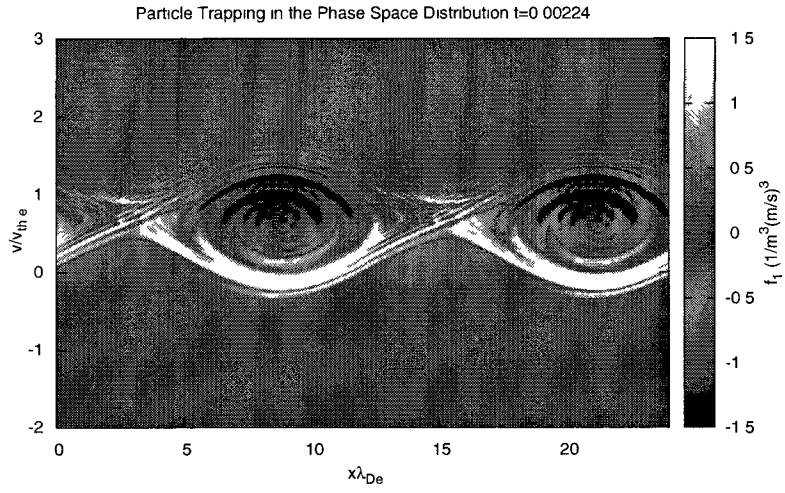

Figure 5-14: Phase Space Distribution for Instability, nonlinear regime
The electron phase space distribution at $t = 0.00224s$

dramatic effect on resistivity as particles scatter off them. These small scale structures may also have some nonlinear effect on the energy of the fastest growing mode.

The most significant finding of the work of Petkaki et al. and Watt et al. [WHF02] is that the quasilinear theory does not well describe the quasilinear regime. Anomalous resistivity is calculated following Sagdeev by using electric field data to calculate energy density. However, Watt states that the energy density is given by $\delta E^2 = \frac{\epsilon_0}{2} \int dk |E_k|^2$. This is clearly a total energy and not a density. They show that it is orders of magnitude smaller than the resistivity values from their code.

This work is followed by Hellinger et al. [HTM04] who do a realistic mass ratio study with a Vlasov-Poisson solver initialized with a spectrum of wavenumbers. They show much better agreement between resistive theory and numerical results. Hellinger

uses the energy form $\delta E^2 = \sum_i^{N_x} \delta E_i^2/N_x$. They show no significant structure in the nonlinear regime of the anomalous resistivity or the electric field. These differences with Petkaki's results are attributed to the use of a real mass ratio.

Here, our own comparison with theory is made. According to Parseval's theorem, the total energy calculations used by Watt and Hellinger are the same. Here we compare the effective collision frequency calculated from equation 5.30 using two different forms of energy density. First we used the space averaged energy, as Hellinger does. Then we use the average energy density from the fastest growing Fourier mode as given in equation 5.41. This is the contribution to fastest growing mode (FGM) to the average energy. To arrive at the equation, first note the discrete form of Parseval's theorem 5.35, where E_i contains the spatial dependence and E_k is the Fourier transformed field.

$$\sum_{i=0}^{N-1} |E_i|^2 = \frac{1}{N} \sum_{k=0}^{N-1} |E_k|^2 \tag{5.35}$$

This means that the actual integral form is related to the summation form as follow.

$$\int |E(x)|^2 dx = \sum_{i=0}^{N-1} |E_i|^2 dx \tag{5.36}$$

$$= \sum_{k=0}^{N-1} |E_k|^2 dx \tag{5.37}$$

Since the space average of energy is directly related to the average of the Fourier transformed version, the single mode average,$Wavg_{FGM}$, is given by equation 5.41

$$W_E = (1/2)\epsilon_0 \frac{\int |E_k|^2 dk}{L} \tag{5.38}$$

$$= (1/2)\epsilon_0 \sum |E_k|^2 dx \tag{5.39}$$

$$W_{FGM} = (1/2)\epsilon_0 |E_{k,FGM}|^2 dx \tag{5.40}$$

$$Wavg_{FGM} = (1/2)\epsilon_0 \frac{|E_{k,FGM}|^2}{nx} \tag{5.41}$$

It turns out that there is not a significant difference between them, but Hellinger's approach fits the data very nicely as shown in figure 5-15. This is not surprising

since the Kinetic Code calculates the effective collision frequency from a space average. From this point on, the Hellinger definition of energy will be used. The figure shows that the analytical estimate remains close to but less than the actual resistivity through the linear regime. Near quasilinear saturation, the analytical estimate overshoots the actual value.

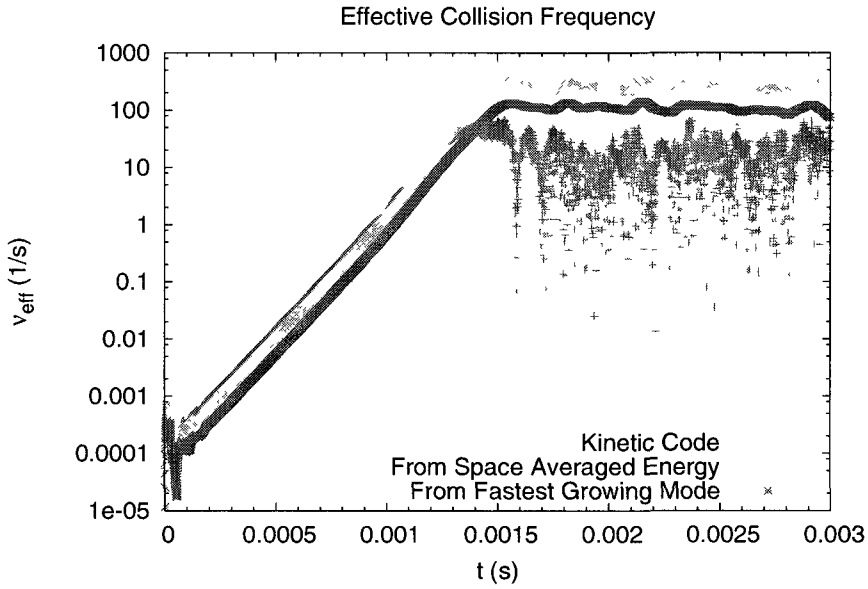

Figure 5-15: Effective Collision Frequency Calculations From Various Energies The effective collision frequency is calculated in the Kinetic Code and compared with Sagdeev's theory using space averaged energy and the average energy from the fastest growing mode only. Both definitions yield qualitatively similar results.

$$\nu = \alpha\omega_{pi}\frac{v_{drift,e}T_e}{C_sT_i} \tag{5.42}$$

Here we also compare with the estimates of Sagdeev based on laboratory experiment, equation 5.42. He fits data and finds that $\alpha = .01$. Table 5.4 shows that this estimate does not agree well with the effective collision frequency at quasilinear saturation. For this equation to fit data from the Kinetic Code, α must be about 0.0002.

T_e/T_i	2	20
Sagdeev Estimate	5066 1/s	50660 1/s
Kinetic Code	55 1/s	563 1/s

Table 5.4: Sagdeev Formula Compared with Saturated Effective Collision Frequency
The Sagdeev formula is given in equation 5.42. The parameters for these data set are given in tables 5.3 and 5.5

Next the role of mass in saturation and resistivity can be examined. Figure 5-16 shows that while the saturated field drops with increasing ion mass, it does not vary over many orders of magnitude. A similar result is obtained from the resistivity study as seen in figure 5-17.

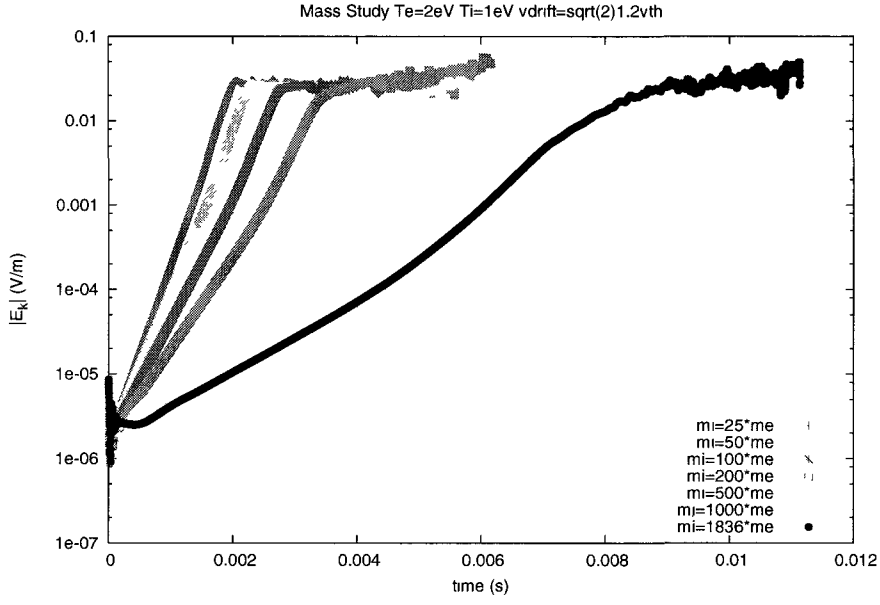

Figure 5-16: Instability and Saturation Dependance on Mass
The saturated wave energy does not vary significantly with change in mass.

Figure 5-18 demonstrates that the anomalous resistivity estimate is not significantly altered for a large mass ratio.

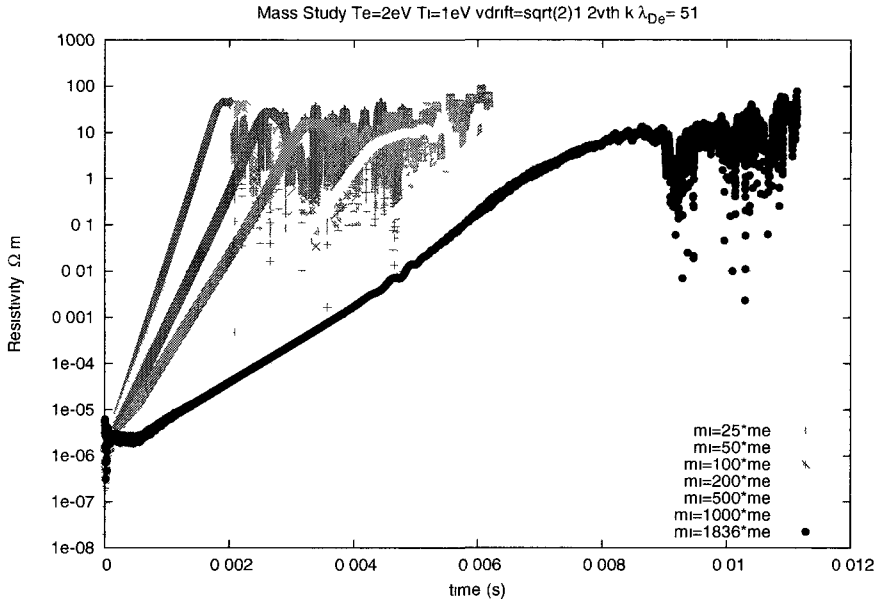

Figure 5-17: Resistivity with varying mass ratio
The resistivity does not show significant change with mass.

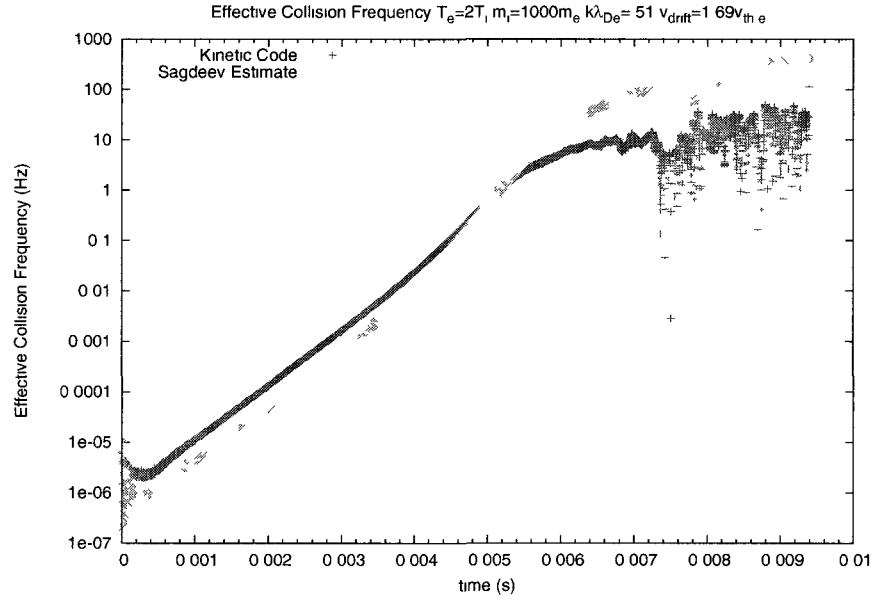

Figure 5-18: Anomalous Resistivity Comparison with Analytical Estimate for mi=1000me.

Corresponding electric field data is given in figure 5-16

Parameter	Value
nx	64
nv	20000
α_i	10^{-5}
α_e	10^{-5}
wavenumber, $k_x\lambda_{De}$	.51
lx	$4\pi/k_x$
U_i	40000
U_e	600000
m_e	$9.11 * 10^{-}31$ kg
m_i	$25m_e$
v_{drift}	$1.7v_{th,e}$
T_e	$20eV$
T_i	$1eV$
n_0	$7 * 10^6(1/m)$
$v_{th,e}$	$1.8742 * 10^6$ m/s
$v_{th,i}$	83816.7 m/s
λ_{De}	12.5712 m
ω_{pe}	$1.49086 * 10^5$ Hz
ω_{pi}	$2.98 * 10^4$ Hz

Table 5.5: Parameters for High Temperature Resistivity Study
This table is a complete list of the parameters implemented for the $T_e = 20T_i$.

5.5 High Temperature Ratio Study

Finally, we present the same study for a high temperature ratio. Table 5.5 gives the parameters for this study. The analytical theories are for the high temperature difference regime. It is tested for major differences from the low temperature study.

We see that there appears to be slightly better agreement with theory in the high temperature case than in the low temperature case, at least through the linear regime. The nonlinear regime does not show any better agreement.

5.6 Discussion

In this chapter, we have shown that the Kinetic Code accurately recovers the ion acoustic and current driven ion acoustic modes. We have recovered a converged

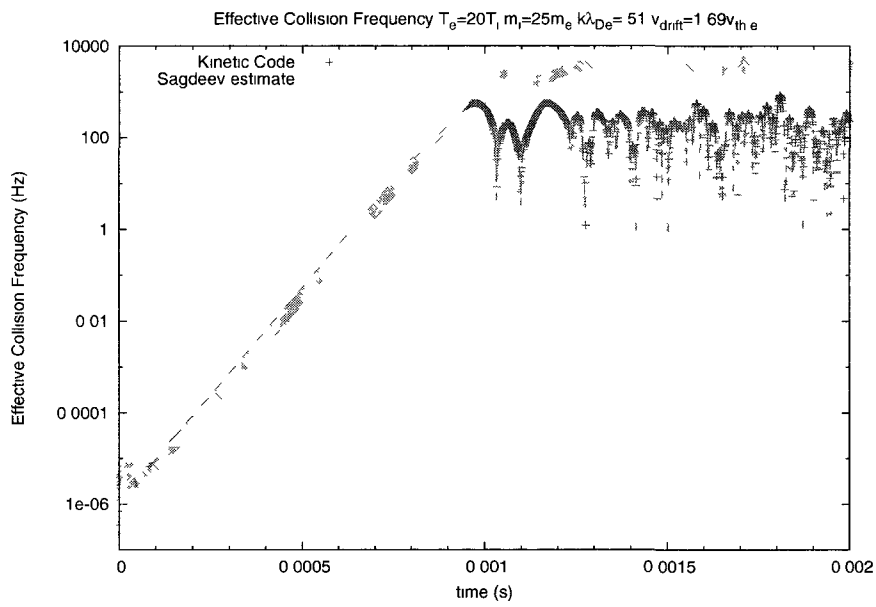

Figure 5-19: Effective Collision Frequency For High Temperature Ratio Comparison of data with analytical estimates. Corresponding electric field data is given in figure 5-16

instability saturation that is in disagreement with other current numerical results, i.e., those of Petkaki and Watt. We find agreement with Hellinger's studies, but argue that the discrepancy with Watt is not due to unrealistic mass ratio. The discrepancy is likely due to dynamic phase space holes seen in their data. The origin of these holes is not yet well understood.

The effective collision frequencies of the instability are also examined. We dispute the findings of Watt et al. that the Sagdeev estimate does not well describe the resistivity at quasilinear saturation in the $T_e \sim T_i$ regime. We show that this agreement also holds for the $T_e > T_i$ regime, the regime for which the theory was derived.

Based on the studies presented here, it is easy to see that distinguishing the linear from weakly nonlinear regime is a subtle task. The estimates of Sagdeev for anomalous resistivity could potentially be used as a diagnostic tool to help identify this boundary.

It would be interesting, in the future, to also examine resistivity generated from ion scattering. This could be considerable and of importance for some systems.

CHAPTER 6

Collisional Ion Acoustic Waves and Instability

When sound waves propagate through air, they are propagating through a medium with high molecular collisionality. The collisional effects have little damping effect on the wave. Ion acoustic waves in plasmas, though analogous to acoustic waves, are highly sensitive to weak particle collisions. For very weak collisionality, changes to the wave particle resonance may be more significant than the viscosity introduced.

In unstable collisional systems, the development of the quasilinear plateau and the effects of collisions play competing roles. The collisions tend to destroy any structures that form in the distributions and return it to the Maxwellian equilibrium. The plateau is very much a non Maxwellian structure. Traditionally, the dominance of one of these effects over the other is determined by the temporal scales (or spatial as the case may be). If the collision time is much smaller than the saturation time, the plateau development will be inhibited or prevented entirely. The saturation time is in part dependent on the size of the wave perturbation. For large perturbations, the quasilinear process can overcome the effect of weak collisions [Ved63], as well.

The various types of particle collisions have different impacts on the instability. Electron-electron collisions will directly compete with the electron plateau formation responsible for saturation. Electron-ion collisions are also likely to compete with the plateau formation as they will act to thermalize electrons. We will note later on

that the effects of these collisions was not clear initially. Ion-ion collisions are a bit subtle in such a system. They do not directly effect the plateau formation in the electron distribution. Their impact is exclusively on the ion distribution function. The modified evolution of the ion distribution leads to changes in the wave, which in turn alter the electron plateau formation. Kulsrud and Shen [KS66] show that ion-ion collisions have two effects on the wave: a viscous damping and a slowing of the wave speed. Because the ion contribution to the instability is one of damping anyway, ion collisions may not have quite as dramatic an effect as electron collisions.

In the ion acoustic system, the ions resonate with the wave and, as we have seen in the Landau damping/quasilinear plateau discussion, the ions take energy from the wave. This energy accelerates particles moving slower than the phase velocity. This leads to what is known as the high energy ion tail.

The weakly collisional regime has interesting consequences for anomalous resistivity, as well. There are no theories for this area of study yet. However, we will show in section 6.2, that the resistivity for an instability drops with the inclusion of weak ion-ion collisions. This is, perhaps, contrary to what one might think initially. However, anomalous resistivity, being due to electron scattering about the resonance, does not directly carry information about the ion interactions. The slowing of the wave speed by the ion collisions reduces the ability of the wave to scatter electrons, at least in part. Also examined are the effects of electron-electron collisions. It is shown that the resistivity rises for this case.

In this chapter, we begin with a discussion of the existing collisional theories for the current driven ion wave in section 6.1. These are used to guide the benchmarking of the collisional Kinetic Code for the instability, as neither an exact theory nor a numerical method has been written for the cases presented here. Besides the existing theories, another growth rate is estimated from data. In section 6.2, numerical re-

sults of the collisional ion acoustic instability are presented. We show that the electric field and effective resistivity both decay with increasing collisionality. The qualitative properties agree with Kulsrud and Shen. The electric field damping rate shows agreement with the theories tested. Comparison of collisionless anomalous resistivity data with the predictions of Sagdeev's collisionless estimates are also presented. There is good agreement between the two for very weak collisions. Finally, we discuss the implications of this and plans for future work in 6.3.

6.1 Existing Collisional Studies

The benchmark of the collisional ion waves has proven challenging. While Skiff et al. [SSMN$^+$98] have studied the collisional ion waves both numerically and experimentally, they recover the ion distribution modes of the spatially damping current driven ion acoustic wave. The Kinetic Code was written for the temporal problem so, one must turn back to the literature for guidance on the problem.

Many studies of collisional modes for the ion acoustic wave have been made [BV05] [BN00] [Kuc64] [Sha90] [TWE$^+$93] and it appears that collisional effects are analogous to that of the Langmuir waves [SSMS98]. However, the current driven wave needs to be considered more carefully. This has been done by Bhadra and Varma [BV64], Stéfant [Ste71] and Kulsrud and Shen [KS66] among others [SK73]. The work of Kulsrud and Shen [KS66] is generally viewed as the standard for same species collisions. Their interspecies collision results were disputed by Epperlein, Short, and Simon [ESS92]. Kulsrud and Shen argue that e-i collisions can enhance the instability. Epperlain et al. showed much later that this effect is always smaller than the equilibrating, viscous effect of the collisions. Thus, collisions will always have a damping effect on the wave. The works of Kulsrud and Shen, and Stéfant are used in this study. Kulsrud and Shen (KS) [KS66] used the Landau (integral Fokker-Planck)

operator in their study. They note that e-e and i-i collisions produce the same effect on the critical current, but on a different scale. They show that the critical current for the i-i collision case should increase as ion viscosity from collisions increases. They also show that the wave speed slows which increases ion Landau damping. This also inhibits the instability. Kulsrud and Shen make an estimate of the ion collisional effects on the phase velocity and critical current using long wavelength approximations and a relaxed high temperature ratio requirement. Equation 6.1 shows the phase velocity equation with the slowing due to i-i collisions.

$$\frac{\omega_r}{k} = \left(\frac{k_B T_e}{m_i}\right)^{1/2} \left[\frac{2T_e + 3T_i}{2T_e} - \frac{1}{\omega_r \tau_i}\frac{1}{3}\sqrt{\frac{\pi}{2}}\left(\frac{T_e}{T_i}\right)^2 exp\left(-\left(\frac{T_e + 3T_i}{2T_e}\right)\right)\right] \tag{6.1}$$

$$\omega_r = \frac{-k}{2} C_s \frac{2T_e + 3T_i}{2T_e} \pm \frac{k}{2}\sqrt{C_s^2\left(\frac{2T_e + 3T_i}{2T_e}\right)^2 - \frac{4\nu_i C_s}{3k\sqrt{8\pi}}\left(\frac{T_e}{T_i}\right)^2 exp\left(-\left(\frac{T_e + 3T_i}{2T_e}\right)\right)} \tag{6.2}$$

This quadratic equation yields a messy solution, but it will be compared nonetheless with numerical results. Here we have used $\tau_i = 2\pi/\nu_i$, where τ_i is the time between ion collisions and $C_s = \sqrt{T_e/m_i}$. This solution says that the wave frequency has a $\nu_i^{1/2}$ dependance rather than the ν dependance of the damping rates. However, the data recovered from simulations do not agree with this result. In general, it is a more difficult problem to recover collisional effects on phase velocity than on growth and damping rates. The lack of agreement suggests that the Lenard and Bernstein operator needs to be evaluated specifically in this context.

Stéfant [Ste71] uses a density and momentum conserving BGK operator (eq. 6.3) to solve the linear current driven problem. (See appendix C.2.) He derives the dispersion relation by integrating along orbit trajectories and assuming small electron

Z-function and large ion Z-function.

$$\frac{\partial f}{\partial t}|_c = -\nu_{s,s}\left[f_{1,s} - (N_{1,s}/N_0) f_{0,s}(v-u_0)\right] + \nu_{s,r}(m_s/k_B T_s)\left[q_r \cdot (v-u_0)\right] f_{0,s}(v-u_0) \tag{6.3}$$

$$q_r = \int v f_{1,r} d^3v - N_{1,r}(u_0/N_0) \tag{6.4}$$

$$\gamma = \gamma_L - \nu/2 \tag{6.5}$$

From this, the critical current and damping rates are found. He recovers the critical velocity of Kulsrud and Shen for the ion-ion collisions, in the long wavelength and $T_e >> T_i$ regime, with the exception of a factor of 16/15 in the ion viscosity term. Thus this damping rate serves as a substitute for Kulsrud and Shen in the high temperature regime. The damping rate is given in equation 6.5, where γ_L is the Landau growth rate. Tables 6.1 and 6.2 show comparisons of data with this theory.

Here, another damping rate is posited. The approaches of NBS, Lenard and Bernstein, and many other approaches, show that collisions will alter the frequencies by a factor of $i\nu$ times some factor. Testing of data to this strict definition did not yield good fits. An educated guess led to the modification of this damping rate by the dimensionless ion sound speed. The following rate is compared with simulation data in the next section and shows a good fit for the low temperature regime.

$$\gamma = \gamma_L - \nu \frac{\sqrt{T_e/T_i}}{\sqrt{m_i/m_e}} \tag{6.6}$$

6.2 Numerical results of collisional ion waves

The Lenard-Bernstein operator is first implemented for ion-ion collisions which minimizes the poor conservation properties of the operator. In this section two temperature ratios are examined $T_e/T_i = 2$ and $T_e/T_i = 20$ for the same wavelength and drift

velocity.

$$\frac{\partial f_e}{\partial t} + v\frac{\partial f_e}{\partial x} + \frac{q_e E}{m_e}\frac{\partial f_e}{\partial v} = 0 \tag{6.7}$$

$$\frac{\partial f_i}{\partial t} + v\frac{\partial f_i}{\partial x} + \frac{q_i E}{m_i}\frac{\partial f_i}{\partial v} = \nu_{ii}\frac{\partial}{\partial v}\left[v f_i + v_{th,i}\frac{\partial f_i}{\partial v}\right] \tag{6.8}$$

$$\nabla \cdot E = \frac{q_e}{\epsilon_o}\int_{-\infty}^{\infty} f_e(v)dv + \frac{q_i}{\epsilon_o}\int_{-\infty}^{\infty} f_i(v)dv \tag{6.9}$$

6.2.1 Wave Simulation Findings

Our simulation with the Lenard-Bernstein operator also sees an increase in critical current and a decrease in the wave speed. Figure 6-2 shows the instability for various collision frequencies at a high temperature ratio. Note that the period of the wave oscillation is increasing as collision frequency increases. We see this behavior for the low temperature ratio as well. See figure 6-1.

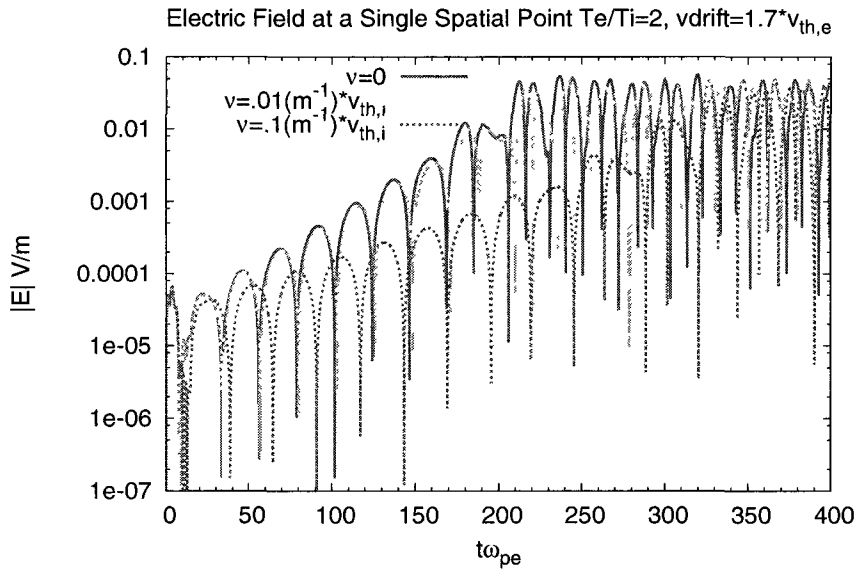

Figure 6-1: $Te/Ti = 2$. Electric field in time for a single point in space. The collision frequency, ν, varies above showing that the instability is inhibited by ion-ion collisions.

Not surprisingly, the Stéfant approach does not fit well in the low temperature

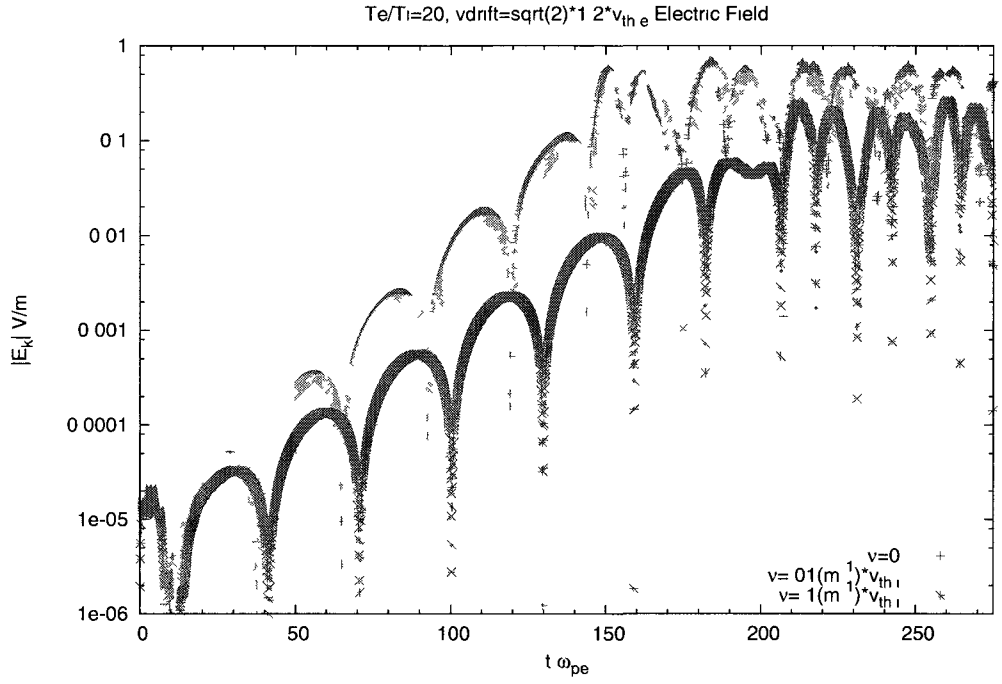

Figure 6-2: High temperature ratio electric field
$Te/Ti = 20$ kλ_{De}=.51. Electric field in time at a single point in space. The collision frequency, ν, varies above showing that the instability is inhibited by ion-ion collisions.

$\nu/v_{th,i}$	0	.01	.1
Data fit (1/s)	4863.64	4631.7	2875.77
r^2	0.99991887	0 99993155	0.99760775
Hypothesis (1/s)	4742.07	4626.57	2492.95
Stéfant (1/s)	measured	4444.56	672.81

Table 6.1: Growth rates for collisional $T_e = 2T_i$ instability
This table shows the predicted growth rates of the instability including ion-ion collisions and those recovered from fits to Kinetic Code data. Here ν is the ion collision frequency. The collisionless value from the data fit is used in the predictions presented here. The collisionless hypothesis growth rate is from the exact root given by the PDF Solver.

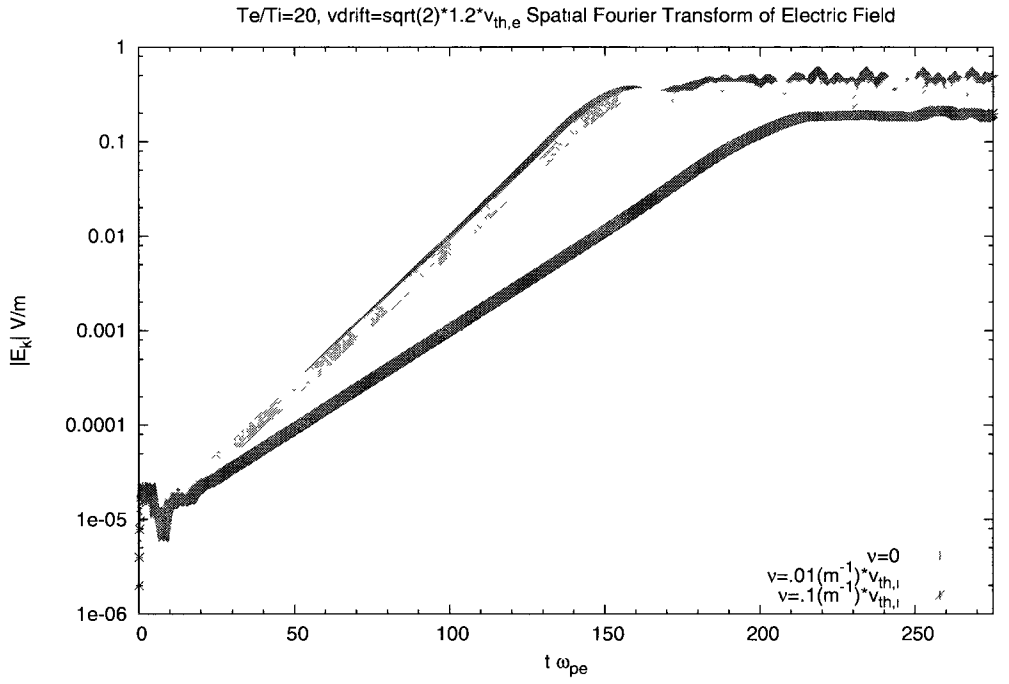

Figure 6-3: Fourier Transformed High Temperature Ratio Electric Field $Te/Ti = 20$ kλ_{De}=.51. Fastest growing mode of the electric field in time. The collision frequency, ν, varies above showing that the instability is inhibited by ion-ion collisions.

$\nu/v_{th,i}$	0	.01	.1
Fit (1/s)	11203.36	10740.74	7592.93
r^2	0.99994322	0.99992346	0.99992372
Stéfant (1/s)		10784.28	7012.525
% difference		.4	8.27
Hypothesis (1/s)		10828.52	7454.95
% difference		.8	1.8

Table 6.2: Growth rates, γ, for collisional $T_e = 20T_i$ instability
This table shows the predicted growth rate and the actual growth rates of instability including ion-ion collisions. Here ν is the ion collision frequency.

ratio regime. The NBS mode work as well as that of Lenard and Bernstein and the various studies mentioned above suggest that the ion acoustic waves should damp as $\gamma_{Landau} - \nu$ Here we examine the best fits to the collisional data with this prediction.

My prediction used for the low temperature ratio, equation 6.6, did not fit the high temperature data well. A cue was taken from Stéfant, which was based on a solid analytical foundation, and a factor of 1/2 was included. This greatly improved the fit.

$$\gamma = \gamma_L - \nu \frac{\sqrt{Te/Ti}}{2\sqrt{mi/me}} \tag{6.10}$$

This data is presented in Table 6.2 which shows that both predictions fit the data reasonably well for the weakly collisional regime. The Stéfant prediction may diverge very quickly from the data in a system with slightly higher collision frequencies. At a minimum, we can say that the collision operator that has been implemented in the Kinetic Code with the ion acoustic instability agrees reasonably well with the theories that exist for similar operators (Krook and Landau) in similar regimes.

6.2.2 Resistivity Simulation Findings

The resistivity is calculated for varying collision frequency and collision type in this section. Results of ion-ion collision tests are shown in figure 6-4. The resistivity

drops as collision frequency increases. This is due to the destruction of the wave-particle resonance by the collisions. However, the collisions are still weak enough not to generate a large resistivity on their own. Thus as collisions are increased, resistivity drops. We then calculated the resistivity from the simulation including weak collisions and see that the resistivity drops as collision frequency increases. As Kulsrud and Shen stated, the ion-ion collisions force the instability's critical velocity up. As a result, the resistivity drops for a given drift velocity.

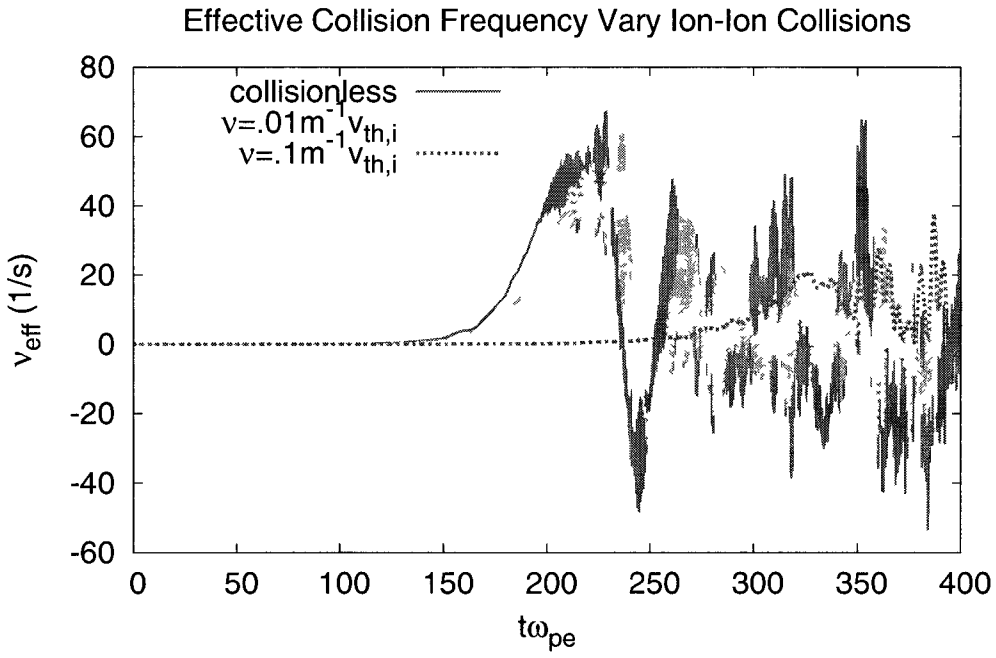

Figure 6-4: $Te/Ti = 2$. $k\lambda_{De} = .51$. Effective collision frequency from wave-particle scattering in time with varying collision frequency, ν.

We also examine the calculation of Sagdeev for the collisional systems. We find that Sagdeev's estimate still agrees with data largely due to its dependence on energy from the simulation. The Sagdeev estimate appears to be very good through the linear regime for a range of temperatures and collisionality. It seems potentially useful as a

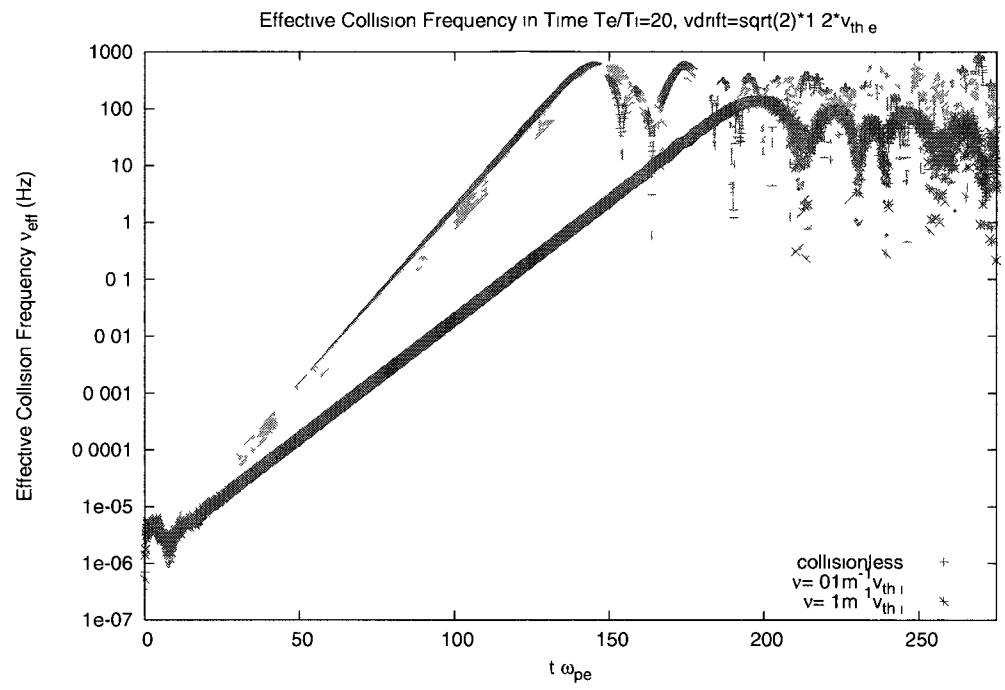

Figure 6-5: $Te/Ti = 20$. Instantaneous resistivity in time with varying collision frequency, ν.

tool to help estimate the onset of saturation.

Finally, the effect of electron-electron collisions on the wave-particle resistivity is explored here, despite the poor conservation properties outlined in Appendix C. A simple hypothesis is that if these collisions are very weak, they will not effect the instability growth. Thus, total collisionality of the system will be the wave-particle collision frequency plus the particle collision frequency. That hypothesis is tested in figure 6-8.

There is a significant perturbation difference between the $\nu_{ee} = 5.927(1/s)$ and collisionless runs. This is largely responsible for the delay in the saturation time. It is also notable that in the $\nu_{ee} = 59.27(1/s)$ run, the instability peaks and then dies away. The high particle collisionality dominates late times and is preventing turbulent scattering from occurring.

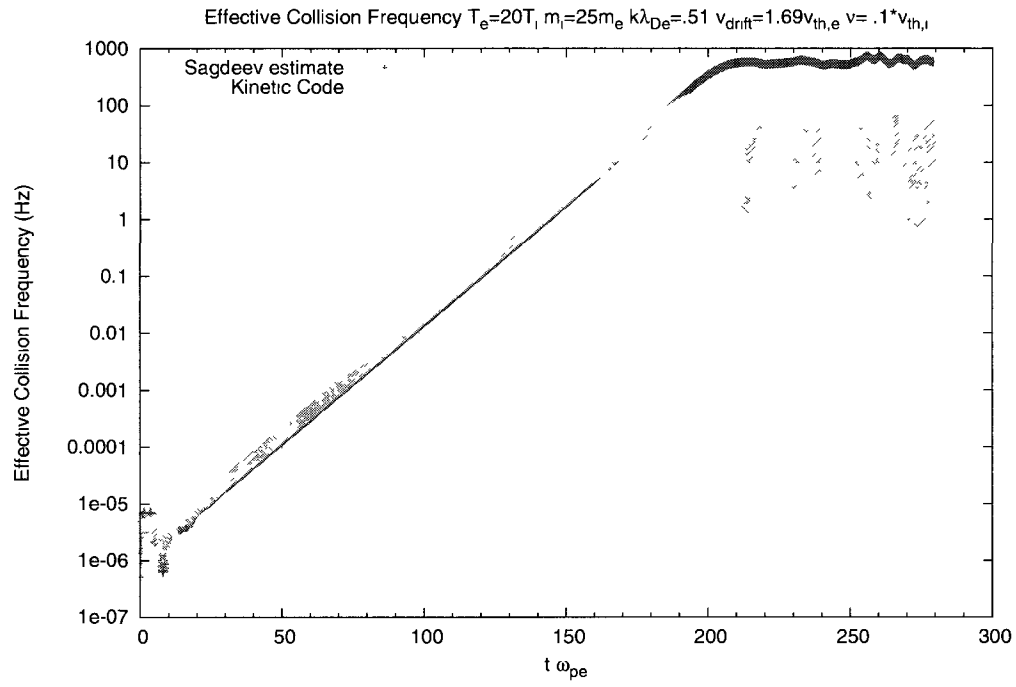

Figure 6-6: $Te/Ti = 20$. Effective collision frequency from the Kinetic Code and the estimates from Sagdeev for $\nu/v_{th,i} = .1$

We can see from figure 6-8 that the total effective collision frequency behaves differently in different temporal regions. Early in the simulation particle collisionality dominates. As the instability grows, so does the wave scattering of particles. At some time this collision frequency equals and then dominates over the particle collision frequency. For weak collisionality it appears that the wave-particle behaviors occur more or less unimpeded by the collisions. The higher e-e collisional study, i.e., e-e collision frequency approximately equal to wave-particle collision frequency at saturation time, demonstrates that in the weakly collisional systems, the total effective collision frequency is the wave-particle collisionality plus the particle collisionality.

We can see this quantitatively as well. The collisionless saturated ν_{eff} is about 50 (1/s). The $\nu_{ee} = 59.27$ has a peak value of 100-102 (1/s) and $\nu_{ee} = 5.927(1/s)$ has a peak value of about 56 (1/s).

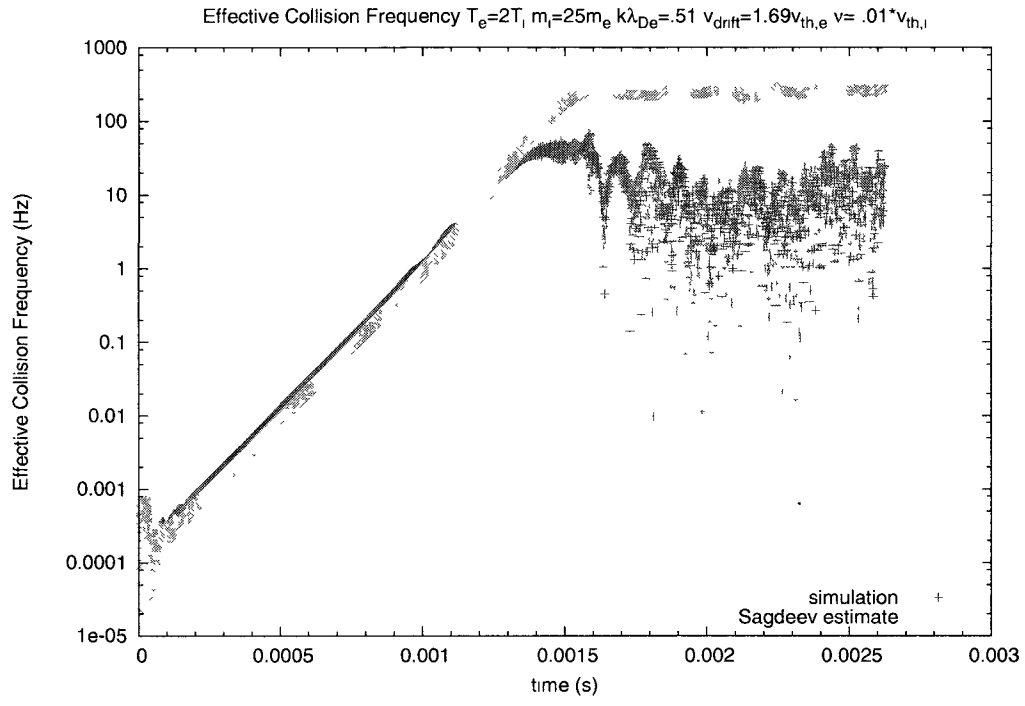

Figure 6-7: $Te/Ti = 2$, $\nu/v_{th,i} = .1$. Effective collision frequency from the Kinetic Code and the estimates from Sagdeev.

6.3 Discussion and Future Work

In this chapter we have presented ion acoustic instability numerical results with ion-ion collisions and electron-electron collisions. It has been demonstrated that ion-ion collisions modify the growth rate of the instability by a term proportional to νt. This is in agreement with the existing theories of operators similar to the Lenard-Bernstein operator. Anomalous resistivity results for the collisional system are also presented here for the first time. It is shown that the ion-ion collisions damp the electron scattering through changes to the wave by the ions.

Future work involves further benchmarking of the Kinetic Code by writing a temporal eigenmode solver for the collisional ion acoustic instability. The method used in the NBS work should be followed. This is critical to identifying the true damping rates and phase frequencies of the collisional ion acoustic wave.

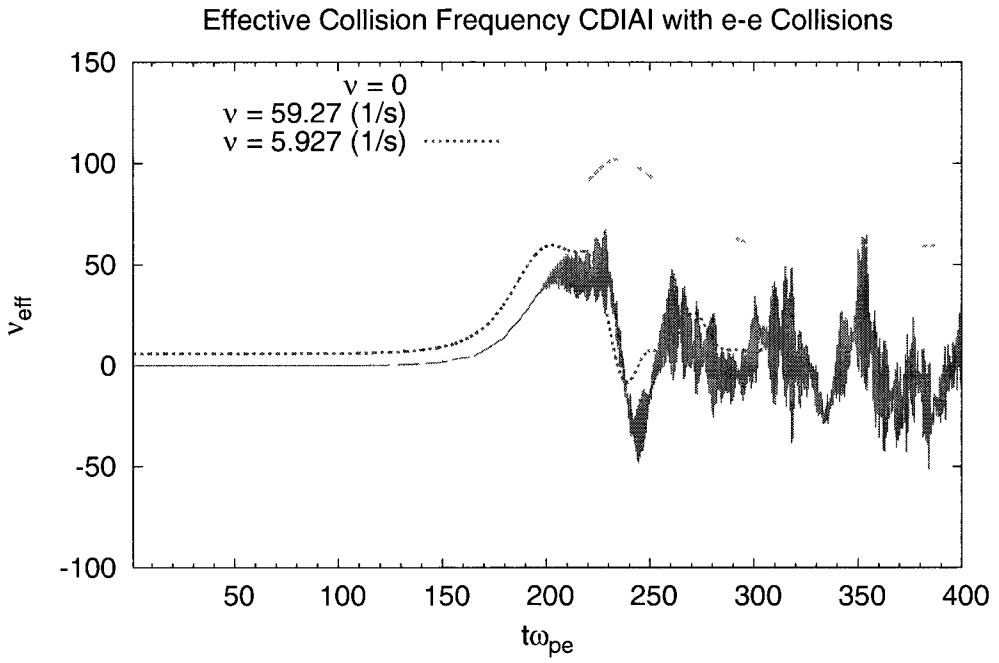

Figure 6-8: Effective Collision Frequency for Electron-Electron Collision Study $Te/Ti = 2.$ $k\lambda_{De} = .51, v_{drift} = 1.5.$ Electron collision frequency ν. The collisionless trial was given a slightly smaller perturbation ($\alpha_i = \alpha_e = 10^-4$) than the other two trials ($\alpha_e = 3.65 * 10^{-4}, \alpha_i = 10^{-4}$

Also, it would be beneficial to advancing theory and for comparison to experiment to implement a fully conservative form of the collision operator such as Dougherty's. This may address some of the discrepancies between the Lenard and Bernstein and Landau operators, such as why the wave frequencies do not agree.

A new anomalous resistivity theory could be developed that includes e-e collisions and follows the NBS approach. This could lead to a better understanding of the onset of the nonlinear regime and the saturation mechanism.

CHAPTER 7

Conclusion

The work presented in this thesis on nonlinear kinetic plasma phenomena was motivated by the experiments of Skiff et al. which demonstrated that theories for collisional plasma waves (Su and Oberman) were insufficient to describe the measured distributions. This led Ng, Bhattacharjee and Skiff to find the eigenmodes of the weakly collisional, Lenard-Bernstein Vlasov-Poisson system. The recovered modes are discrete and contain the Landau damped root as the least damped eigenmode. In this work, we set out to examine the effects of the spectrum discretization in various systems.

This was carried out using a new Vlasov-Poisson solver called the Kinetic Code written by Kai Germaschewski and modified to include the Lenard-Bernstein operator and multiple species options. This 1-D, 1-V code makes use of a velocity Hermite spectral method and finite difference spatial method with explicit time stepping.

The first nonlinear phenomena examined was the plasma wave echo. This was chosen for two reasons. Primarily, Su and Oberman had intended their study for the echo. Strictly speaking, the problem solved was for the collisional impact on the first order distribution. The echo is actually a second order phenomenon, but one that is generated from the first order interferences. The second reason for examining the echo was to determine if the NBS modes, which are the linear eigenmodes, are identifiable in the nonlinearity.

The study presented here shows that Su and Oberman's boundary layer approach

fits the data well. It fits very weakly collisional systems better than those with slightly larger collisionality, as is characteristic of an asymptotic solution. It appears that Su and Oberman obtained the appropriate general form for some time regime, perhaps not the long time regime.

The asymptotic solution shows that on the short time scale, the collisions do not have any effect on the system. For longer time scales, the effects of collisions on the resonance regime become important. This approximate solution does not apparently converge on the eigenmodes (the NBS modes). There is no indication that the asymptotic analysis recovers the discrete spectrum or the least damped eigenmode. Since a system will settle to its eigenmodes in the $t \rightarrow \infty$ limit, it is suggested that the very long time solution is not well approximated by the Su and Oberman analysis.

While the continuous eigenmode spectrum is destroyed in collisional systems, the behavior of the weakly collisional discrete modes may be very similar to and difficult to distinguish from the continuous spectrum. It is possible that the Su and Oberman result is recoverable from a summation of the NBS eigenmodes, given the very highly damped nature of some of these modes. However, this has been difficult to show.

The NBS approach needs to be implemented in the context of the echo. One test would be to decompose the echo into the eigenmode spectrum. This would indicate which modes are interfering to create the echo. The NBS modes contain the collisional contribution and may help to clarify the effect on the echo. However, numerical examinations of the NBS modes were not well enough resolved to carry this out. The collisional echo could be derived analytically using the hermite expansion of velocity space which reduces the Lenard-Bernstein operator to a single term. This may make the analysis easier. In any event, the interference of NBS modes is not easily predicted and should be examined to determine the discrepancy between Su

and Oberman and NBS.

As stated in Chapter 4, there may be some regime where the modes are dominated by a super-exponential collisional damping followed by a regime where the modes experience an exponential damping. I believe that the asymptotic matching of resonant and non-resonant regimes in the particle distributions needs to be revisited. The result for the resonant regime appears to be patched to the non resonant regime. The non resonant regime is assumed to suffer no collisions, but this is not entirely accurate. As collisionality increases, even for very weakly collisional plasmas, this non resonant contribution may become important.

The second part of this work focused on the ion acoustic instability and anomalous resistivity in collisional and collisionless systems. There are few analytical estimates or numerical studies on quasilinear saturation properties and anomalous resistivity. Collisionless results are compared with both types of studies. We show that agreement with the analytical estimates, which are dependent on the input from data, are in agreement in the quasilinear regime with code results. This agrees with other Vlasov-Poisson studies. Uniquely, we show this for two different temperature regimes.

The collisional study is also complicated by the lack of exact theories for the Lenard-Bernstein operator and the current driven wave. Analytical results for Landau and Krook collisions were compared with the numerical results. The Lenard-Bernstein, Krook and Landau operators all belong to the same family. It is shown that the ion-ion collisions contribute an exponential damping to the mode. The anomalous resistivity drops in this case due to its dependance on electron scattering only. An anomalous resistivity study of electron-electron collisions, shows that the total resistivity is approximately a sum of contributions from the particle collisions and the wave scattering. It is hypothesized that a similar calculation of the ion resistivity would yield the same relation.

Several future and ongoing projects have been presented so far. Foremost is the examination of the plasma wave echo under strong particle trapping in the collisional and collisionless systems. On the ion acoustic front, further examination of electron collisional effects on anomalous resistivity and calculation of ion resistivity is ongoing.

One final comment needs to be made on the unifying theme of this thesis. The underlying current of this project is to examine the spectral change imposed on eigenmodes by collisions. However, extensive study of different operators needs to be made to determine if this is a unique property to Lenard and Bernstein operator. A totally conservative operator which well defines experimental data may contain a singular perturbation. Indeed, we have seen indications of this in the work of Skiff. If truly natural collisions exhibit this behavior, the implications need to be examined in more depth.

Bibliography

[BE06] Jörg Büchner and Nina Elkina. Anomalous resistivity of current-driven isothermal plasmas due to phase space structuring. *Physics of Plasma*, 13(8), 2006.

[Bel06] Paul M. Bellan. *Fundamentals of Plasma Physics*. Cambridge University Press, 2006.

[BGK54] P. L. Bhatnagar, E. P. Gross, and M. Krook. A Model for Collision Processes in Gases. I. Small Amplitude Processes in Charged and Neutral One-Component Systems. *Physical Review*, 94:511–525, May 1954.

[BMRT05] V.Yu Bychenkov, J. Myatt, W. Rozmus, and V.T. Tokhanchuk. Kinetic theory of ion acoustic waves in a plasma with collisional electrons. *Physical Review E*, 52(6):6759–6776, December 2005.

[BN00] A. V. Bobyliv and K. Nanbu. Theory of collisional algorithms for gases and plasmas based on the boltzmann equation and the landau-fokker-planck equation. *Physical Review E*, 61(4), 2000.

[BO99] C. M. Bender and S.A. Orszag. *Advanced Mathematical Methods for Scientists and Engineers: Asymptotic Methods and Perturbation Theory*. Springer-Verlag Inc., 1999.

[Bun59] O. Buneman. Dissipation of currents in ionized media. *Physical Review*, 115(3), 1959.

[BV64] D. Bhadra and R.K. Varma. Collisional damping of ion waves in a plasmas. *Physics of Fluids*, 7(7), 1964.

[BV05] R.L. Berger and E.J. Valeo. The frequency and damping of ion acoustic waves in collisional and collisionless two-species plasmas. *Physics of Plasma*, 12(3), 2005.

[Cas59] K. M. Case. Plasma Oscillations. *Annals of Physics*, 7:349–364, 1959.

[CFL67] R. Courant, K. Friedrichs, and H. Lewy. On the partial difference equations of mathematicalphysics. *IBM Journal*, pages 215 – 234, March 1967.

[DG75] R.C. Davidson and N.T. Gladd. Anomalous transport properties associated with the lower-hybrid-drift instability. *Physics of Fluids*, 18(10):1327–1335, October 1975.

[DRB+05] F. Detering, W. Rozmus, A. Brantov, V.Y Bychenkov, C.E. Capjack, and R. Sydora. Particle-in-cell simulations of heat flux driven ion acoustic instability. *Physics of Plasma*, 12(1), 2005.

[DSMSS99] S. De Souza-Machado, M. Sarfaty, and F. Skiff. Kinetic modes in a hot magnetized and weakly collisional plasma. *Physics of Plasma*, 6(6), June 1999.

[EA72] Kent Estabrook and Igor Alexeff. Ion-acoustic wave and pseudowave generation in a plasma. *Physics of Fluids*, 15(11):2026–2033, November 1972.

[ESS92] E.M. Epperlein, R.W. Short, and A. Simon. Damping of ion-acoustic waves in the presence of electron-ion collisions. *Physical Review Letters*, 69(12), September 1992.

[FC62] B.D. Fried and S.B. Conte. *The Plasma Dispersion Function.* Academic, 1962.

[Fun93] Daniele Funaro. Fortran routines for spectral methods. online at http://cdm.unimo.it/home/matematica/funaro.daniele/rout.html, 1993.

[GB05] Donald A. Gurnett and Amitava Bhattacharjee. *Introduction to Plasma Physics with Space and Laboratory Applications.* Cambridge University Press, 2005.

[GCP06] L. Galeotti, F. Califano, and F. Pegoraro. Echography of Vlasov codes. *Physics Letters A*, 355(4-5):381–385, 2006.

[Gre73] John M. Greene. Improved bhatnagar-gross-krook model of electron-ion collisions. *Physics of Fluids*, 16(11), November 1973.

[GS84] A.A. Galeev and R.Z. Sagdeev. Current instabilities and anomalous resistivity of plasmas. In A.A. Galeev and R.N. Sudan, editors, *Basic Plasma Physics*, volume 2, pages 271–303. North-Holland Physics Publishing, 1984.

[Hin91] E. J. Hinch. *Perturbation Methods.* Springer-Verlag Inc., 1991.

[HTM04] P. Hellinger, P. Travnicek, and J.D. Menietti. Effective collision frequency due to ion-acoustic instability: Theory and simulations. *Geophysical Research Letters*, 31, 2004.

[Ich73] S. Ichimaru. *Basic principles of plasma physics, a statistical approach.* Benjamin, 1973.

[IH81] O. Ishihara and A. Hirose. Quasilinear mechanism of high-energy ion tail formation in the ion-acoustic instability. *Physical Review Letters*, 46(12), March 1981.

[IH83] O. Ishihara and A. Hirose. High-energy ion tail formation in the ion-acoustic instability - three dimensional quasilinear approach. *Physics of Fluids*, 26(1), January 1983.

[IH84] O. Ishihara and A. Hirose. Turbulent heating and anomalous k spectrum in the quasilinear evolution of current-driven ion-acoustic instability. *Physics of Fluids*, 27(2), 1984.

[Kar67] V. I. Karpman. 'singular' solutions of the equations for plasma oscillations. *Soviet Journal of Physics*, 24(3):603–607, March 1967.

[Kli87] A. Klimas. A method for overcoming the velocity space filamentation problem in collisionless plasma model solutions. *Journal of Computational Physics*, 68:202–226, 1987.

[KS66] R. Kulsrud and C.S. Shen. The effect of weak collisions ion waves. *Physics of Fluids*, 9(1):177–186, January 1966.

[KT73] Nicholas A. Krall and Alvin W. Trivelpiece. *Principles of Plasma Physics.* McGraw-Hill, Inc., 1973.

[Kuc64] A. F. Kuckes. Effect of collisions upon plasma ion oscillations. *Physics of Fluids*, 7(4):511–519, April 1964.

[Lan46] L. Landau. On the vibrations of an electronic plasma. *Journal of Soviet Physics*, 10(1):25–34, 1946

[LB58] A. Lenard and I.B. Bernstein. Plasma oscillations with diffusion in velocity space. *Physical Review*, 112(5):1456–1459, December 1958.

[LSH53] Jr Lyman Spitzer and Richard Härm. Transport phenomena in a completely ionized gas. *Physical Review*, 89(5):977–981, March 1953.

[LT88] J. Labelle and R.A. Treumann. Plasma waves at the dayside magnetopause. *Space Science Review*, 47:175–202, 1988.

[MD05] Robert L. Merlino and Nicola D'Angelo. Electron and ion inertia effects on current-driven collisional dust acoustic, dust ion acoustic, and ion acoustic instabilities. *Physics of Plasma*, 12, 2005.

[MWGO68] J. H. Malmberg, C. B. Wharton, R. W. Gould, and T. M. O'Neil. Observation of Plasma Wave Echoes. *Physics of Fluids*, 11:1147–1153, June 1968.

[NBS99] C.S. Ng, A. Bhattacharjee, and F. Skiff. Kinetic eigenmodes and discrete spectrum of plasma oscillations in a weakly collisional plasma. *Physical Review Letters*, 83(10):1974–1977, September 1999.

[NBS04] C.S. Ng, A. Bhattacharjee, and F. Skiff. Complete spectrum of kinetic eigenmodes for plasma oscillations in a weakly collisional plasma. *Physical Review Letters*, 96(2), 2004.

[Nic83] Dwight R. Nicholson. *Introduction to Plasma Theory.* Wiley, 1983.

[OG68] T.M. O'Neil and R.W. Gould. Temporal and spatial plasma wave echoes. *Physics of Fluids*, 11(1):134–142, January 1968.

[O'N65] T. O'Neil. Collisionless Damping of Nonlinear Plasma Oscillations. *Physics of Fluids*, 8:2255–2262, December 1965.

[O'N68] T.M. O'Neil. Effect of Coulomb collisions and microturbulence on the plasma wave echoes. *Physics of Fluids*, 11(11):2420–2425, November 1968.

[PF08] P. Petkaki and M.P. Freeman. Nonlinear dependence of anomalous ion-acoustic resistivity and electron drift velocity. *The Astrophysical Journal*, pages 686–693, October 2008.

[PFK+06] P. Petkaki, M.P. Freeman, T. Kirk, C.E.J. Watt, and R.B. Horne. Anomalous resistivity and the nonlinear evolution of the ion-acoustic instability. *Journal of Geophysics Research*, 111, 2006.

[PWHF03] P. Petkaki, C.E.J. Watt, R.B. Horne, and M.P. Freeman. Anomalous resistivity in non-maxwellian plasmas. *Journal of Geophysics Research*, 108(A12), 2003.

[Ris89] H. Risken. *The Fokker-Planck equation. Methods of solution and applications.* Springer-Verlag Inc., 1989.

[RMJ57] M. N. Rosenbluth, W. M. MacDonald, and D. L. Judd. Fokker-Planck Equation for an Inverse-Square Force. *Physical Review*, 107:1–6, July 1957.

[SDR+06] R.D. Sydora, F. Detering, W. Rozmus, V.Y. Bychenkov, A. Brantov, and C.E. Capjack. Collisional particle simulation of ion acoustic instability. *Journal of Plasma Physics*, 72(6):1295–1298, 2006.

[SG69] R.Z. Sagdeev and A.A. Galeev. *Nonlinear Plasma Theory.* W.A. Benjamin, Inc., 1969.

[SH98] J.W. Schumer and J.P. Holloway. Vlasov simulations using velocity-scaled hermite representations. *Journal of Computational Physics*, 144:626–661, 1998.

[Sha90] S.K. Sharma. Kinetic theory of ion acoustic instability in a collisional plasma. *Journal of the Physical Society of Japan*, 59(2):130–137, January 1990.

[SK73] A.K Sundaram and P.K. Kaw. Current-driven ion acoustic instability in a collisional plasma. *Physics of Fluids*, 16(4):563–564, April 1973.

[SO68] C. H. Su and C. Oberman. Collisional damping of a plasma echo. *Physical Review Letters*, 20(9), 1968.

[SOC96] L.K. Spentzouris, J.-F. Ostiguy, and P.L. Colestock. Direct measurement of diffusion rates in high energy synchrotrons using longitudinal beam echoes. *Physical Review Letters*, 76(4), January 1996.

[SS02] R.W. Short and A. Simon. Damping of perturbations in weakly collisional plasmas. *Physics of Plasmas*, 9(8), 2002.

[SSMN+98] F. Skiff, S. De Souza-Machado, W.A. Noonan, A. Case, and T. N. Good. Linear kinetic modes in weakly collisional plasma. *Physical Review Letters*, 81(26):5820–5823, December 1998.

[SSMS96] M. Sarfaty, S. De Souza-Machado, and F. Skiff. Direct determination of ion wave fields in a hot magnetized and weakly collisional plasma. *Physics of Plasma*, 3(12):4316–4324, December 1996.

[SSMS98] M. Sarfaty, S. De Souza-Machado, and F. Skiff. Wave-particle resonance in a magnetized plasma. *Physical Review Letters*, 80(15):3252–3255, April 1998.

[Ste71] R. J. Stefant. Influence of electron-ion collisions on ion acoustic waves. *Physics of Fluids*, pages 2245–2246, 1971.

[Sti92] Thomas Howard Stix. *Waves in Plasmas.* Springer-Verlag Inc., 1992.

[Tho63] K.I. Thomassen. Evidence of anomalous resistance in plasmas. *Physical Review Letters*, 10(3):80–81, February 1963.

[TL29] Lewi Tonks and Irving Langmuir. A general theory of the plasma of an arc. *Phys. Rev.*, 34(6):876–922, Sep 1929.

[Tre01] Rudolf A. Treumann. Origin on Resistivity in reconnection. *Earth Planets Space*, 53:453–462, 2001.

[TWE+93] M.D. Tracy, E. A. Williams, K. G. Estabrook, J.S. De Groot, and S. M. Cameron. Eigenvalue solution for the ion-collisional effects on ion-acoustic and entropy waves. *Physics of Fluids B*, 5(5):1430–1439, May 1993.

[van55] N. G. van Kampen. On the theory of stationary waves in plasmas. *Physica*, 21:949–963, 1955.

[Ved63] A. A. Vedenov. Quasi-linear plasma theory (theory of a weakly turbulent plasma). *Journal of Nuclear Energy*, 5:169–186, January 1963.

[Vla45] A. Vlasov. On the kinetic theory of an assembly of particles with collective interaction. *Soviet Journal of Physics*, 9(1), 1945.

[WHF02] C.E.J. Watt, R.B. Horne, and M.P. Freeman. Ion-acoustic resistivity in plasmas with similar ion and electron temperatures. *Geophysical Research Letters*, 29(1):1004, 2002.

APPENDIX A

Plasma-Wave-Derivations

The work in this appendix, particularly the derivation of the plasma wave echo was taken largely from Bellan's textbook [Bel06]. The organization of this appendix is as follows.
A.1. Expand Vlasov
A.2. Fourier-Laplace of linear VP System
A.3. Fourier-Laplace of nonlinear VP System
A.4. The Double Impulse Source Function

A.1 Expand Vlasov Poisson System

In the usual linear theory for the Vlasov-Poisson system, we apply perturbation theory by expanding about a time and space independent equilibrium. Assuming that each successive order is much smaller than the previous one, we can neglect all terms or order $n > 1$.

$$\frac{\partial f}{\partial t} + v\frac{\partial f}{\partial x} + \frac{qE}{m}\frac{\partial f}{\partial v} = 0 \tag{A.1}$$

$$\nabla^2\Phi = \frac{q}{\epsilon_o}\int_{-\infty}^{\infty} f(v)dv \tag{A.2}$$

$$\frac{\partial f}{\partial t} + v\frac{\partial f}{\partial x} + \frac{qE}{m}\frac{\partial f}{\partial v} = \nu\frac{\partial}{\partial v}\left[vf + {v_{th}}^2\frac{\partial f}{\partial v}\right]. \tag{A.3}$$

$$\begin{aligned}
&\frac{\partial}{\partial t}(f_0(v) + f_1(x,v,t) + ...) + v\frac{\partial}{\partial x}(f_0(v) + f_1(x,v,t) + ...) \\
&+\frac{q}{m}(E_0 + E_1(x,t) + E_2(x,t) + ...) \times \frac{\partial}{\partial v}(f_0(v) + f_1(x,v,t) + ...) \\
&= \nu\frac{\partial}{\partial v}\left[v(f_0(v) + f_1(x,v,t) + ...) + {v_{th}}^2\frac{\partial}{\partial v}(f_0(v) + f_1(x,v,t) + ...)\right]
\end{aligned} \tag{A.4}$$

$$\frac{\partial E(x,t)}{\partial x} = \frac{q}{\epsilon_o}\int_{-\infty}^{\infty}(f_0(v) + f_1(x,v,t) + f_2(x,v,t)...)dv \tag{A.5}$$

As we are interested in the linear behavior, the equilibrium Vlasov equation is subtracted off and the nonlinear terms are dropped. Also note that we have chosen $E_0 = 0$ for simplicity.

$$\frac{\partial f_1}{\partial t} + v\frac{\partial f_1}{\partial x} + \frac{qE_1}{m}\frac{\partial f_0}{\partial v} = \nu\frac{\partial}{\partial v}\left[vf_1 + {v_{th}}^2\frac{\partial f_1}{\partial v}\right] \tag{A.6}$$

$$\frac{\partial E_1(x,t)}{\partial x} = \frac{q}{\epsilon_o}\int_{-\infty}^{\infty} f_1(x,v,t)dv \tag{A.7}$$

A.2 Fourier-Laplace of linear VP

In this section, we take the Fourier transform in space and the Laplace transform in time of the Vlasov-Poisson system. Note that the external potential can be a pulse. The second term in Poisson's equation is the response to the external field.

$$(p + ikv)\widetilde{f_1} + \frac{ike}{m}\widetilde{\phi_1}\frac{df_0}{dv} = 0 \tag{A.8}$$

$$-k^2\widetilde{\phi_1} = -k^2\widetilde{\phi_{ext}} - \frac{1}{\epsilon_o}\int_{-\infty}^{\infty}\widetilde{f_1}dv \tag{A.9}$$

Rewrite f_1 from Vlasov:

$$\widetilde{f_1} = \frac{-ike\widetilde{\phi_1}}{m(p+ikv)}\frac{df_0}{dv} \tag{A.10}$$

$$\tag{A.11}$$

Now rewrite ϕ_1.

$$-k^2\widetilde{\phi_1} = -k^2\widetilde{\phi_{ext}} - \frac{1}{\epsilon_o}\int_{-\infty}^{\infty}\frac{-ike\widetilde{\phi_1}}{m(p+ikv)}\frac{df_0}{dv}dv \tag{A.12}$$

$$\widetilde{\phi_1} = \frac{\widetilde{\phi_{ext}}}{\epsilon(p,k)} \tag{A.13}$$

$$\epsilon(p,k) = 1 - \int_{-\infty}^{\infty}\frac{ie^2}{m\epsilon_0 k(p+ikv)}\frac{df_0}{dv} \tag{A.14}$$

$$\widetilde{\phi_1} = \frac{\widetilde{\phi_{ext}}}{1 - \int_{-\infty}^{\infty}\frac{ie^2}{m\epsilon_0 k(p+ikv)}\frac{df_0}{dv}} \tag{A.15}$$

Finally we get f_1 in terms of the external field.

$$\widetilde{f_1} = \frac{-ike\widetilde{\phi_{ext}}}{m\epsilon(p,k)(p+ikv)}\frac{df_0}{dv} \tag{A.16}$$

$$= \frac{-ike\widetilde{\phi_{ext}}}{m(p+ikv)\left(1 - \int_{-\infty}^{\infty}\frac{ie^2\widetilde{\phi_1}}{m\epsilon_0 k(p+ikv)\frac{df_0}{dv}}\right)\frac{df_0}{dv}} \tag{A.17}$$

A.3 Fourier-Laplace of nonlinear VP System

Begin with the second order equation.

$$\frac{\partial f_2}{\partial t} + v\frac{\partial f_2}{\partial x} - \frac{eE_1}{m}\frac{\partial f_1}{\partial v} - \frac{eE_2}{m}\frac{\partial f_0}{\partial v} = 0 \tag{A.18}$$

Fourier-Laplace transform

$$(p + ikv)\widetilde{f_2} + \frac{ike}{m}\widetilde{\phi_2}\frac{df_0}{dv} = -\frac{e}{m}\frac{\partial}{\partial v}L\left[F\left[\nabla\phi_1 f_1\right]\right] \tag{A.19}$$

$$-\frac{e}{m}\frac{\partial}{\partial v}L\left[F\left[\nabla\phi_1 f_1\right]\right] \tag{A.20}$$

$$= -\frac{e}{m}\frac{\partial}{\partial v}\left[\frac{1}{2\pi}\int_{-\infty}^{\infty}dk'\int_{b-i\infty}^{b+i\infty}dp'\frac{ik'}{2\pi i}\widetilde{f}_1(p-p',k-k')\widetilde{\phi}_1(p',k')\right] \tag{A.21}$$

$$\bar{k'} = k - k' \tag{A.22}$$

$$\bar{p'} = p - p' \tag{A.23}$$

$$(p + ikv)\widetilde{f_2} + \frac{ike}{m}\widetilde{\phi_2}\frac{df_0}{dv} = -\frac{e}{m}\frac{\partial}{\partial v}\left[\frac{1}{2\pi}\int_{-\infty}^{\infty}dk'\int_{b-i\infty}^{b+i\infty}dp'\frac{ik'}{2\pi i}\widetilde{f}_1(\bar{p'},\bar{k'})\widetilde{\phi}_1(p',k')\right] \tag{A.24}$$

Now substitute in the definitions of ϕ_1, eq.(A.15), and f_1, eq.(A.16), from the previous section.

$$(p + ikv)\widetilde{f_2} + \frac{ike}{m}\widetilde{\phi_2}\frac{df_0}{dv} = \frac{\partial\chi(p,k,v)}{\partial v} \tag{A.25}$$

$$\chi(p,k,v) = \frac{e^2}{m^2}\left[\frac{i}{(2\pi)^2}\int_{-\infty}^{\infty}dk'\int_{b-i\infty}^{b+i\infty}dp'\frac{\bar{k'^2}\widetilde{\phi}_{ext}(\bar{p'},\bar{k'})}{\epsilon(\bar{p'},\bar{k'})(\bar{p'}+i\bar{k'}v)}\frac{df_0}{dv}\frac{\widetilde{\phi}_{ext}(k',p')}{\epsilon(p',k')}\right] \tag{A.26}$$

$$\widetilde{f_2} = \frac{1}{(p+ikv)}\left[\frac{\partial\chi}{\partial v} - \frac{ike}{m}\widetilde{\phi_2}\frac{df_0}{dv}\right] \tag{A.27}$$

Find the second moment of the potential by substituting in f_2

$$\widetilde{\phi_2} = \frac{e}{k^2\epsilon_0}\int_{-\infty}^{\infty}f_2(v)dv \tag{A.28}$$

$$= \frac{e}{k^2\epsilon_0\epsilon(p,k)}\int_{-\infty}^{\infty}\frac{1}{(p+ikv)}\frac{\partial\chi}{\partial v}dv \tag{A.29}$$

$$= \frac{e}{k^2\epsilon_0\epsilon(p,k)}\int_{-\infty}^{\infty}\frac{ik\chi}{(p+ikv)^2}dv \tag{A.30}$$

$$\widetilde{\phi}_2 = \frac{-\omega_p\ e/m}{4\pi^2 k^2 \epsilon(p,k)} \int_{-\infty}^{\infty} dv \frac{k}{(p+ikv)^2} \times \left[\int_{-\infty}^{\infty} dk' \int_{b-\imath\infty}^{b+\imath\infty} dp' \frac{\bar{k}'k'\widetilde{\phi}_{ext}(\bar{p}',\bar{k}')}{\epsilon(\bar{p}',\bar{k}')(\bar{p}'+i\bar{k}'v)} \frac{df_0}{dv} \frac{\widetilde{\phi}_{ext}(k',p')}{\epsilon(p',k')} \right] \quad \text{(A.31)}$$

Now we are ready to substitute in the external potential to analyze the second order behavior.

A.4 Double Impulse Source Function

To create the echo we apply and external pulse at two different times.

$$\Phi_{ext} = \phi_a cos(k_a x)\delta(\omega_p t) + \phi_b cos(k_b x)\delta(\omega_p(t-\tau)) \quad \text{(A.32)}$$

$$\quad \text{(A.33)}$$

Fourier-Laplace transform the external potential.

$$\widetilde{\Phi}_{ext} = \int_{-\infty}^{\infty} dt \int_{-\infty}^{\infty} dx \left(\phi_a cos(k_a x)\delta(\omega_p t) + \phi_b cos(k_b x)\delta(\omega_p(t-\tau))\right) e^{-\imath kx - pt} \quad \text{(A.34)}$$

$$= \frac{1}{\omega_p} \int_{-\infty}^{\infty} dx \left(\phi_a cos(k_a x) + \phi_b cos(k_b x) e^{-p\tau}\right) e^{-\imath kx} \quad \text{(A.35)}$$

$$= \frac{\pi}{\omega_p} \sum_{\pm} \left(\phi_a \delta(k \pm k_a) + \phi_b \delta(k \pm k_b) e^{-p\tau}\right) \quad \text{(A.36)}$$

Substitute the transformed potential into the ϕ_2 equation, eq.(A.31).

$$\begin{aligned}\widetilde{\phi}_2 &= \frac{-\omega_p\ e/m}{4\pi^2k^2\epsilon(p,k)}\int_{-\infty}^{\infty}dv\frac{k}{(p+ikv)^2}\int_{-\infty}^{\infty}dk' \\ &\times\int_{b-i\infty}^{b+i\infty}dp'\frac{\bar{k}'k'\widetilde{\phi}_{ext}(\bar{p}',\bar{k}')}{\epsilon(\bar{p}',\bar{k}')(\bar{p}'+i\bar{k}'v)}\frac{df_0}{dv}\frac{\widetilde{\phi}_{ext}(k',p')}{\epsilon(p',k')} \qquad \text{(A.37)} \\ &= \frac{-\omega_p\ e/m}{4\pi^2k^2\epsilon(p,k)}\int_{-\infty}^{\infty}dv\frac{k}{(p+ikv)^2}\int_{-\infty}^{\infty}dk' \\ &\int_{b-i\infty}^{b+i\infty}dp'\frac{\bar{k}'k'\frac{df_0}{dv}}{\epsilon(\bar{p}',\bar{k}')(\bar{p}'+i\bar{k}'v)\epsilon(p',k')}\frac{\pi^2}{\omega_p^2} \\ &\times\sum_{\pm}\left(\phi_a\delta(k'\pm k_a)+\phi_b\delta(k'\pm k_b)e^{-p'\tau}\right)\times\sum_{\pm}\left(\phi_a\delta(\bar{k}'\pm k_a)+\phi_b\delta(\bar{k}'\pm k_b)e^{-\bar{p}'\tau}\right) \qquad \text{(A.38)} \\ &= \frac{-\pi e/m}{4\pi k^2\epsilon(p,k)}\int_{-\infty}^{\infty}dv\frac{k}{(p+ikv)^2}\int_{b-i\infty}^{b+i\infty}dp' \\ &\left[\frac{(\pm)k_a(k\mp k_a)\widetilde{\phi}_{ext}(\bar{p}',k\mp k_a)\phi_a\frac{df_0}{dv}}{\epsilon(\bar{p}',k\mp k_a)(\bar{p}'+i(k\mp k_a)v)\epsilon(p',\mp k_a)}+\frac{(\pm)k_b(k\mp k_b)\widetilde{\phi}_{ext}(\bar{p}',k\mp k_b)\phi_b\frac{df_0}{dv}e^{-p'\tau}}{\epsilon(\bar{p}',k\mp k_b)(\bar{p}'+i(k\mp k_b)v)\epsilon(p',\pm k_b)}\right] \qquad \text{(A.39)}\end{aligned}$$

We are interested only in "cross" terms, those that give interactions of k_a and k_b. The other terms give no interaction behavior.

$$\begin{aligned}\widetilde{\phi}_2(p,k) &= \frac{-e/m}{4\omega_pk^2\epsilon(p,k)}\int_{-\infty}^{\infty}dv\frac{k}{(p+ikv)^2}\int_{b-i\infty}^{b+i\infty}dp'\frac{df_0}{dv}\phi_a\phi_b \\ &\times\left[\frac{(\pm)k_a(k\mp k_a)\delta(k\mp k_a\pm k_b)e^{-\bar{p}'\tau}}{\epsilon(\bar{p}',k\mp k_a)(\bar{p}'+i(k\mp k_a)v)\epsilon(p',\pm k_a)}+\frac{(\pm)k_b(k\mp k_b)\delta(k\pm k_a\mp k_b)e^{-p'\tau}}{\epsilon(\bar{p}',k\mp k_b)(\bar{p}'+i(k\mp k_b)v)\epsilon(p',\pm k_b)}\right] \qquad \text{(A.40)}\end{aligned}$$

Do the spatial inverse Fourier transform.

$$\begin{aligned}\widetilde{\phi}_2(p,x) &= \frac{1}{2\pi}\int_{-\infty}^{\infty}dk\ e^{ikx}\frac{-e/m}{4\omega_pk^2\epsilon(p,k)}\int_{-\infty}^{\infty}dv\frac{k}{(p+ikv)^2}\int_{b-i\infty}^{b+i\infty}dp'\frac{df_0}{dv}\phi_a\phi_b \\ &\left[\frac{(\pm)k_a(k\mp k_a)\delta(k\mp k_a\pm k_b)e^{-\bar{p}'\tau}}{\epsilon(\bar{p}',k\mp k_a)(\bar{p}'+i(k\mp k_a)v)\epsilon(p',\pm k_a)}+\frac{(\pm)k_b(k\mp k_b)\delta(k\pm k_a\mp k_b)e^{-p'\tau}}{\epsilon(\bar{p}',k\mp k_b)(\bar{p}'+i(k\mp k_b)v)\epsilon(p',\pm k_b)}\right] \qquad \text{(A.41)} \\ &= \frac{1}{2\pi}\int_{-\infty}^{\infty}dk\ e^{ikx}\frac{-e/m}{4\omega_pk^2\epsilon(p,k)}\int_{-\infty}^{\infty}dv\frac{k}{(p+ikv)^2}\int_{b-i\infty}^{b+i\infty}dp'\frac{df_0}{dv}\phi_a\phi_b \\ &\times\left[\frac{(\pm)k_a(k\mp k_a)\delta(k\mp k_a\pm k_b)e^{-\bar{p}'\tau}}{\epsilon(\bar{p}',k\mp k_a)(\bar{p}'+i(k\mp k_a)v)\epsilon(p',\pm k_a)}+\frac{(\pm)k_b(k\mp k_b)\delta(k\pm k_a\mp k_b)e^{-p'\tau}}{\epsilon(\bar{p}',k\mp k_b)(\bar{p}'+i(k\mp k_b)v)\epsilon(p',\pm k_b)}\right] \qquad \text{(A.42)}\end{aligned}$$

Let's examine the first term for the upper set of signs. Later, we can come back to examine the other terms.

$$\widetilde{\phi}_2^{upper}(p,x) = \frac{1}{2\pi}\int_{-\infty}^{\infty} dk\; e^{ikx}\frac{-e/m}{4\omega_p k^2\epsilon(p,k)}\int_{-\infty}^{\infty} dv\frac{k}{(p+ikv)^2}$$
$$\int_{b-i\infty}^{b+i\infty} dp'\frac{df_0}{dv}\phi_a\phi_b\frac{k_a(k-k_a)\delta(k-k_a+k_b)e^{-\bar{p}'\tau}}{\epsilon(\bar{p}',k-k_a)(\bar{p}'+i(k-k_a)v)\epsilon(p',k_a)} \tag{A.43}$$
$$= \frac{1}{2\pi}e^{i(k_a-k_b)x}\frac{-e/m}{4\omega_p(k_a-k_b)^2\epsilon(p,k_a-k_b)}\int_{-\infty}^{\infty} dv\frac{k_a-k_b}{(p+i(k_a-k_b)v)^2}$$
$$\int_{b-i\infty}^{b+i\infty} dp'\frac{df_0}{dv}\phi_a\phi_b\frac{k_a(k_a-k_b-k_a)e^{-\bar{p}'\tau}}{\epsilon(\bar{p}',k_a-k_b-k_a)(\bar{p}'+i(k_a-k_b-k_a)v)\epsilon(p',k_a)} \tag{A.44}$$

$$= \frac{-e\phi_a\phi_b e^{i(k_a-k_b)x}}{2\pi m4\omega_p(k_a-k_b)^2\epsilon(p,k_a-k_b)}\int_{-\infty}^{\infty} dv\frac{k_a-k_b}{(p+i(k_a-k_b)v)^2}$$
$$\int_{b-i\infty}^{b+i\infty} dp'\frac{df_0}{dv}\frac{-k_bk_ae^{-\bar{p}'\tau}}{\epsilon(\bar{p}',-k_b)(\bar{p}'+i(-k_b)v)\epsilon(p',k_a)} \tag{A.45}$$

Inverse Laplace transform

$$\widetilde{\phi}_2^{upper}(p,x) = \frac{-e\phi_a\phi_b e^{i(k_a-k_b)x}}{2\pi m4\omega_p(k_a-k_b)^2\epsilon(p,k_a-k_b)}\int_{-\infty}^{\infty} dv\frac{k_a-k_b}{(p+i(k_a-k_b)v)^2}$$
$$\times\int_{b-i\infty}^{b+i\infty} dp'\frac{df_0}{dv}\frac{-k_bk_ae^{-\bar{p}'\tau}}{\epsilon(\bar{p}',-k_b)(\bar{p}'+i(-k_b)v)\epsilon(p',k_a)} \tag{A.46}$$
$$\widetilde{\phi}_2^{upper}(t,x) = \int_{b-i\infty}^{b+i\infty}\frac{dp\;e^{pt}}{2\pi i}\frac{-e\phi_a\phi_b e^{i(k_a-k_b)x}}{2\pi m4\omega_p(k_a-k_b)^2\epsilon(p,k_a-k_b)}\int_{-\infty}^{\infty} dv\frac{k_a-k_b}{(p+i(k_a-k_b)v)^2} \tag{A.47}$$

$$\int_{b-i\infty}^{b+i\infty} dp'\frac{df_0}{dv}\frac{-k_bk_ae^{-\bar{p}'\tau}}{\epsilon(\bar{p}',-k_b)(\bar{p}'+i(-k_b)v)\epsilon(p',k_a)} \tag{A.48}$$

To do this we need to consider the terms carefully. First do the p' integral. Remember also that $\bar{p}' = p - p'$ There is a first order pole in the $\bar{p}' + i(-k_b)v$ term at $p' = p - ik_bv$. Using residue theory we find:

$$\widetilde{\phi}_2^{upper}(t,x) = \int_{b-i\infty}^{b+i\infty}\frac{dp}{2\pi i}\frac{-e\phi_a\phi_b e^{i(k_a-k_b)x}}{2\pi m4\omega_p(k_a-k_b)^2\epsilon(p,k_a-k_b)}\int_{-\infty}^{\infty} dv\frac{k_a-k_b}{(p+i(k_a-k_b)v)^2}$$
$$\times\int_{b-i\infty}^{b+i\infty} dp'\frac{df_0}{dv}\frac{-k_bk_ae^{-(p-p')\tau}e^{pt}}{\epsilon(p-p',-k_b)(p-p'+i(-k_b)v)\epsilon(p-ik_bv,k_a)} \tag{A.49}$$
$$= \int_{b-i\infty}^{b+i\infty}\frac{dp}{2\pi i}\frac{-e\phi_a\phi_b e^{i(k_a-k_b)x}}{2\pi m4\omega_p(k_a-k_b)^2\epsilon(p,k_a-k_b)}\int_{-\infty}^{\infty} dv\frac{k_a-k_b}{(p+i(k_a-k_b)v)^2}$$
$$\times\frac{df_0}{dv}\frac{-k_bk_ae^{-ik_bv\tau}e^{pt}}{\epsilon(ik_bv,-k_b)\epsilon(p-ik_bv,k_a)} \tag{A.50}$$

(A.51)

Next do the p integral noting that there is a second order pole at $p = i(k_b - k_a)v$ This allows us to use residue theorem for $n = 2$ which contains a derivative in p. Remember that $k_b - k_a$ is the interference wave number.

$$Res[\frac{G(p)}{(p + i(k_a - k_b)v)^2}, p = ikv] = \frac{d}{dz}G(p = i(k_a - k_b)v) \tag{A.52}$$

$$\begin{aligned}\widetilde{\phi}_2^{upper}(t,x) = &\frac{ei\phi_a\phi_b k_b k_a}{2\pi 2\pi m 4\omega_p(k_b - k_a)}\int_{b-i\infty}^{b+i\infty} dp \int_{-\infty}^{\infty} dv \frac{df_0}{dv}\frac{e^{i(k_a-k_b)x}}{\epsilon(p, k_a - k_b)} \\ &\times \frac{e^{-ik_b v\tau}e^{pt}}{(p + i(k_a - k_b)v)^2\epsilon(ik_b v, -k_b)\epsilon(p - ik_b v, k_a)}\end{aligned} \tag{A.53}$$

$$\begin{aligned}\widetilde{\phi}_2^{upper}(t,x) = &\frac{ei\phi_a\phi_b k_b k_a}{2\pi 2\pi m 4\omega_p(k_b - k_a)}\int_{-\infty}^{\infty} dv \frac{df_0}{dv}\frac{e^{i(k_a-k_b)x}}{\epsilon(ik_b v, -k_b)} \\ &\times \frac{d}{dp}\left[\frac{e^{-ik_b v\tau}e^{pt}}{\epsilon(p, k_a - k_b)\epsilon(p - ik_b v, k_a)}\right]|_{p=i(k_b-k_a)v}\end{aligned} \tag{A.54}$$

Now note that the largest p dependence is in the exponential term. Keep only this term.

$$\begin{aligned}\widetilde{\phi}_2^{upper}(t,x) = &\frac{ei\phi_a\phi_b k_b k_a}{2\pi 2\pi m 4\omega_p(k_b - k_a)}\int_{-\infty}^{\infty} dv \frac{df_0}{dv}\frac{e^{i(k_a-k_b)x}}{\epsilon(ik_b v, -k_b)} \\ &\times \left[\frac{te^{-ik_b v\tau}e^{i(k_b-k_a)vt}}{\epsilon(i(k_b - k_a)v, k_a - k_b)\epsilon(-ik_a v, k_a)}\right]\end{aligned} \tag{A.55}$$

First lets write $k_c = k_b - k_a$.

$$\begin{aligned}\widetilde{\phi}_2^{upper}(t,x) = &\frac{ei\phi_a\phi_b k_b k_a}{2\pi 2\pi m 4\omega_p k_c}\int_{-\infty}^{\infty} dv \frac{df_0}{dv}\frac{e^{ik_c x}}{\epsilon(ik_b v, -k_b)} \\ &\times \left[\frac{te^{-ik_b v\tau}e^{ik_c vt}}{\epsilon(ik_c v, -k_c)\epsilon(-ik_a v, k_a)}\right]\end{aligned} \tag{A.56}$$

Then note that this integral will phase mix to a nonzero value at $t = k_b\tau/k_c$. This is the echo time, τ'.

$$\widetilde{\phi}_2^{upper}(t,x) = \frac{ei\phi_a\phi_b k_b k_a}{2\pi 2\pi m 4\omega_p k_c}\int_{-\infty}^{\infty} dv \frac{df_0}{dv}\frac{te^{-ik_c v(t-\tau')}e^{ik_c x}}{\epsilon(ik_b v, -k_b)\epsilon(ik_c v, -k_c)\epsilon(-ik_a v, k_a)} \tag{A.57}$$

The dispersion terms are all equal to 1 if there is no dispersion and less than one for dispersive effects. When differentiating the exponential term, a linear time dependence arises in the second order potential. This indicates that the dispersion relations act only on their designated waves with no disturbance to the other waves.

APPENDIX B

Quasilinear Theory

B.1. Expand Vlasov-Poisson System
B.2. Take Space Average
B.3. Linear Solution
B.4. Finding the Quasilinear Equation
B.5. Quasilinear Diffusion Coefficient
B.6. Quasilinear Conservation Properties
B.7. Definition of Resistivity
B.8. Anomalous Resistivity

B.1 Expand Vlasov

In the usual linear theory for the Vlasov-Poisson system, we linearize about a time independent equilibrium. For quasilinear theory we linearize about a time dependent, spatially averaged equilibrium. We impose the requirement of a spatially homogeneous equilibrium. This is like linearizing about the space average of the distribution, where the non-equilibrium terms are the fluctuations.

$$\frac{\partial f}{\partial t} + v\frac{\partial f}{\partial x} + \frac{qE}{m}\frac{\partial f}{\partial v} = 0 \tag{B.1}$$

$$\nabla^2\Phi = \frac{q}{\epsilon_o}\int_{-\infty}^{\infty} f(v)dv \tag{B.2}$$

$$\frac{\partial(f_0(v,t) + f_1(x,v,t) + ...)}{\partial t} + v\frac{\partial(f_0(v,t) + f_1(x,v,t) + ...)}{\partial x}$$
$$+ \frac{q}{m}(E_0 + E_1(x,t) + E_2(x,t) + ...) + \frac{\partial(f_0(v,t) + f_1(x,v,t) + ...)}{\partial v} = 0 \tag{B.3}$$

$$\frac{\partial E(x,t)}{\partial x} = \frac{q}{\epsilon_o}\int_{-\infty}^{\infty}(f_0(v,t) + f_1(x,v,t) + f_2(x,v,t)...)dv \tag{B.4}$$

As we are interested in the nonlinear behavior, the linearized Vlasov equation is subtracted off.

$$\frac{\partial f_1}{\partial t} + v\frac{\partial f_1}{\partial x} + \frac{qE_1}{m}\frac{\partial f_0}{\partial v} = 0 \tag{B.5}$$

Also note that $E_0 = 0$ and the equilibrium is spatially invariant. This leaves us with:

$$\frac{\partial(f_0 + f_2 + ...)}{\partial t} + v\frac{\partial(f_2 + ...)}{\partial x} + \frac{q}{m}(E_2 + ...)\frac{\partial f_0}{\partial v} + \frac{q}{m}(E_1 + E_2 + ...)\frac{\partial(f_1 + ...)}{\partial v} = 0 \tag{B.6}$$

$$\nabla^2\Phi = \frac{q}{\epsilon_o}\int_{-\infty}^{\infty}(f_0(v) + f_1(v) + f_2(v)...)dv \tag{B.7}$$

B.2 Space Average

The next step is to space average the nonlinear collisional Vlasov equation and keep only the lowest order terms. According to Bellan, we will assume that space averages of E_n's are zero because they are waves. Again, f_0 is spatially independent, we can drop any $< E_n f_0 >$ terms. This leaves us with the following equation. Note that once the equilibrium changes from Maxwellian, the collision operator will have an effect on f_0.

$$\frac{\partial f_0(v,t)}{\partial t} + \frac{q}{m}\frac{\partial}{\partial v}\langle E_1(x,t)f_1(x,v,t)\rangle\, 0 \tag{B.8}$$

B.3 Linear Theory

We need to find f_1 as a function of E_1 to plug into eq[B.8]. We revert to the typical solution for linear theory by Fourier transforming the VP system in space and time. This gives:

$$\tilde{f}_1(k,v,\omega) = \frac{\imath e}{m}\tilde{E}_1(k)\frac{\partial f_0/\partial v}{\omega - kv} \tag{B.9}$$

Noting now that equilibrium is allowed to have time dependence and ω is dependent on both k and t, f_1 is

$$\tilde{f}_1(k,v,t) = \tilde{f}_1(k,v)e^{-\imath\omega(k,t)t} \tag{B.10}$$

$$\tilde{E}_1(k,t) = \tilde{E}_1(k)e^{-\imath\omega(k,t)t} \tag{B.11}$$

and (B.9) is

$$\tilde{f}_1(k,v) = \frac{\imath e}{m}\tilde{E}_1(k)\frac{\partial f_0/\partial v}{\omega - kv}. \tag{B.12}$$

This will be substituted into (B.8).

B.4 Quasilinear Equation rewritten

Now we rewrite the quasilinear term to take the Fourier transformed distribution, $\tilde{f}_1(k,v)$.

$$\langle E_1(x,t)f_1(x,v,t)\rangle = \frac{1}{L}\int dx\,\frac{1}{2\pi}\int \tilde{E}(k,t)e^{\imath kx}dk\,\frac{1}{2\pi}\int \tilde{f}_1(k',v,t)e^{\imath k'v}dk' \tag{B.13}$$

$$= \frac{1}{2\pi L}\int dk\int dk'\tilde{E}(k,t)\tilde{f}_1(k',v,t)\frac{1}{2\pi}\int dx e^{\imath(k+k')x} \tag{B.14}$$

$$= \frac{1}{2\pi L}\int dk\tilde{E}(-k,t)\tilde{f}_1(k,v,t) \tag{B.15}$$

$$= \frac{1}{2\pi L}\frac{ie}{m}\int dk\tilde{E}(-k)e^{-\imath\omega(-k,t)t}\tilde{E}_1(k)\frac{\partial f_0/\partial v}{\omega - kv}e^{-\imath\omega(k,t)t} \tag{B.16}$$

At this point we need to analyze the Fourier transforms of E and E^* (i.e. exploit parity). We end up with the following relations.

$$\tilde{E}_1(-k) = \tilde{E}_1^*(k) \qquad\qquad \omega(k) = -\omega_1^*(-k) \tag{B.17}$$

This leads to

$$\tilde{E}_1(-k)\tilde{E}_1(k) = \tilde{E}_1(k)\tilde{E}_1^*(k) \tag{B.18}$$

$$\omega(k) + \omega(-k) = 2i\omega_i(k) \tag{B.19}$$

Finally, the quasilinear equation can be rewritten.

$$\frac{\partial f_0(v,t)}{\partial t} = \frac{1}{2\pi L}\frac{ie^2}{m^2}\frac{\partial}{\partial v}\int dk|\tilde{E}_1(k)|^2\frac{\partial f_0/\partial v}{\omega - kv}e^{-2\omega_i(k,t)t} \tag{B.20}$$

B.5 Quasilinear Diffusion Coefficient

Here we can condense eq(B.20) into something with a Fokker-Planck form.

$$\frac{\partial f_0(v,t)}{\partial t} = \frac{\partial}{\partial v}\left[D_{QL}(v,t)\frac{\partial f_0(v,t)}{\partial v}\right] \tag{B.21}$$

$$D_{QL} = \frac{1}{2\pi L}\frac{ie^2}{m^2}\int \frac{|\tilde{E}_1(k)|^2e^{-2\omega_i(k,t)t}}{\omega(k,t) - kv}dk \tag{B.22}$$

B.6 Conservation Properties

Since we know the equilibrium is completely conservative, we will solve for the expansion term: $f = f_0 + (df_0/dt)dt$. Using that the distribution and its derivatives go

to zero at $\pm\infty$. Conservation of Particle Number Density.

$$n_0 = \int f_{e0} dv \tag{B.23}$$

$$\frac{dn_0}{dt} = \int \frac{df_{e0}}{dt} dv \tag{B.24}$$

$$= \int \frac{\partial}{\partial v} \left[D_{QL}(v,t) \frac{\partial f_0(v,t)}{\partial v} \right] dv \tag{B.25}$$

$$= \int d \left[D_{QL}(v,t) \frac{\partial f_0(v,t)}{\partial v} \right] \tag{B.26}$$

$$= \left[D_{QL}(v,t) \frac{\partial f_0(v,t)}{\partial v} \right]_{-\infty}^{\infty} \tag{B.27}$$

$$= 0 \tag{B.28}$$

$$\tag{B.29}$$

Conservation of Momentum

$$p = m \int v f_{e0} dv \tag{B.30}$$

$$\frac{dp}{dt} = m \int v \frac{df_{e0}}{dt} dv \tag{B.31}$$

$$= m \int v \frac{\partial}{\partial v} \left[D_{QL}(v,t) \frac{\partial f_0(v,t)}{\partial v} \right] dv \tag{B.32}$$

$$\tag{B.33}$$

Integrate by parts

$$\frac{dp}{dt} = -m \int D_{QL}(v,t) \frac{\partial f_0(v,t)}{\partial v} dv \tag{B.34}$$

$$= -m \int \frac{1}{2\pi L} \frac{ie^2}{m^2} \int \frac{|\tilde{E}_1(k)|^2 e^{-2\omega_i(k,t)t}}{\omega(k,t) - kv} dk \frac{\partial f_0(v,t)}{\partial v} dv \tag{B.35}$$

$$\tag{B.36}$$

The dispersion relation tells us that

$$-k = \omega_p^2 \int dv \frac{\partial f_0}{\partial v} \frac{1}{\omega - kv} \tag{B.37}$$

Thus,

$$\frac{dp}{dt} = m \frac{1}{2\pi L} \frac{ie^2}{m^2} \int k |\tilde{E}_1(k)|^2 e^{-2\omega_i(k,t)t} dk \tag{B.38}$$

$$= 0 \tag{B.39}$$

Because the last equation is an odd function of k under symmetric limits, momentum is conserved between the particles and the wave.

Conservation of Energy

$$W_{particle} = \int dv \ \frac{mv^2}{2} f_0(v) \tag{B.40}$$

$$\frac{\partial W_p}{\partial t} = \int dv \ \frac{mv^2}{2} \frac{\partial f_0(v)}{\partial t} \tag{B.41}$$

$$= \int dv \ \frac{mv^2}{2} \frac{\partial}{\partial v} \left[D_{QL} \frac{\partial f_0(v)}{\partial v} \right] \tag{B.42}$$

$$\tag{B.43}$$

Integration by parts yields.

$$\frac{\partial W_p}{\partial t} = - \int dv \ mv D_{QL} \frac{\partial f_0(v)}{\partial v} \tag{B.44}$$

$$= - \int dv \ mv \frac{\partial f_0(v)}{\partial v} \frac{ie^2}{2\pi L m^2} \int \frac{|\tilde{E}_1(k)|^2 e^{-2\omega_i(k,t)t}}{\omega(k,t) - kv} dk \tag{B.45}$$

$$\tag{B.46}$$

Add zero $(\omega - \omega)$, then separate integrals.

$$\frac{\partial W_p}{\partial t} = - \int dv \ mv D_{QL} \frac{\partial f_0(v)}{\partial v} \tag{B.47}$$

$$= -\frac{mie^2}{2\pi L k m^2} \int dv \ (kv + \omega - \omega) \frac{\partial f_0(v)}{\partial v} \int \frac{|\tilde{E}_1(k)|^2 e^{-2\omega_i(k,t)t}}{\omega(k,t) - kv} dk \tag{B.48}$$

$$= -\frac{mie^2}{2\pi L k m^2} \int dv \frac{\partial f_0(v)}{\partial v} \int |\tilde{E}_1(k)|^2 e^{-2\omega_i(k,t)t} \frac{\omega}{\omega(k,t) - kv} dk$$

$$+ \frac{mie^2}{2\pi L k m^2} \int dv \frac{\partial f_0(v)}{\partial v} \int |\tilde{E}_1(k)|^2 e^{-2\omega_i(k,t)t} dk \tag{B.49}$$

$$= -\frac{mie^2}{2\pi L k m^2} \int dv \frac{\partial f_0(v)}{\partial v} \int |\tilde{E}_1(k)|^2 e^{-2\omega_i(k,t)t} \frac{\omega}{\omega(k,t) - kv} dk$$

$$+ \frac{mie^2}{2\pi L k m^2} f_0(v)|_{\infty}^{\infty} \int |\tilde{E}_1(k)|^2 e^{-2\omega_i(k,t)t} dk \tag{B.50}$$

$$= -\frac{mie^2}{2\pi L k m^2} \int dv \frac{\partial f_0(v)}{\partial v} \int |\tilde{E}_1(k)|^2 e^{-2\omega_i(k,t)t} \frac{\omega}{\omega(k,t) - kv} dk \tag{B.51}$$

Now using the definition of the dispersion function, $\epsilon = 0$

$$1 = -\frac{\omega_p^2}{k} \int dv \frac{\partial f_0(v)}{\partial v} \frac{1}{\omega(k,t) - kv} \tag{B.52}$$

$$\frac{\partial W_p}{\partial t} = - \int \omega |\tilde{E}_1(k)|^2 e^{-2\omega_i(k,t)t} dk \tag{B.53}$$

$$= \int (\omega_r + i\omega_i) |\tilde{E}_1(k)|^2 e^{-2\omega_i(k,t)t} dk \tag{B.54}$$

We have already see that ω_r is an odd function of k and ω_i is an even function. This reduces the above result and tells us is that the particle energy change is equal to the wave energy change.

$$\frac{\partial W_p}{\partial t} = \int \omega_i |\tilde{E}_1(k)|^2 e^{-2\omega_i(k,t)t} dk \tag{B.55}$$

B.7 Classical Resistivity

Classical resistivity comes from collisions. This simplest approach to deriving resistivity is to consider two competing forces - interspecies collisions (dissipation of relative velocity) and the creation of a relative flow (velocity) due to the acceleration of particles in opposite directions by an electric field.

$$0 = -eE - \nu_{ei} m_e u_{rel} \tag{B.56}$$

$$E = \eta J \tag{B.57}$$

$$J = -neu_{rel} \tag{B.58}$$

$$0 = -e\eta(-neu_{rel}) - \nu_{ei} m_e u_{rel} \tag{B.59}$$

$$\eta = \frac{m\nu_{ei}}{ne^2} \tag{B.60}$$

That is simple enough.

B.8 Anomalous (Collisionless) Resistivity

In a collisionless system, resistivity comes about as particles scatter due to mechanisms such as resonances. In wave-particle interactions, resonances between the particles and waves will cause a resistivity in the plasma. The scattering of particles does not become apparent until the quasilinear regime when the plateau begins to form. Davidson and Gladd [DG75] derive a useful form of resistivity. Here $p_e = m_e \int v f_{e0} dv$ is momentum. This is most simply derived by a definition of the frictional force due to collisions.

$$F = \frac{dp_e}{dt} = -mn\nu_{eff} v = -\nu_{eff} p_e \tag{B.61}$$

This gives ν and η from Eq(B.60).

$$\nu = -\frac{1}{p_e}\frac{\partial p_e}{\partial t} \tag{B.62}$$

$$\eta = \frac{m_e}{n_e q_e^2}\left(-\frac{1}{p_e}\frac{\partial p_e}{\partial t}\right) \tag{B.63}$$

Sagdeev in his book "Nonlinear Plasma Theory" [SG69] spends sometime deriving an explicit form for the quasilinear contributions to resistivity. He begins by deriving the quasilinear equation in the following form:

$$\frac{\partial f_{e0}}{\partial t} = \frac{\partial}{\partial v} D_{QL} \frac{\partial f_0}{\partial v} \tag{B.64}$$

$$= \frac{e^2}{2\pi m^2} \int \frac{\partial}{\partial v} \frac{\gamma k^2 |\phi|^2}{(w - kv)^2 + \gamma^2} \frac{\partial f_0}{\partial v} dk \tag{B.65}$$

This get substituted into the definition of force.

$$F = \frac{dp_e}{dt} = m \int v \frac{df_{e0}}{dt} dv \tag{B.66}$$

$$= m \int v \frac{\partial}{\partial v} D_{QL} \frac{\partial f_0}{\partial v} dv \tag{B.67}$$

$$= -m \int D_{QL} \frac{\partial f_0}{\partial v} dv \tag{B.68}$$

$$\frac{dp_e}{dt} = \frac{e^2}{2\pi m^2} \int dv \int \frac{\gamma k^2 |\phi|^2}{(w - kv)^2 + \gamma^2} \frac{\partial f_0}{\partial v} dk \tag{B.69}$$

Noting that the dispersion relation is:

$$\epsilon = 1 - \sum_s \frac{\omega_{ps}^2}{k} \int dv \frac{\partial f_s 0 / \partial v}{\omega + i\gamma - kv} \tag{B.70}$$

$$\frac{\partial \epsilon}{\partial \omega} = \sum_s \frac{\omega_{ps}^2}{k} \int dv \frac{\partial f_s 0 / \partial v}{(\omega + i\gamma - kv)^2} \tag{B.71}$$

Sagdeev goes on to say that:

$$mn\nu_{eff} u(t) = - \int dk \frac{\gamma k}{2\pi} \frac{\partial \epsilon(\omega)}{\partial \omega} \frac{k^2 |\phi|^2}{8\pi} \tag{B.72}$$

Estimates are then made for the $T_e >> T_i$ regime that yields the following equation.

$$\nu_{an} \sim \omega_{pi} \frac{v_{de} T_e}{c_s T_i} \tag{B.73}$$

The anomalous resistivity is estimated by Petkaki via Labelle and Treumann. Labelle and Treumman also use the Sagdeev formula for ion-acoustic waves in the following form.

$$\nu_{an} = \frac{\omega_e \epsilon_o \delta E^2}{2nT_e} \tag{B.74}$$

$$\nu_{an} = \frac{\omega_e W}{nT_e} \tag{B.75}$$

$$W = \frac{\epsilon_o \delta E^2}{2} \tag{B.76}$$

$$\nu_{an} \approx 10^{-2} \omega_{pi} \frac{v_{de} T_e}{c_s T_i} \tag{B.77}$$

APPENDIX C

Collisions

C.2. Krook Operator
C.3. Fokker-Planck
C.4. Landau Operator
C.5. Lenard-Bernstein
C.6. Dougherty Fix to Lenard-Bernstein
C.7. Derivation of the NBS Modes

C.1 Spitzer-Harm

Spitzer and Harm [LSH53] derive that the conductivity in a plasma with stationary noninteracting ions and mobile electrons. They include the effects of electron-ion and electron-electron collisions [GB05] and show that resistivity is proportional to $(k_B T_e)^{-3/2}$.

C.2 The Krook Operator

The Bhatnagar-Gross-Krook, or Krook, operator simply accounts for a constant drag on the particles. It is appropriate for close range collisions, hard sphere scattering. It conserves mass and momentum and is generally applicable in the weak collisions limit. Despite lacking conservation of energy, it is simple to work with in the following form.

$$\frac{\partial f}{\partial t}|_c = \nu(f_0 - f_1) \tag{C.1}$$

Greene [Gre73] made modifications to include conservation of energy. Here u is the fluid drift velocity.

$$\frac{\partial f}{\partial t}|_c = \nu_{s,s}(f_{1,s} - (n_s/n_0 + m_e(v - u_0) \cdot \mathbf{u}_s/T_{0,s})$$

$$+ \nu_{s,s}((m_s(v - u_0)^2/2T_{0,s} - 3/2) \cdot T_s/T_{0,s}) f_{0,s}(v - u_0, T_{0,s})) \tag{C.2}$$

$$\tag{C.3}$$

It still, however, fails to account for the well known velocity dependence of collision frequencies as described by Spitzer collisions. It also does not account for diffusive behaviors. Greene states that this operator is only good "when there are no large gradients in the velocity space distribution". After that, the full Fokker-Planck form is needed.

C.3 Fokker-Planck

This section largely follows [GB05], chapter 11. The Fokker-Planck collisions were applied to plasmas by Rosenbluth, MacDonald, and Judd [RMJ57]. The operator can be found from expanding the distribution in moments in velocity. It is fully conservative and accounts for both particle drift and diffusion.

$$\left(\frac{\partial f}{\partial t}\right)_C = -\nabla_v \cdot \left[\left\langle \frac{\Delta \mathbf{v}}{\Delta t} \right\rangle_s f_s\right] + \frac{1}{2}\nabla_v \nabla_v : \left[\left\langle \frac{\Delta \mathbf{v}\Delta \mathbf{v}}{\Delta t} \right\rangle_s f_s\right] \tag{C.4}$$

The first term is known as the dynamical friction vector. It describes the drag imposed by the collision in velocity space.

$$\left\langle \frac{\Delta \mathbf{v}}{\Delta t} \right\rangle_s = \sum_{s'} 4\pi ln\Lambda_s \left(\frac{e_s e_{s'}}{4\pi\epsilon\mu_{ss'}}\right)^2 \frac{\mu_{ss'}}{m_s} \int_{-\infty}^{\infty} f_{s'}(\mathbf{v}') \frac{\mathbf{v}-\mathbf{v}'}{|\mathbf{v}-\mathbf{v}'|^3} d^3v' \tag{C.5}$$

The collision frequency between species s and s' is given by $\mu_{ss'}$. Also note that $N_{D,s}$ is the number of particles of species, s, in the Debye sphere.

$$\Lambda_s = 12\pi N_{D,s} \tag{C.6}$$

The second term is the aptly named diffusion tensor. It accounts for diffusive effects in the velocity space of the particle distributions.

$$\left\langle \frac{\Delta \mathbf{v}\Delta \mathbf{v}}{\Delta t} \right\rangle_s = \sum_{s'} ln\Lambda_s \left(\frac{e_s^2 e_{s'}^2}{4\pi\epsilon_o^2\mu_{ss'}}\right) \frac{\mu_{ss'}}{m_s} \int_{-\infty}^{\infty} \frac{f_{s'}(\mathbf{v}')}{|\mathbf{v}-\mathbf{v}'|} \left[\mathbf{1} - \frac{(\mathbf{v}-\mathbf{v}')(\mathbf{v}-\mathbf{v}')}{|\mathbf{v}-\mathbf{v}'|^2}\right] d^3v' \tag{C.7}$$

C.4 Landau Operator

The Landau operator is an integral form of the Fokker-Planck operator. It conserves mass, momentum and energy.Kulsrud and Shen write it as:

$$\left(\frac{\partial f}{\partial t}\right)_C = \frac{\Gamma}{m}\frac{\partial}{\partial \bar{v}} \cdot \sum_s \int d^3v' \bar{G} \cdot \left[\frac{1}{m}\frac{\partial f(\bar{v})}{\partial \bar{v}} f_s(\bar{v}') - \frac{1}{m_s}\frac{\partial f_s(\bar{v}')}{\partial \bar{v}} f(\bar{v})\right] \tag{C.8}$$

$$\bar{G} = (g^2 I - \bar{g}\bar{g})/g^2 \tag{C.9}$$

$$\bar{g} = \bar{v} - \bar{v}' \tag{C.10}$$

note that $f = f_e$ and s is for any species.

C.5 Lenard-Bernstein

The Lenard- Bernstein operator comes about from simplifying the Fokker-Planck operator. The constant collision frequency, single dimension in space and velocity,

and linearized assumptions are made to achieve Lenard and Bernstein's operator. It conserves particle number and momentum only for non drifting distribution. The Maxwellian is the equilibrium. This is shown in the next section

$$\left(\frac{\partial f}{\partial t}\right)_C = \nu \frac{\partial}{\partial v}\left[vf + v_{th}^2 \frac{\partial f}{\partial v}\right] \tag{C.11}$$

C.6 Dougherty Fix to Lenard and Bernstein Operator

Dougherty derives a conservative form of a reduced Fokker-Planck operator. This provides a method for fixing some of the conservation properties of the Lenard-Bernstein operator. It works for both drifting and non drifting distributions. Eq. C.11 is the non-linearized Lenard-Bernstein operator. Eq. C.12 is Dougherty's modified non-linearized Lenard-Bernstein operator. Subsequently, the conservation properties are shown in section C.6.1. This is followed by analysis of the linearized form of Dougherty's operator with its conservation properties in section C.6.2.

The starting point for the Dougherty form is eq. C.12. Here u is the "local" drift velocity.

$$\left(\frac{\partial f}{\partial t}\right)_C = \beta \frac{\partial}{\partial v_i}\left[(v_i - u_i)f + \frac{KT}{m}\frac{\partial f}{\partial v_i}\right] \tag{C.12}$$

C.6.1 Analysis of Nonlinear Dougherty Form

It adheres to the H-theorem and the non drifting velocity ($u = 0$) Maxwellian is its equilibrium.

$$f_0(v) = \frac{n_0}{\sqrt{2\pi v_{th}^2}} e^{-\frac{v^2}{2v_{th}^2}} \tag{C.13}$$

$$\left(\frac{\partial f}{\partial t}\right)_C = \beta \frac{\partial}{\partial v}\left[vf + v_{th}^2 \frac{\partial f}{\partial v}\right] \tag{C.14}$$

$$= \beta \frac{n_0}{\sqrt{2\pi v_{th}^2}}\left[f + v\frac{\partial f}{\partial v} + v_{th}^2 \frac{\partial^2 f}{\partial v^2}\right] \tag{C.15}$$

$$= \beta \frac{n_0}{\sqrt{2\pi v_{th}^2}}\left[e^{-\frac{v^2}{2v_{th}^2}} + v\frac{\partial (e^{-\frac{v^2}{2v_{th}^2}})}{\partial v} + v_{th}^2 \frac{\partial^2 (e^{-\frac{v^2}{2v_{th}^2}})}{\partial v^2}\right] \tag{C.16}$$

$$= \frac{\beta n_0 (e^{-\frac{v^2}{2v_{th}^2}})}{\sqrt{2\pi v_{th}^2}}\left[1 + v\frac{-v}{v_{th}^2} + v_{th}^2 \frac{v^2}{v_{th}^4} + v_{th}^2 \frac{-1}{v_{th}^2}\right] \tag{C.17}$$

$$= 0 \tag{C.18}$$

This is the drifting case.

$$f_0(v) = \frac{n_0}{\sqrt{2\pi v_{th}^2}} e^{-\frac{(v-v_d)^2}{2v_{th}^2}} \tag{C.19}$$

$$\left(\frac{\partial f}{\partial t}\right)_C = \beta\frac{\partial}{\partial v}\left[(v-v_d)f + v_{th}^2\frac{\partial f}{\partial v}\right] \tag{C.20}$$

$$= \beta\frac{n_0}{\sqrt{2\pi v_{th}^2}}\left[f + (v-v_d)\frac{\partial f}{\partial v} + v_{th}^2\frac{\partial^2 f}{\partial v^2}\right] \tag{C.21}$$

$$= \beta\frac{n_0}{\sqrt{2\pi v_{th}^2}}\left[e^{-\frac{(v-v_d)^2}{2v_{th}^2}} + (v-v_d)\frac{\partial(e^{-\frac{(v-v_d)^2}{2v_{th}^2}})}{\partial v} + v_{th}^2\frac{\partial^2(e^{-\frac{(v-v_d)^2}{2v_{th}^2}})}{\partial v^2}\right] \tag{C.22}$$

$$= \frac{\beta n_0(e^{-\frac{(v-v_d)^2}{2v_{th}^2}})}{\sqrt{2\pi v_{th}^2}}\left[1 + (v-v_d)\frac{-(v-v_d)}{v_{th}^2} + v_{th}^2\frac{(v-v_d)^2}{v_{th}^4} + v_{th}^2\frac{(-1)}{v_{th}^2}\right] \tag{C.23}$$

$$= 0 \tag{C.24}$$

Now we proceed to the conservation properties beginning with conservation of particle number.

$$\int_{-\infty}^{\infty}\left(\frac{\partial f}{\partial t}\right)_C dv = \int_{-\infty}^{\infty}\beta\frac{\partial}{\partial v}\left[(v-v_d)f + v_{th}^2\frac{\partial f}{\partial v}\right]dv \tag{C.25}$$

$$= \beta\left[(v-v_d)f + v_{th}^2\frac{\partial f}{\partial v}\right]_{-\infty}^{\infty} = 0 \tag{C.26}$$

Note that the exponential decay of the function, f, outweighs the algebraic growth of the other v terms. Next is conservation of momentum. Use integration by parts. $\int udv = uv - \int vdu$

$$\int_{-\infty}^{\infty} v\left(\frac{\partial f}{\partial t}\right)_C dv = \int_{-\infty}^{\infty} v\beta\frac{\partial}{\partial v}\left[(v-v_d)f + v_{th}^2\frac{\partial f}{\partial v}\right]dv \tag{C.27}$$

$$= \beta v\left[(v-v_d)f + v_{th}^2\frac{\partial f}{\partial v}\right]_{-\infty}^{\infty} - \beta\int_{-\infty}^{\infty}\left[(v-v_d)f + v_{th}^2\frac{\partial f}{\partial v}\right]dv \tag{C.28}$$

$$= \beta n_0 < (v-v_d) > -\beta v_{th} f|_{-\infty}^{\infty} \tag{C.29}$$

$$= -\beta n_0 < (v-v_d) >= 0 \tag{C.30}$$

Conservation of energy.

$$\int_{-\infty}^{\infty} v^2 \left(\frac{\partial f}{\partial t}\right)_C dv = \beta \int_{-\infty}^{\infty} v^2 \frac{\partial}{\partial v}\left[(v-v_d)f + v_{th}^2 \frac{\partial f}{\partial v}\right] dv \tag{C.31}$$

$$= \beta v^2 \left[(v-v_d)f + v_{th}^2 \frac{\partial f}{\partial v}\right]_{-\infty}^{\infty} - \beta \int_{-\infty}^{\infty} 2v \left[(v-v_d)f + v_{th}^2 \frac{\partial f}{\partial v}\right] dv \tag{C.32}$$

$$= -2\beta \int_{-\infty}^{\infty} \left[(v^2 - v_d v)f + v_{th}^2 v \frac{\partial f}{\partial v}\right] dv \tag{C.33}$$

$$= -2\beta \int_{-\infty}^{\infty} \left[(v-v_d)^2 f + v_d^2 f - v_d v f + v_{th}^2 v \frac{\partial f}{\partial v}\right] dv \tag{C.34}$$

$$= -2\beta n_0 \left[v_{th}^2 + v_d^2 - v_d^2\right] - 2\beta v_{th}^2 [vf|_{-\infty}^{\infty} - \int_{-\infty}^{\infty} f dv] \tag{C.35}$$

$$= -2\beta n_0 v_{th}^2 + 2\beta n_0 v_{th}^2 = 0 \tag{C.36}$$

C.6.2 Analysis of Non-drifting Linear Dougherty Form

Assuming an equilibrium with no drift velocity and expanding the new operator to first order we get:

$$\left(\frac{\partial f_1}{\partial t}\right)_C = \beta \frac{\partial}{\partial v_i}\left[v f_1 - u_1 f_0 + \frac{KT_0}{m}\frac{\partial f_1}{\partial v} + \frac{KT_1}{m}\frac{\partial f_0}{\partial v}\right] \tag{C.37}$$

Where u is the first order fluid correction. It is necessary to use the following definitions

$$n_1 = \int_{-\infty}^{\infty} f_1 dv \tag{C.38}$$

$$n_0 u_1 = \int_{-\infty}^{\infty} v f_1 dv \tag{C.39}$$

$$n_0 v_{th,1}^2 + n_1 v_{th,0}^2 = \int_{-\infty}^{\infty} v^2 f_1 dv \tag{C.40}$$

Conservation particle number.

$$\int_{-\infty}^{\infty} \left(\frac{\partial f}{\partial t}\right)_C dv = \int_{-\infty}^{\infty} \beta \frac{\partial}{\partial v}\left[v f_1 - u_1 f_0 + \frac{KT_0}{m}\frac{\partial f_1}{\partial v} + \frac{KT_1}{m}\frac{\partial f_0}{\partial v}\right] dv \tag{C.41}$$

$$= \frac{\partial}{\partial v}\left[v f_1 - u_1 f_0 + \frac{KT_0}{m}\frac{\partial f_1}{\partial v} + \frac{KT_1}{m}\frac{\partial f_0}{\partial v}\right]|_{-\infty}^{\infty} \tag{C.42}$$

$$= 0 \tag{C.43}$$

Conservation of momentum.

$$\int_{-\infty}^{\infty} v \left(\frac{\partial f}{\partial t}\right)_C dv = \int_{-\infty}^{\infty} v\beta \frac{\partial}{\partial v}\left[vf_1 - u_1 f_0 + \frac{KT_0}{m}\frac{\partial f_1}{\partial v} + \frac{KT_1}{m}\frac{\partial f_0}{\partial v}\right] dv \tag{C.44}$$

$$= \beta v\left[vf_1 - u_1 f_0 + \frac{KT_0}{m}\frac{\partial f_1}{\partial v} + \frac{KT_1}{m}\frac{\partial f_0}{\partial v}\right]|_{-\infty}^{\infty}$$

$$- \beta \int_{-\infty}^{\infty}\left[vf_1 - u_1 f_0 + \frac{KT_0}{m}\frac{\partial f_1}{\partial v} + \frac{KT_1}{m}\frac{\partial f_0}{\partial v}\right] dv \tag{C.45}$$

$$= -\beta n_0 u_1 + \beta n_0 u_1 - \beta v_{th,0}^2 f_1|_{-\infty}^{\infty} - \beta v_{th,1}^2 f_0|_{-\infty}^{\infty} \tag{C.46}$$

$$= 0 \tag{C.47}$$

Conservation of energy.

$$\int_{-\infty}^{\infty} v^2 \left(\frac{\partial f}{\partial t}\right)_C dv = \int_{-\infty}^{\infty} v^2\beta \frac{\partial}{\partial v}\left[vf_1 - u_1 f_0 + \frac{KT_0}{m}\frac{\partial f_1}{\partial v} + \frac{KT_1}{m}\frac{\partial f_0}{\partial v}\right] dv \tag{C.48}$$

$$= \beta v^2\left[vf_1 - u_1 f_0 + \frac{KT_0}{m}\frac{\partial f_1}{\partial v} + \frac{KT_1}{m}\frac{\partial f_0}{\partial v}\right]|_{-\infty}^{\infty}$$

$$- \beta \int_{-\infty}^{\infty} 2v\left[vf_1 - u_1 f_0 + \frac{KT_0}{m}\frac{\partial f_1}{\partial v} + \frac{KT_1}{m}\frac{\partial f_0}{\partial v}\right] dv \tag{C.49}$$

$$= -\beta \int_{-\infty}^{\infty} 2\left[v^2 f_1 - vu_1 f_0 + vv_{th,0}^2\frac{\partial f_1}{\partial v} + vv_{th,1}^2\frac{\partial f_0}{\partial v}\right] \tag{C.50}$$

$$= -2\beta\left[n_0 v_{th,1}^2 + n_1 v_{th,0}^2\right] - 2\beta v_{th,0}^2\left[vf_1|_{-\infty}^{\infty} - \int_{-\infty}^{\infty} f_1 dv\right]$$

$$- 2\beta v_{th,1}^2\left[vf_0|_{-\infty}^{\infty} - \int_{-\infty}^{\infty} f_0 dv\right] \tag{C.51}$$

$$= -2\beta\left[n_0 v_{th,1}^2 + n_1 v_{th,0}^2\right] + 2\beta v_{th,0}^2 n_1 + 2\beta v_{th,1}^2 n_0 \tag{C.52}$$

$$= 0 \tag{C.53}$$

C.6.3 Analysis of Full Linear Dougherty Form

Assuming an equilibrium with drift velocity and expanding the new operator to first order we get:

$$\left(\frac{\partial f_1}{\partial t}\right)_C = \beta \frac{\partial}{\partial v_i}\left[vf_1 - u_0 f_1 - u_1 f_0 + \frac{KT_0}{m}\frac{\partial f_1}{\partial v} + \frac{KT_1}{m}\frac{\partial f_0}{\partial v}\right] \tag{C.54}$$

Where u is the fluid correction. It is necessary to use the following definitions

$$n_1 = \int_{-\infty}^{\infty} f_1 dv \tag{C.55}$$

$$n_0 u_1 + n_1 u_0 = \int_{-\infty}^{\infty} v f_1 dv \tag{C.56}$$

$$n_0 v_{th,1}^2 + n_1 v_{th,0}^2 = \int_{-\infty}^{\infty} v^2 f_1 dv \tag{C.57}$$

Conservation particle number.

$$\int_{-\infty}^{\infty} \left(\frac{\partial f}{\partial t}\right)_C dv = \int_{-\infty}^{\infty} \beta \frac{\partial}{\partial v}\left[v f_1 - u_0 f_1 - u_1 f_0 + \frac{KT_0}{m}\frac{\partial f_1}{\partial v} + \frac{KT_1}{m}\frac{\partial f_0}{\partial v}\right] dv \tag{C.58}$$

$$= \frac{\partial}{\partial v}\left[v f_1 - u_0 f_1 - u_1 f_0 + \frac{KT_0}{m}\frac{\partial f_1}{\partial v} + \frac{KT_1}{m}\frac{\partial f_0}{\partial v}\right] |_{-\infty}^{\infty} \tag{C.59}$$

$$= 0 \tag{C.60}$$

Conservation of momentum.

$$\int_{-\infty}^{\infty} v \left(\frac{\partial f}{\partial t}\right)_C dv = \int_{-\infty}^{\infty} v\beta \frac{\partial}{\partial v}\left[v f_1 - u_0 f_1 - u_1 f_0 + \frac{KT_0}{m}\frac{\partial f_1}{\partial v} + \frac{KT_1}{m}\frac{\partial f_0}{\partial v}\right] dv \tag{C.61}$$

$$\begin{aligned} =& \beta v \left[v f_1 - u_0 f_1 - u_1 f_0 + \frac{KT_0}{m}\frac{\partial f_1}{\partial v} + \frac{KT_1}{m}\frac{\partial f_0}{\partial v}\right] |_{-\infty}^{\infty} \\ & - \beta \int_{-\infty}^{\infty} \left[v f_1 - u_0 f_1 - u_1 f_0 + \frac{KT_0}{m}\frac{\partial f_1}{\partial v} + \frac{KT_1}{m}\frac{\partial f_0}{\partial v}\right] dv \end{aligned}$$

$$= -\beta \left[n_0 u_1 + n_1 u_0 - n_1 u_0 - n_0 u_1 + v_{th,0}^2 f_1 |_{-\infty}^{\infty} + v_{th,1}^2 f_0 |_{-\infty}^{\infty}\right] \tag{C.62}$$

$$= 0 \tag{C.63}$$

Conservation of energy.

$$\int_{-\infty}^{\infty} v^2 \left(\frac{\partial f}{\partial t}\right)_C dv = \int_{-\infty}^{\infty} v^2 \beta \frac{\partial}{\partial v}\left[v f_1 - u_0 f_1 - u_1 f_0 + \frac{KT_0}{m}\frac{\partial f_1}{\partial v} + \frac{KT_1}{m}\frac{\partial f_0}{\partial v}\right] dv \tag{C.64}$$

$$\begin{aligned} =&\beta v^2 \left[v f_1 - u_0 f_1 - u_1 f_0 + \frac{KT_0}{m}\frac{\partial f_1}{\partial v} + \frac{KT_1}{m}\frac{\partial f_0}{\partial v}\right] |_{-\infty}^{\infty} \\ &- \beta \int_{-\infty}^{\infty} 2v \left[v f_1 - u_0 f_1 - u_1 f_0 + \frac{KT_0}{m}\frac{\partial f_1}{\partial v} + \frac{KT_1}{m}\frac{\partial f_0}{\partial v}\right] dv \end{aligned} \tag{C.65}$$

$$= -\beta \int_{-\infty}^{\infty} 2 \left[v^2 f_1 - v u_0 f_1 - v u_1 f_0 + v v_{th,0}^2 \frac{\partial f_1}{\partial v} + v v_{th,1}^2 \frac{\partial f_0}{\partial v}\right] \tag{C.66}$$

$$\begin{aligned} =& -2\beta \left[n_0 v_{th,1}^2 + n_1 v_{th,0}^2\right] - u_0(n_0 u_1 + n_1 u_0) - u_1 u_0 n_0 \\ &- 2\beta v_{th,0}^2 [v f_1|_{-\infty}^{\infty} - \int_{-\infty}^{\infty} f_1 dv] - 2\beta v_{th,1}^2 [v f_0|_{-\infty}^{\infty} - \int_{-\infty}^{\infty} f_0 dv] \end{aligned} \tag{C.67}$$

$$\begin{aligned} =& -2\beta \left[n_0 v_{th,1}^2 + n_1 v_{th,0}^2\right] - u_0(2n_0 u_1 + n_1 u_0) \\ &+ 2\beta v_{th,0}^2 n_1 + 2\beta v_{th,1}^2 n_0 \end{aligned} \tag{C.68}$$

$$= -u_0(2n_0 u_1 + n_1 u_0) \tag{C.69}$$

This is the full first order expansion of the Lenard-Bernstein operator, but unless the equilibrium is not drifting it does not conserve energy. Thus, Dougherty presents the case of a non drifting equilibrium for his fully conservative form.

C.7 NBS mode derivation

Here, the linear eigenmodes of the collisional plasma wave are derived as in [NBS99]. Let's look at the Hermite expansion of the Lenard-Bernstein-Vlasov-Poisson system. After re-normalizing equations C.70 and C.71 using equation C.72. Assume that the velocity dependence goes as equation C.73]. Note that for the normal mode solutions, we also assume that $f(x,v,t) = \tilde{f}(k,\omega,v)exp[i(kx - \omega t)]$.

$$\frac{\partial f_1}{\partial t} + v\frac{\partial f_1}{\partial x} + \frac{qE^{(1)}}{m}\frac{\partial f_0}{\partial v} = \nu \frac{\partial}{\partial v}\left[v f_1 + {v_{th}}^2 \frac{\partial f_1}{\partial v}\right] \tag{C.70}$$

$$\frac{\partial E^{(1)}}{\partial x} = \frac{q}{\epsilon_o}\int_{-\infty}^{\infty} f_1(v) dv \tag{C.71}$$

Normalizations:

$$\begin{aligned} u &= \frac{v}{\sqrt{2}v_{th}} & \Omega &= \frac{\omega}{\sqrt{2}kv_{th}} \\ \mu &= \frac{\nu}{\sqrt{2}kv_{th}} & \alpha &= \frac{\omega_p^2}{k^2 v_{th}^2} \\ g &= \frac{\sqrt{2}v_{th}\tilde{f}}{n_0} \end{aligned} \tag{C.72}$$

$$g(u,k,\omega) = \sum_{n=0}^{\infty} a_n(\Omega) H_n(u) e^{-u^2} \tag{C.73}$$

$$= \sum_{n=0}^{\infty} g_n(\Omega, u) \tag{C.74}$$

$$g_0 = \frac{H_0 e^{-u^2}}{\sqrt{\pi}} \tag{C.75}$$

Note that the hermite polynomials are normalized by a factor $(\sqrt{2^n \pi n!})^{-1}$ so that f_n's are orthonormal. The Vlasov-Poisson system reduces to:

$$(\Omega - u)g = \frac{-\alpha a_0}{2}\frac{dg_0}{du} + i\mu \frac{d}{du}\left[ug + \frac{dg}{du}\right] \tag{C.76}$$

Fully expand in the Hermite polynomials we would recover the equation from which the coefficients are found by exploiting orthogonality.

$$(\Omega - i\mu n)g_n(u) = \sqrt{\frac{n+1}{2}}g_{n+1}(u) + \sqrt{\frac{n}{2}}g_{n-1}(u) - \frac{\alpha a_0}{2}\frac{dg_0}{du} \tag{C.77}$$

If instead we expand g in the hermite series and exploit the recursion relations for the collision terms, we recover:

$$(\Omega - u - i\mu n)g_n = \frac{-\alpha a_0}{2}\frac{dg_0}{du} \tag{C.78}$$

$$\sum_{n=0}^{\infty} g_n(u) = \sum_{n=0}^{\infty} \frac{-\alpha a_0}{2(\Omega - u - i\mu n)}\frac{dg_0}{du} \tag{C.79}$$

The coefficients, a_n, are:

$$a_1 = \sqrt{2}\Omega a_0 \tag{C.80}$$

$$a_2 = (\Omega + i\mu)a_1 - \frac{1+\alpha}{\sqrt{2}}a_0$$

$$a_{n+1} = \sqrt{\frac{2}{n+1}}\left((i\mu n + \Omega)a_n - \sqrt{\frac{n}{2}}a_{n-1}\right) \quad n \geq 2$$

We find a_0 from Poisson's equation by exploiting orthogonality.

$$ik\tilde{E}(k,\omega) = \frac{-en_0}{\epsilon_0}\int \sum a_n H_n(u) e^{-u^2} du \tag{C.81}$$

$$a_0 = \frac{-ik\epsilon_0}{en_0}\tilde{E}(k,\omega) \tag{C.82}$$